INCREASING THE DEGREE OF DEFORMATION IN ALUMINUM ALLOYS IN A DOUBLE STAGED DEEP DRAWING PROCESS THROUGH AN INTERMEDIATE THERMAL TREATMENT

Diploma Thesis

Johann Erwin Gruber

Graz University of Technology
Institute Tools & Forming
Univ.-Prof. Dr.-Ing. Ralf Kolleck

Tutors:
Univ.-Prof. Dr.-Ing. Ralf Kolleck
DI. Wolfgang Weiss

STATUTORY DECLARATION

I declare that I have authored this thesis independently, that I have not used any other than the declared sources / resources, and that I have explicitly marked all material which has been quoted either literally or by content form the used sources.

Graz, 30 May 2011   _____

                                                    Signature

Danksagung

Abstract

The effect of recovery/ recrystallization on the aluminum alloy EN AW-5182 in a double staged deep drawing process with an intermediate thermal treatment was investigated. For the description of complex stress conditions, an X-shaped cross tool was used. A microstructure analysis was completed to evaluate the influence of the recovery/ recrystallization on the increase in the degree of deformation of the 2nd drawing stage.

Kurzfassung

Vorliegende Arbeit untersucht die Auswirkung von Erholung/ Rekristallisation auf die Erhöhung des Umformgrades der Aluminiumlegierung EN AW-5182. Die Versuchsdurchführung erfolgte in einem zweistufigen Tiefziehprozess mit zwischengelagerter Wärmebehandlung. Zur Abbildung möglichst komplexer Spannungszustände wurde ein X-förmiges Kreuzwerkzeug verwendet. Der Einfluss des erholten/ rekristallisierten Gefüges auf den Umformgrad wurde an Hand einer Gefügeanalyse festgestellt.

Table of content

1   Introduction

Lightweight construction is one of the major topics in the automotive vehicle development, currently and in the future. The reduction of weight, the continuous increase of energy costs and the fulfillment of legal regulations are all strong impulsive forces for further developments in this field. The approaches to reach these targets are manifold, they affect nearly every vehicle sector, and they range from power train applications up to the development of new alloys.

Lightweight construction

Due to its low specific weight, its mechanical properties and its widespread availability, aluminum has big potential as a construction material in the automotive sector, in order to promote further development of the material and its application.

Aluminum in the automotive sector

The application of aluminum in deep drawing is among those of greatest importance. According to the DIN 8584-3 definition, "Deep drawing is a sheet metal forming process by which a sheet metal blank is radially drawn into a forming die through the mechanical action of a punch."

DIN 8584-3

Automotive body parts of aluminum are usually drawn on the same equipment used to draw body parts made of steel. Special consideration must be given to the higher springback of aluminum sheet metal during mold and die production. Additionally, arrangements must be made to prevent the tool and die from flaking and cold bonding with the blank.

Tool and Die

The formability and the fields of application of aluminum are also limited by strain hardening during deformation, resulting in lower degrees of deformation.

Strain hardening

The approach of this work is to increase the formability of aluminum as a sheet metal through an intermediate thermal treatment in a double staged deep drawing process.

Increase of formability

1

2 State of the Art

Recovery/recrystallization through thermal treatment is a common practice to influence the mechanical properties of a material. In the case of steel as a construction material, it has been verified and controlled due to its long application history. In comparison, the application of aluminum as a construction material in the automotive industry is relatively new and detailed information about the softening processes of specific aluminum alloys are rare.

The most important alloy groups for the automotive industry are the 5xxx and 6xxx aluminum alloy groups. The 6xxx group is used for body shell part production, while the 5xxx group is applied in body structure parts.

The strain hardening effect of alloys in the 5xxx group is desirable in order to increase the material's strength, yet it also limits its formability and because of this, its fields of application. The limited formability affects the application of the alloy unfavorably and is the reason for applications of this material that are limited to structural body parts.

Previous research projects mainly covered recovery/recrystallization, grain growth and grain size following cold rolling in the manufacturing process of the blank material. As the degree of deformation of nearly 30 % appears during the manufacturing process, a comparison with deformations appearing in the sheet metal forming of aluminum is not useful. (Huda 2009), (Miller, et al. 2000), (Wen and Morris 2004)

The following chapter provides an overview concerning the physical basics and technologies used for test performance and evaluation.

2.1 Properties of Aluminum

Aluminum is the third most common element in the earth's crust following oxygen and silicon. Due to its strong affinity to react with non-metal elements, such as oxygen, aluminum does not exist in its pure form naturally. The chemical combinations used as a raw material for the production of aluminum are called bauxite and aluminum silicates. Bauxite is a decomposition product of lime and silicate stones. Aluminum silicates can be found in clay or black coal ash. (Ostermann 1998, 5)

Source

At 2.6989 kg dm^{-3}, the specific weight of aluminum is one third that of steel, aluminum can be classified as a light metal. This is the main reason for automotive industry to pursue the idea of lightweight construction and begin to change from using steel to aluminum. The strength of the material correlates with the modification of the involved elements in alloys and thermo-mechanical treatments involved. Aluminum is an outstanding conductor of heat and electricity

Periodic table
Properties

and is the most commonly used material in power transmission lines. (Krammer 2009, 81 ff.)

The production of aluminum is very cost-intensive, due to its high-energy consumption. The re-melting of the recycled metal requires only about 5 percent of the energy as compared to the extraction of aluminum in the primary production process. This makes aluminum very attractive and profitable as a recycling material.

2.2 Classification of Aluminum Alloys

Aluminum as a construction material is divided into cast alloys and wrought alloys. The focus of wrought alloys lies on plastic formability and cast alloys focus on castability. This work tries to increase degree of deformation and formability of aluminum sheet metal.
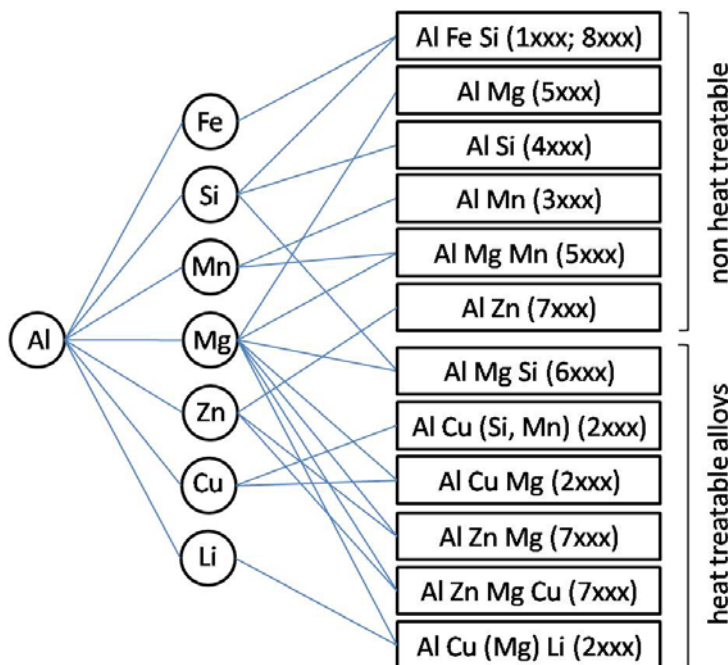

Figure 2-1:   Notation of wrought aluminum alloys (Krammer 2009, 413)

Different properties in regards to stress, strain, corrosion and strength of the material can be reached by different types, quantities and combinations of alloying elements and/or variations in thermo-mechanical processing. This leads to a further classification of wrought aluminum alloys into heat treatable and non-heat treatable alloys (Figure 2-1). Heat treatable alloys use the effect of age harden-ing to strengthen the material, whereas non-heat treatable alloys make use of the effects of solute hardening and cold work. Thermal processing can increase the mechanical properties of heat treatable alloys while non-heat treatable alloys lose their strength of material when tempered.(Krammer 2009, 143 ff)

Those alloys belonging to the 2xxx, 6xxx and 7xxx series are members of the group of heat treatable alloys and reach their final state properties through thermal treatments following deformation. The range of possible temper states is wide, as every change in temperature and/ or duration delivers a different microstructure and a wide variety of mechanical properties. The EN AW-6xxx series plays an important role in the field of lightweight vehicle construction. When used for body shell parts, the material receives its final mechanical properties during the bake hardening of the finish in the paintshop.(European Aluminium Association 2001-2010)

Heat treatable

The 1xxx, 3xxx, 4xxx and 5xxx series belong to the non-heat treatable alloys. The effects of hot and/or cold working mechanisms are used to define the mechanical properties of these alloys. Worthy of mention here are EN AW-3xxx and EN AW-5xxx, as they are the most important wrought aluminum alloys for the automobile industry.(European Aluminium Association 2001-2010)

Non-heat treatable

2.2.1 Non heat treatable Aluminum Alloys EN AA-5xxx

The mechanical properties of an alloy are defined by the mass fractures of different alloying elements and their cooperation among each other. In general, each major alloying element stands for a different attribute of the alloy.

Alloys of the EN AW-5xxx group are influenced by magnesium as their main alloying element. The addition of magnesium leads to solid solution hardening and strain hardening which results in a medium strength material. This is because of the big difference in the atomic radius of aluminum and magnesium. Normally, the magnesium percentage varies between 0.8 and 6 percent. Both tensile strength and yield strength increase with the addition of magnesium. In general, 5xxx series alloys show a higher strength than those of the 3xxx series, while their formability is comparable. With a magnesium level below 3 %, the material becomes susceptible for intergranular corrosion. On the other hand, the ultimate elongation decreases with a magnesium percentage above 3 %.

Magnesium

Compared to all other wrought aluminum alloys, those of the 5xxx series have a superior resistance to corrosion and outstanding properties for applications in seawater and marine atmospheres. Even at low temperatures, this material shows a high resistance to brittleness. Good formability, weldability (Mg > 2.7 %) and the excellent corrosion resistance predestine this material for building architecture (e.g. electro-colored facade panels), scaffolding and marine applications. The automotive industry uses aluminum of the 5xxx series for press-formed body structure parts and chassis components.

Depending on the magnesium percentage in the alloy, n (strain hardening coefficient) and Z (Poisson ratio) exhibit reciprocal properties. Both variables are vital for the prediction of the formability behavior. Alloys with a mass fraction of magnesium below 1 % display a high lateral contraction Z, from which a good deep drawing performance can be derived. As a result of this, alloys with a mass fraction of magnesium greater than 4 % show a high strain hardening coefficient n and a good performance in stretch forming.(Krammer 2009, 146)

Manganese

Alloys of the 5xxx series with added manganese tend to streak and strain mark formations on the material surface as a result of inhomogeneous forming. Stretcher strain marks lead to a higher friction coefficient and limited applications of the 5xxx series in chassis components. Stretcher strain marks are visible even after painting and tend to crater formation in the course of natural aging. This means for painted chassis components, the stretcher strain marks that are readily identifiable after the paint shop, tend to form unaesthetic porosities by natural aging. Due to this, the main areas of application for the 5xxx alloys in the automotive industry are press formed body structure parts.(Krammer 2009, 150)

Chromium

Another important alloying element is chromium. The main reason for the addition of chromium is the ability to control grain size and the formation of microstructure in aluminum-magnesium alloys. Chromium forms a finely dispersed phase, responsible for the anticipation of nucleation and grain growth. With a mass fraction of chromium below 0.35 %, the electrical resistivity increases. At levels above 0.35 %, chromium builds rough compounds with other impurities such as iron, titanium or manganese. The fibrous structure of chromium in the solid solution reduces the susceptibility of stress corrosion cracking and increases hardness and strength. The alliance of chromium and manganese is specific to aluminum-magnesium alloys to achieve a reduction of the susceptibility of inter-granular corrosion as stress corrosion cracking and exfoliation.(European Aluminium Association 2001-2010)

1.1.2 Heat-treatable Aluminum Alloys EN AA-6xxx

Heat-treatable

The presence of the alloying elements silicon and magnesium ranging between 0.3 and 1.5 percent enables a strengthening of the material through thermo-mechanical processing and enables precipitation hardening. Silicon improves the corrosion resistance and the fluidity of the melt. With a silicon level of more than 13 percent, the machinability is continuously reduced. In the group of age hardenable alloys, the 6xxx series have a lower strength than the 2xxx and 7xxx series alloys. Still, their formability and weldability are good.(European Aluminium Association 2001-2010)

Due to the combination of strength, formability, corrosion resistance and weldability, alloys of the 6xxx series are used in the automotive sector (outer body panels), on building suites (ladders, doors, windows), for marine applications (offshore structures), in the optical industry and in the food industry. Anodizing is possible and leads to an even better resistance to corrosion, a harder surface or a different surface color. The addition of low melting phase elements such as lead, bismuth and/or tin leads to a good machinability and a dedication in extrusions.(Krammer 2009, 151)

Two minor alloying elements of the 6xxx group are lead and bismuth. Lead improves machinability, has a low melting point and restricted solubility. In aluminum, lead forms a low-melting phase, benefits chip breaking and supports tool lubrication. Due to its toxicity, the amount of lead in alloys is restricted to a level of 0.4 percent by law. Bismuth has a similar influence on the alloy as lead, but it is primarily added to compensate the lead shrinkage during solidification by its own expansion. It is non-toxic and has no legal limitations.(European Aluminium Association 2001-2010)

2.3 Influence on Material Properties through Thermo-mechanical Processing

The properties of a material are not only affected through their alloying elements. They are also dependent upon the crystal structure and defects, as they can also be influenced by thermo-mechanical treatment. The following chapter provides an overview of crystal structure defects and the influence on material properties caused by thermo-mechanical processing.

2.3.1 Material Defects

All mechanical properties can be seen as a result of deviations from a perfect crystal lattice structure. The defects in the crystal lattice are classified into point defects, linear defects and planar defects. For aluminum, the most important microstructure faults are dislocations (two dimensional defects).

Point defects

Point defects are zero dimensional defects in the crystal lattice and can appear in two different types.

- Vacancy defects
- Interstitial defects

Vacancy defects are unoccupied positions in a crystal lattice. Other atoms can substitute these gaps. If an atom from the surrounding area moves into the vacancy, the vacancy defect moves in the opposite direction of the atom movement.(Hirth and Lothe 1991)

Interstitial defects are caused by atoms present in the crystal lattice in locations where usually there are no designated atomic placements. In this case, the interstitial defect is created by a foreign atom; the crystal is called substitution crystal.(Bargel, et al. 2008, 5)
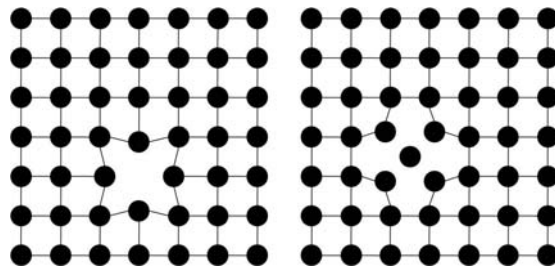
Figure 2-2:   Point defects; left: Vacancy defect; right: Interstitial defect; (Bargel, et al. 2008, 5)

Linear defects

"Dislocations are linear defects around which some of the atoms of the crystal lattice are misaligned."[1]

Dislocations can exist either as edge-dislocations (Figure 2-3) or screw-dislocations (Figure 2-4). Both lattice imperfections result in lattice strain. Usually, edge- and screw-dislocations do not occur alone; rather, they generally appear in combination. Dislocations can begin or end at the edge of the crystal, or form closed loops within the crystal. (Bargel, et al. 2008)
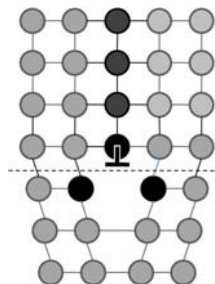
Figure 2-3:   Edge-dislocation (Röhr 2011)

---

[1](Hirth und Lothe 1991)
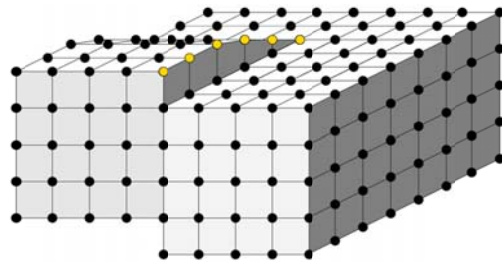
Figure 2-4:   Screw-dislocation (Röhr 2011)

A plastic deformation and work hardening of aluminum will only take place through the movement of dislocations. In aluminum, the formability behavior is influenced by the concentration of dislocations, their re-production, their mobility as well as their reaction among each other and with other lattice defects. With an increasing deformation, the number of dislocations will increase to the point where formation and erasure of dislocations return into balance. Figure 2-5 shows the action of work hardening in an aluminum Al-Si1MgMn-0 alloy.

Effects of dislocation movement
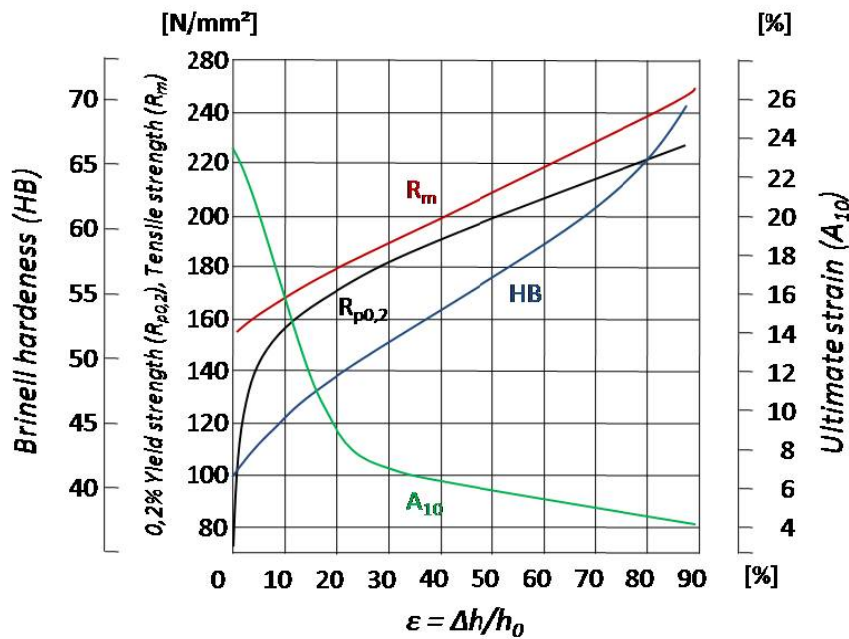
Figure 2-5:   Work hardening behaviour of AlSiMgMn-0
                (Ostermann 1998, 49)

Two-dimensional defects

Two-dimensional defects are variations in the ideal crystal over its entire surface. Two-dimensional defects are:

- Grain boundaries
- Sub-grain boundaries

A grain boundary splits areas of similar crystal structure but different orientation.

Grain boundary
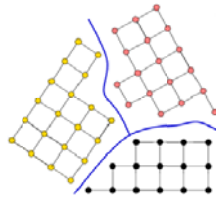
Figure 2-6:   Grain boundary (Röhr 2011)

In sub-grain boundaries, the deviation of orientation has to be equal to or less than 15 degrees. Sub-grain boundaries build rows of edge dislocations, interrupted by coherent lattice areas.

Sub-grain boundary
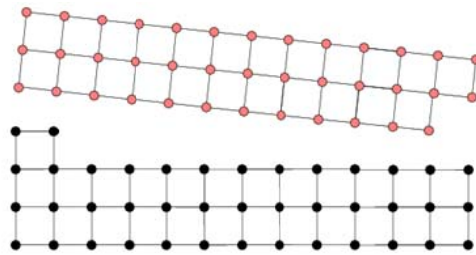
Figure 2-7:   Sub-grain boundaries (Röhr 2011)

2.4   Strengthening of Aluminum

Various types of hardening processes can be applied to improve the properties of aluminum and its alloys. Work hardening, solid solution hardening and precipitation hardening are used to strengthen the material.

2.4.1 Work Hardening

Work hardening, also known as strain hardening, is a direct result of ductile deformation. Plastic deformation produces and shifts dislocations through the crystal structure. With an increasing number of dislocations, they obstruct their own movement in the crystal lattice. The effect of work hardening is that the strength of the material increases, while its elongation drops.(Krammer 2009, 295 f)

Ductile deformation

2.4.2 Solid Solution Hardening

Solid solution hardening occurs through the placement of foreign atoms into the aluminum matrix. It must be distinguished between interstitial solid solution and substitution solid solution. Substitution solid solution takes place when a matrix lattice atom is replaced by a foreign atom. Conditions necessary for a replacement are a) a similar lattice structure and b) a difference in atomic radius less than or equal to 15 percent. Interstitial solid solution is caused by a transfer of foreign atoms to intermediate matrix lattice locations. Hydrogen, carbon, nitrogen and boron are the most important interstitial solid solution elements. Interstitial solid solution can work when the relation of matrix atom to foreign atom is not higher than 0.41. (Figure 2-8) (Bargel, et al. 2008, 34 ff)

Disturbance of the matrix
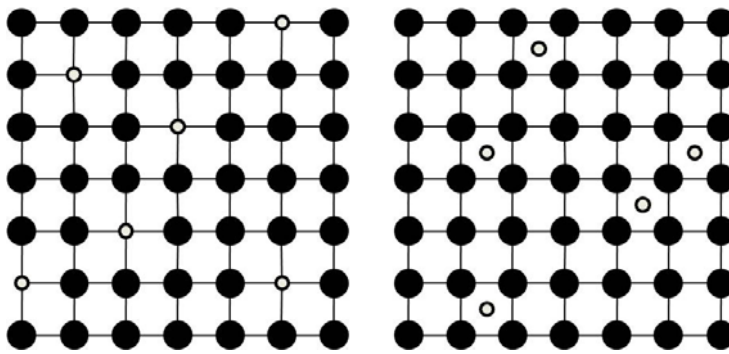
Figure 2-8:   Principle of solid solution hardening; left: Substitutional solid solution; right: Interstitial solid solution (Bargel, et al. 2008, 35)

The alloy atom deforms the matrix lattice and this induces lattice strain over the matrix deformation. Because of the difference in atomic radius of the alloying element, all of the surrounding aluminum atoms are forced slightly out of place. This deformation hinders the movement of dislocations, further resulting in stronger dislocation reactions within the crystal.(Ostermann 1998, 51 ff.)

2.4.3 Precipitation Hardening

In precipitation hardening, finely dispersed precipitates block the movement of dislocations along their gliding planes. During ductile deformation, the moving dislocations have to either separate or bypass the precipitates. Depending upon the size, type, amount and arrangement of the precipitates, as well as the degree of coherence between dispersion and aluminum matrix, the dislocation can move through or around the dispersion.
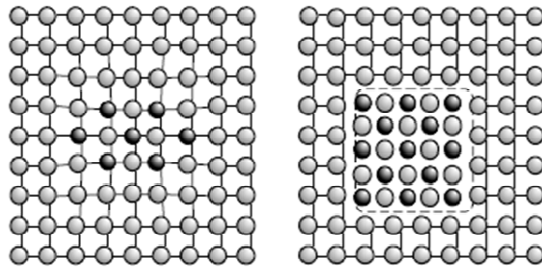
Block of dislocation movement

| Figure 2-9: | Precipitation hardening; left: Coherent dispersion; right: Incoherent dispersion (Bargel, et al. 2008, 53) |

(Figure 2-9) shows possible arrangements of the dispersions in the matrix lattice. The lattice parameters of coherent dispersions deviate marginally from those of the base matrix. Due to this, the grids can be merged without requiring large deformations of the matrix lattice. The phase interface is coherent. Nevertheless, the adaptation of the phase limit that is still required induces lattice strain in the matrix. Hardening through the use of coherent dispersions is very effective and comes as a result of the overlapping of intermediate compounds and the strain they induce in the matrix lattice. Semi-coherent dispersions achieve access to the matrix lattice through the formation of new dislocations around the phase interface. The matrix lattice also becomes denser, but the hardening effect is weaker than with coherent dispersions. Incoherent dispersions appear as submicroscopic corn boundaries in dislocations. A connection between dispersion lattice and matrix lattice is impossible, due to the big differences between the lattice structures.(Bargel, et al. 2008, 52 ff)

For a more detailed description of the formation of precipitates, a referral to specialized literature has to be made at this point. As an example, a detailed description of the various types of formation of precipitations can be found in (Ostermann 1998, 53 ff.).

2.4.4 Softening of Aluminum according to (Krammer 2009, 301 ff.)

Work hardened material can be softened through thermal treatments at high temperatures. The hardening as a result of deformation (2.4) can be partially or completely reversed. A total softening will take place if the thermal treatment is a recrystallization. To achieve this state, the temperature of the thermal treatment must lie above the recrystallization temperature. At temperatures below recrystallization temperature, only a partial softening can be reached. A thermal treatment below the recrystallization temperature is called recovery.

Recovery/ Recrystallization

The border between recrystallization and recovery is called the recrystallization barrier. The recrystallization barrier is primarily dependent upon temperature and time. Other influencing factors of the recrystallization barrier are the composure of alloying elements and further

Recrystallization barrier

contents of the material, heating rate and the microstructure of the initial state.

Recovery does not lead to any changes in the microstructure that are visible under a light microscope. Recovery takes place through a transposition of atoms and gaps in the material lattice. Another effect of recovery can be the formation of sub grain boundaries (2.3.1). The reduction of defects in the crystal structure of the material through recovery is insignificant. Recovery improves the arrangement of the defects and reduces the inner energy of the material due to this. The tensile strength is not essentially changed, ultimate elongation is also increased by recovery. (Figure 5-5) shows a typical softening curve of aluminum [Al99.5]. Section 1 describes the area of recovery. In section 2, recrystallization occurs; heat treatment in the area of section 3 will lead to coarse grain formation.

Recovery

Thermal treatment above the recrystallization barrier leads to a partial or total softening of the material, because of the recrystallization of the primary crystallization. Recrystallization usually begins by nucleation of crystal lattice areas most disturbed through cold work. New crystals grow to the point where they reach other, still growing crystals. The previous cold work, the temperature, as well as the duration of the thermal treatment, are the most important factors influencing the course of recrystallization and grain size of the recrystallized microstructure.

Recrystallization

The degree of deformation is one of the strongest influences to the recrystallization process. By increasing the degree of deformation, the tendency for recrystallization increases, and the recrystallization barrier also sinks to lower temperatures. Material that has a high degree of deformation has a large density of strongly tensed up areas, which have, compared to less deformed areas, a much higher amount of nucleation. Because of this, the recrystallized microstructure is much finer in strongly deformed areas than it is in less deformed sections. Figure 2-10 shows the influence of the degree of deformation on the grain size on pure aluminum (Al 99.99).
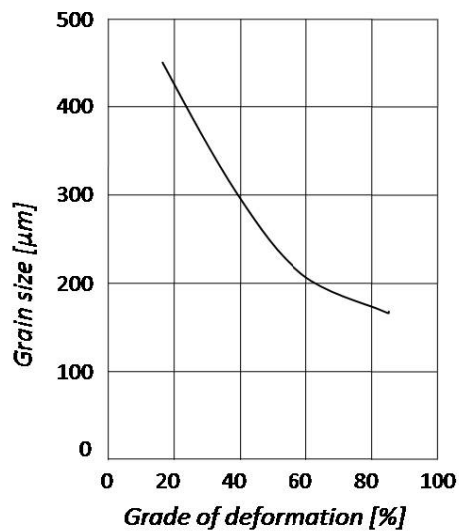
Degree of deformation

Figure 2-10: Grain size in relation to degree of deformation (Krammer 2009, 306)

Figure 2-11 shows a graphical representation of the influence of the degree of deformation on recrystallization and grain size. From left to right, the grain size decreases with the increase of the degree of deformation.
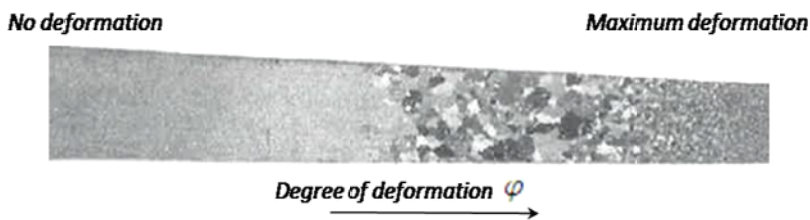

Figure 2-11: Key Tensile Bar (Krammer 2009, 307)

In order to predict the temperature region where recrystallization can take place, recrystallization diagrams are used. A recrystallization diagram shows the relation of the degree of deformation, annealing temperature and grain size.

Recrystallization diagram

13
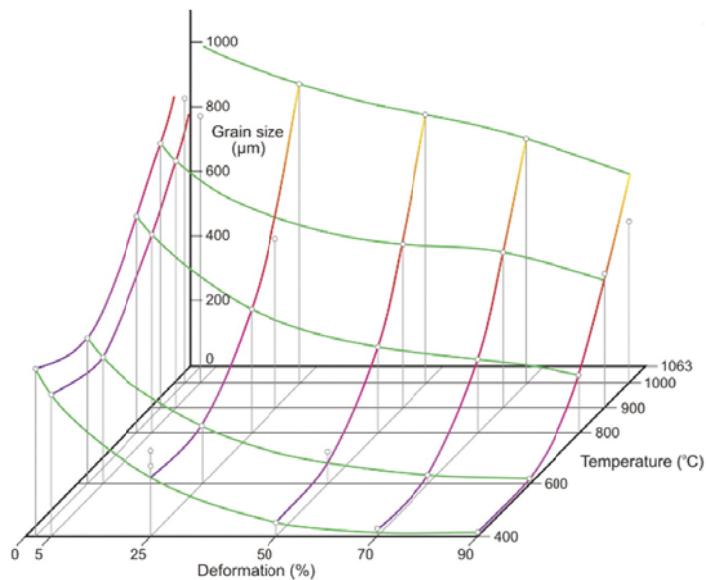
Figure 2-12: Recrystallization Diagram (GeoScienceWorld 2011)

Figure 2-13 shows the chronological steps of an aluminum micro-structure [Al 99.5] from a deformed initial state with stretched grains to a totally recrystallized microstructure.

Deformed microstructure [Al 99,5], natural strain 90%

First recrystallized grains [Al 99,5], natural strain 90%, 320°C, 1h

100% recrystallization [Al 99,5], natural strain 90%, 320°C, 10h
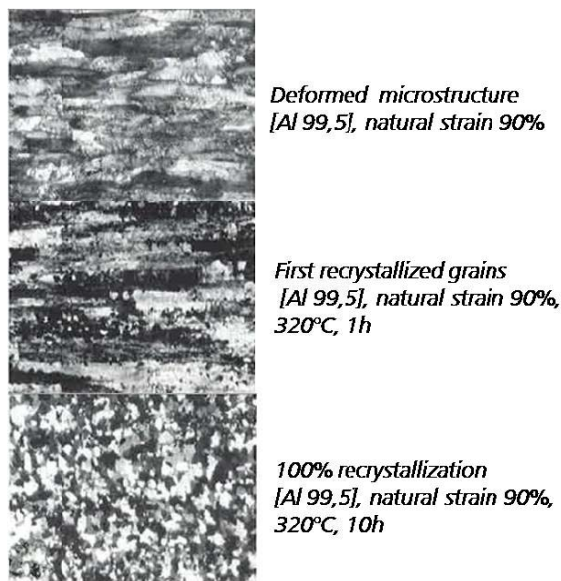
Figure 2-13: Microstructure comparison (Krammer 2009, 304)

2.5 Deep Drawing of Aluminum Sheet Metal

The process of deep drawing is limited by material properties and the force transmission in the deformation zone. During the deformation, the force flow moves from the punch over the part bottom into the flange where the actual deformation takes place. The limit of a deep

drawing process is reached when force transformation into the flange stops and lateral contraction begins.

Through the separation of a deep drawing process into multiple drawing steps, higher depths can be reached. Deformation of the first stage ends once a certain amount of tension has been reached in the transmission zone.

According to (Ostermann 1998, 360), load zones in the deep drawing procedure can be described as follows (Figure 2-14):

- The load introduction zone is the area under the front of the punch.
- The load transmission zone is the finished formed part area between bottom and draw die radius outlet
- The deformation zone contains the area between the outer edge of the flange and the draw die radius inlet.
- The bending zone is the area between draw die radius entry and outlet.
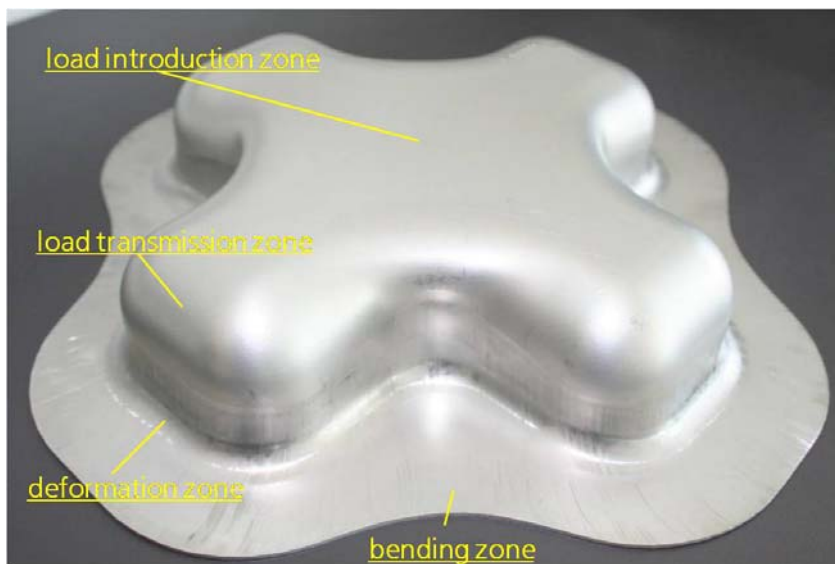
Figure 2-14:   Load Zones

2.5.1 Drawing Ratio

The drawing ratio β_{max} is the ratio of the biggest blank diameter (Formula 2-1) in relation to the die diameter that can be drawn without material failures such as the formation of cup base fractures.

$$\beta_0 = \frac{d_0}{d_{st}}$$

Formula 2-1:   Drawing ratio

β_{max} is reached when the highest occurring drawing force cannot be forwarded into the deformation zone any further. The cup base fracture force has reached its maximum once the first cracks appear in the outlet of the punch edge radius. Other influencing factors on the maximum drawing ratio are lubrication (3.5) as well as anisotropy (2.5.5). An increase of the friction coefficient μ leads to a decrease of the drawing ratio β_{max}. On the other hand, a higher strain hardening coefficient n leads to a higher maximum drawing ratio β_{max}.(Lange 1990, 325 f)

According to (Krammer 2009, 248) the maximum drawing ratio β_{max} of aluminum, tested under laboratory conditions, lies between 1.85 and 2.05. In comparison, the maximum drawing ratio of steel is between 1.9 and 2.2. These numerical values depend on blank thickness, tool geometry and lubrication and are not completely transferable to industrial situations.

2.5.2 Deep Drawing with Blank Holders

In the normal deep drawing procedure, a deformation of the flange is produced by tangential compression and radial tensile force. Through the use of a blank holder, an additional compression force F_N in normal direction to the flange is induced.
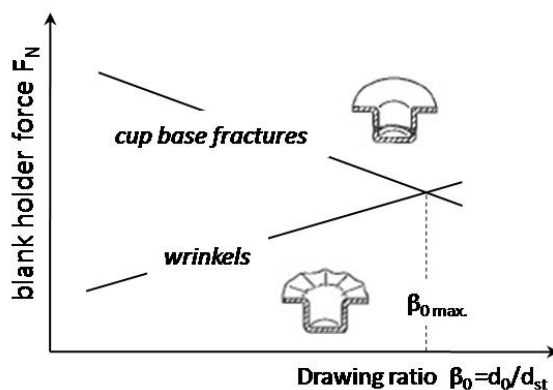
Figure 2-15:   Influence of blank holder force (Lange 1990, 325)

A correct level of blank holder force is important for the production of useable parts. Figure 2-15 shows the influence of the blank holder force on the drawing ratio. If the blank holder force F_N is too high, this leads to losses through friction, resulting in cup base fractures; an insufficient blank holder force F_N leads to wrinkling. Both types of failures are operational limitations to the drawing ratio. (Lange 1990, 325)

2.5.3 Evaluation of Deep Drawing

The evaluation of a deep drawing process can be done through measurement of strain and stress, thinning or other criteria, such as accuracy of shape or material defects.

For an evaluation through strain measurement and thinning, a defined dot matrix has to be applied to the unformed blank. The following optical forming analysis measures the deviation of the dots through deformation and compares it to a reference matrix.
The optical forming analysis is completed using the ARGUS system, a metrology system from GOM "Gesellschaft für Optische Messtechink" situated in Braunschweig, Germany.

ARGUS is a measuring solution to analyze the forming of sheet metal parts. Circular dots are electrochemically etched onto the original sheet metal (3.4). The regular spacing between the dots varies between 0.3 and 5 mm prior to the forming process. The dots applied to the blank surface follow the deformation during the forming process. The center of these dots can be seen as a reference for the determination of coordinates and a following deformation analysis. In the next step the deformed part is recorded with a digital camera from various view angles. Following a photogrammetric algorithm, the system determines the 3D coordinates of the deformed points and compares it to a previously defined dot matrix.(Friebe, Klein and Galanulis 2010)

Through the program's algorithm, a calculation of strain and stress, thinning and a validation of the forming process according to criteria of the Forming Limit Curve is possible.

2.5.4 Forming Limit Curve

The Forming Limit Curve shows the limits of sheet metal forming under different deformation conditions. The Forming Limit Diagram (FLD) is used to evaluate the properties of blanks after deformation through a defined dot matrix or a line network.

The development of a FLD is similar to its application (2.5.3). Information regarding the deformation of the dots alone does not provide any evidence when material failures such as lateral contractions or cracking will occur. Experiments under laboratory conditions with an equal material deliver the Forming Limit Curves (Nakazima test). The deformation analysis of the real part is compared with the FLC curve, developed under laboratory conditions and a conclusion to the resistance against material failures can be made. The simplification of this system lies in the fact that material failures produced by lateral contraction, or breakage are only defined through the planar state of stress. Because of this, the local deformation can be measured. The distortion of the points is equal to the local deformation of the blank. (Ostermann 1998, 338)

Figure 2-16 shows the principle of a forming limit diagram. Good parts are produced as long as the strain remains below the forming limit curve where lateral contraction occurs. The four dashed lines mark four natural strain ratios $\varphi_1 : \varphi_2$ with the ideal conditions of deformation.
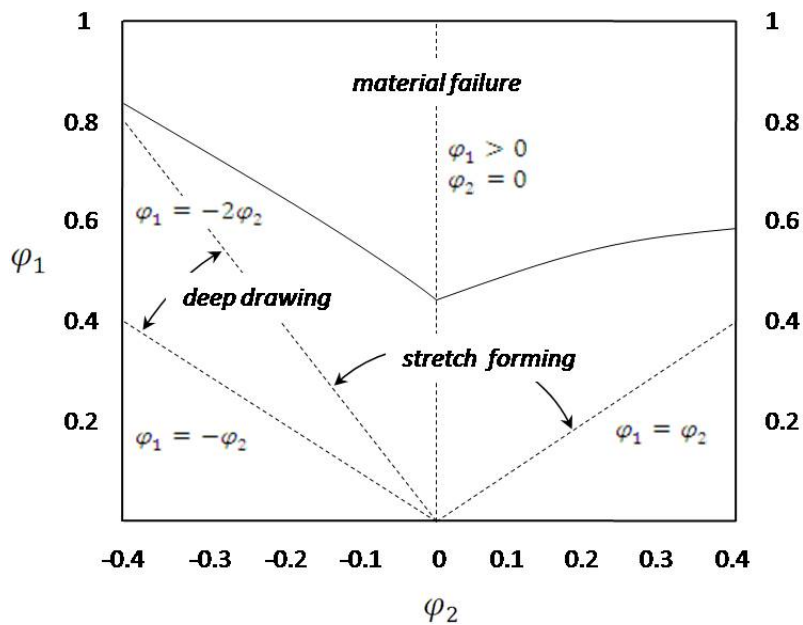

Figure 2-16:   Forming Limit Curve (Ostermann 1998, 340)

Biaxial stretch forming - the elongation in both major axes increases; the material is stretched in planar directions.

$$\varphi_1 = \varphi_2$$

Formula 2-2:   Biaxial stretch forming

Plane strain - one major axis is stretched, the second major axis stays in the initial state.

$$\varphi_1 > 0$$
$$\varphi_2 = 0$$

Formula 2-3:   Plane strain

Uniaxial tension - deep drawing in narrow sense, one major axis is stretched; the second major axis is compressed.

$$\varphi_1 = -2\varphi_2$$

Formula 2-4:   Uniaxial tension

Consistent stretch forming, pure deep drawing, one major axis is stretched; the second major axis is compressed.

$$\varphi_1 = -\varphi_2$$

Formula 2-5:   Consistent stretch forming

2.5.5 Anisotropy

An important factor for sheet metal forming is the anisotropy r. Anisotropy is a synonym for the directionality of sheet metal and is defined as the ratio of the logarithmical strain (grade of deformation) in length and width. An example for the influence of anisotropy on the deformation process is the earing of a radial blank during the drawing process.

Directionality of sheet metal

Anisotropy influences the maximum drawing ratio β_{max} possible in sheet metal forming, and the material flow in massive forming. Anisotropy itself originates in the crystal anisotropy combined with texture and microstructure anisotropy. The texture labels the orientation of all crystallites in a crystalline microstructure. For sheet metals, the texture is influenced by the rolling process. Other factors influencing anisotropy are grain size and how the different grain forms are arranged together.(Lange 2002, 80 f)

Influences on Anisotropy

The anisotropy r is not constant and can vary across the blank. Depending on the location of the sample relative to the rolling direction, anisotropy can have different values. In order to be able to estimate the chance of earing, anisotropy r is measured in three different directions (r_0, r_{45} and r_{90}). The index indicates the angle of the sample axis in relation to the rolling direction. Generally, r>1 indicates a greater resistance to an alternation in thickness than in width by the application of a tensile load. Blanks with anisotropy r<1 show a greater resistance against deformation in width. (Klocke und König 2006, 83)

Variation on Anisotropy

2.5.6 Strain hardening Coefficient

The strain hardening coefficient n is a measure for the maximum achievable deformation based on the drawing ratio β_{max}. Sheet metals with higher strain hardening coefficients achieve higher drawing ratios β_{max}. Through uniform elongation, the affinity of the material for lateral contraction during stretch forming is reduced by increasing the strain hardening coefficient n.

Maximum achievable deformation

3 Test description

The following chapter describes a double-staged deep drawing process with an intermediate heat treatment. As a material, aluminum EN AW-5182 with the material thickness of 1.2 mm is used. A heat treatment is utilized in order to reach recovery/recrystallization following the premier deformation. This thermal treatment should increase the formability of the blank material for the second drawing stage. Compared to a conventional deep drawing process (single draw, lack of a thermal treatment), an increased drawing depth is anticipated.

The test preparation began with an evaluation of the ideal blank geometry with respect to anisotropy and sheet metal thickness. Electrochemical surface etching followed the development of the blank geometry and a number of trial runs on the press were conducted. Further on, the influence of a lubricant, in combination with the blank holder force was tested and forming parameters such as blank holder force, punch velocity and the amount of lubrication to be used were defined.

After the maximum drawing depth was found, a series of x-shaped cross-parts with decreasing depth was produced. A stress and strain analysis according to the criteria of the forming limit curve for the used material followed and delivered the ideal drawing depth. The recrystallization and/or recovery process was done in a batch furnace by a defined temperature and various times.

Finally, a detailed analysis of microstructure diagrams of sections with high strains was done and a connection between recovery/recrystallization and total drawing depth established.

3.1 X – Shaped Cross Tool

Tool

The test runs were carried out using an x-shaped cross tool with a contour-adapted blank holder. The x-shaped cross tool is generally used to validate the formability of different grades of steel. With its complex contour and the alternation between convex and concave radii, it is a model for all complex states of stress which may occur in a real deep drawing process.

The main dimensions of the x-shaped cross tool can be taken from (Figure 3-1).
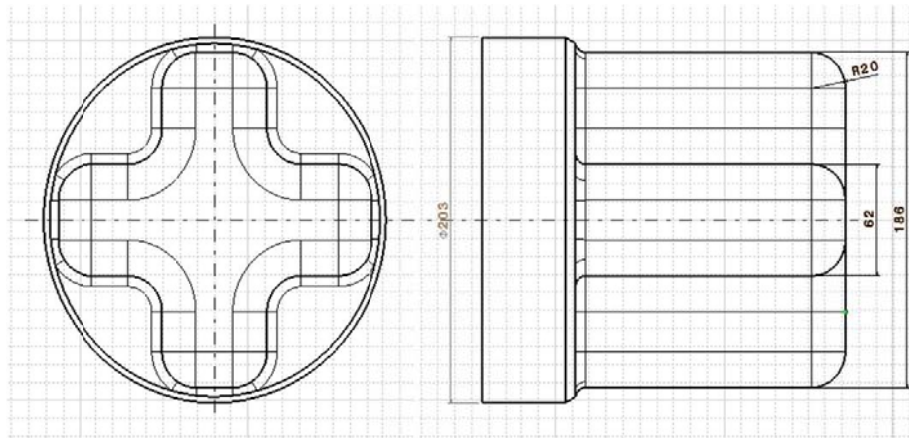
Figure 3-1:   X-shaped cross tool – Punch

The parts produced have two critical areas where highest strains can be found. These two critical areas are further mentioned as Section 1 and Section 2.

Figure 3-2:   Arrays with high strains

As displayed in (Figure 3-2) Section 1 marks the area of the punch-edge at the end of the bars (load transmission zone – deformation zone). Section 2 defines the area where the inner radius of the changeover between frame and flange lies (deformation zone – bending zone)(2.5).

3.2 Material

EN AW-5182 [Al Mg4,5Mn0,4] with a thickness of 1.2 mm from "NOVELIS" was used as a material for these tests. The mass fractions of the alloying elements can be found in (Table 3-1).

Element	Si	Fe	Cu	Mn	Mg	Cr	Zn	Ti
Mass fraction [%]	0,20	0,35	0,15	0,20 - 0,50	4,00 - 5,00	0,10	0,25	0,10

Table 3-1:   Alloying Elements of EN AW-5182

EN AW-5182 has been delivered in the temper state H111, which stands for insignificant strain-hardening, reached through annealing and an enclosed strain-hardening process such as stretch forming, for example.

Table 3-2 shows all mechanical properties and formability parameters of EN AW-5182.

Test direction	R_m	$R_{p0.2}$	A_{80}	A_u	n	r
	Mpa	Mpa	%	%	2 - 20 %	2 - 20 %
longitudinal	272	130	24,60	21,30	0,330	0,85
diagonal	268	129	25,30	24,50	0,330	0,77
transverse	267	128	26,00	23,30	0,331	0,78

Table 3-2:   Mechanical Properties and Formability Parameters
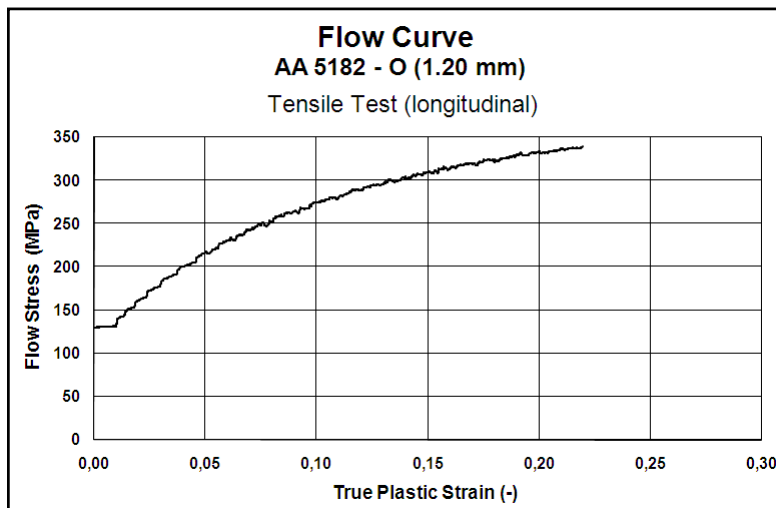
Figure 3-3:   Flow Curve EN AW-5182
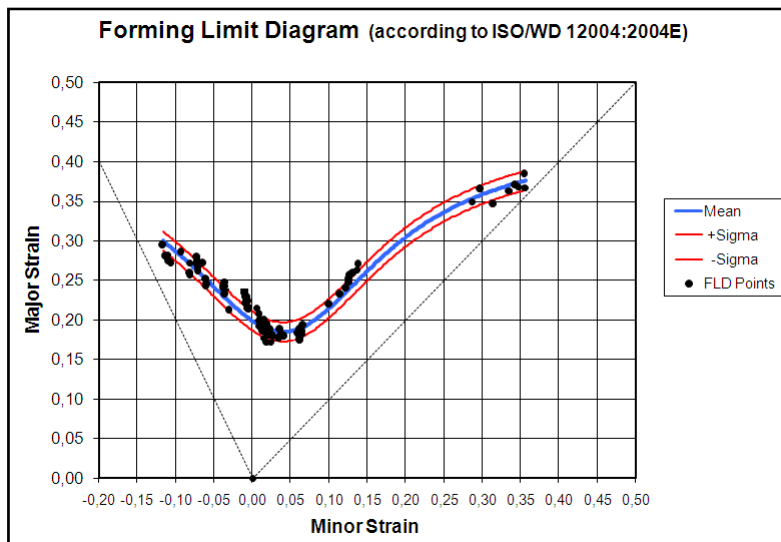
Figure 3-4: Forming Limit Diagram EN AW-5182

All mechanical properties and formability parameters, as well as the flow curve and forming limit diagram have been provided by "NOVELIS".

3.3 Process Limit Estimation and Simulative Blank Geometry Development

The blank geometry was developed with special consideration to factors like the anisotropy of the material, the size and form of the drawn part. First steps were completed by simulation in order to be able to estimate process limits and to predetermine the influence of the above mentioned factors. Trial runs with hand cut blanks alternated with further simulations concerning the size and form of the blank. A blank geometry that could easily be drawn, independent of its placement in the tool and its anisotropy was determined.

Blank geometry

The simulations were done using AutoForm, a simulation software covering the fields of part design, purchasing and planning, process layout and die design, as well as process design and optimization. The description of the yield curve followed the "BARLAT" model and the element formulation was done as an elastic plastic shell. The Forming Limit Curve and the hardening curve were implemented with the values provided by NOVELIS.

AutoForm simulation

Due to the fact that Auto Form R 1.1 XP32 is not able to demonstrate a two-step deep drawing process with an intermediate heat treatment, the simulation was simplified so that the first and second step both begin with the same material parameters. Additionally, the second step was modeled with the actual thinning at the end of the first step; the strain levels were reset for the second drawing stage.

Simplifications in AutoForm

23

The first deep drawing stage was limited to a depth of 20mm according to the forming limit curve criteria of EN AA-5182. The concept to remain within the limits of major strain, minor strain and thinning, in order to provide enough material for the second drawing stage was followed. Thinning should remain below a maximum of 20 percent. According to (Figure 3-5), the maximum thinning was predicted on the inner radii of the cross part. Maximum thinning is 15 %.
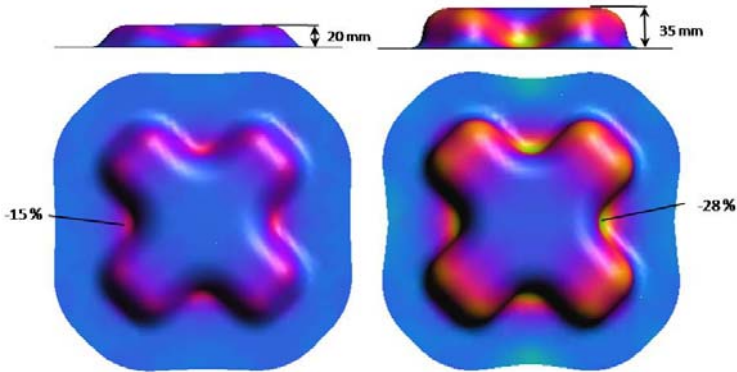
Figure 3-5:   Thinning AutoForm; right: 1st stage; h=20mm
              left: 2nd stage; h=35mm

According to FLC criteria's, the 2nd drawing stage of the AutoForm simulation was limited to a total depth of 35mm. Maximum thinning of the second stage occurred on the inner radius of the cross part and was 28 % (Figure 3-6).
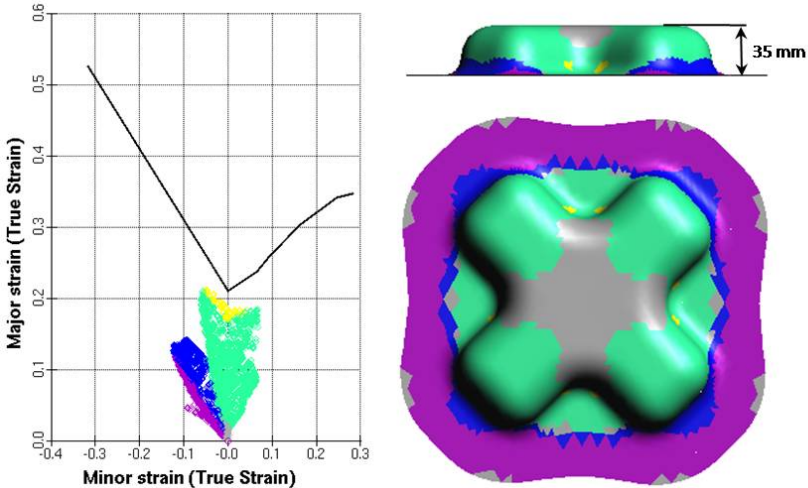
Figure 3-6:   Forming Limit Diagram AutoForm; 2nd stage;
              h=35mm

Lubrication has been considered with the value of $\mu=0.1$. For comparison, AutoForm proposes $\mu=0.15$ as a standard value for steel applications.

The material EN AA-5182 has similar characteristics for longitudinal r_0, diagonal r_{45} and transversal r_{90} anisotropy. Anisotropy values for EN AA-5182 can be found in (Table 3-3).

r_0	0,85
r_{45}	0,77
r_{90}	0,78
r_m	0,793
Δ_r	0,045

Table 3-3:   Anisotropy values of EN AA-5182

The final form of the blank can be seen in (Figure 3-7).
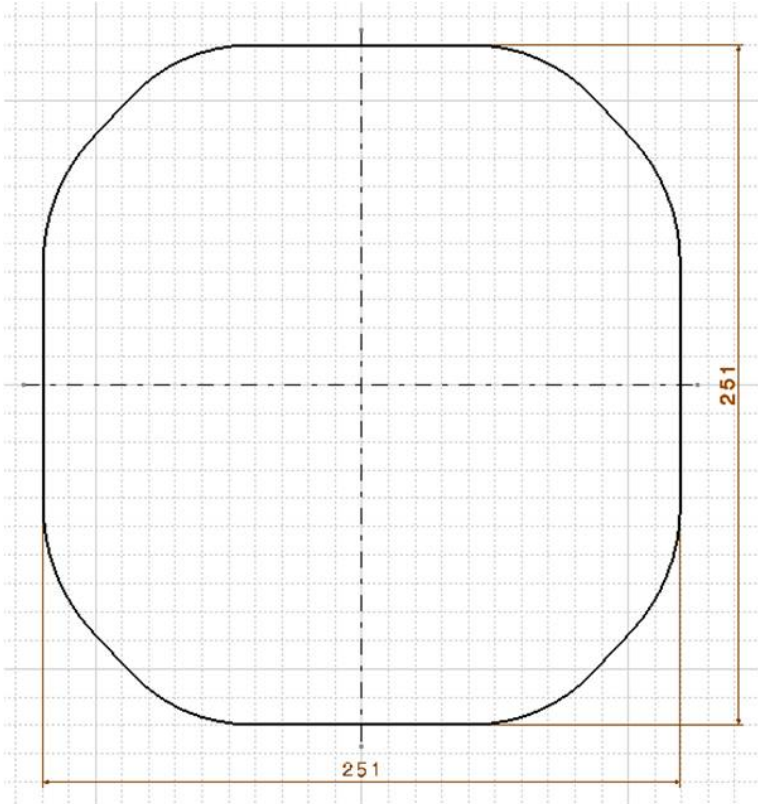
Figure 3-7:   Blank geometry

3.4 Electrochemical Etching

After the ideal blank geometry and the theoretical process limits were found, real test preparation started with electrochemical etching.

Electrochemical surface etching is necessary to enable stress and strain measurement after deformation. The principle is to transfer a copy of a defined dot matrix on the surface of the blank and measure deviations in dot distance and initial shape after deformation as compared to the unformed matrix. Dot diameter and distance are constant over the whole matrix. Depending on the strain, the etched dots change their form and position during blank deformation. (Figure 3-8) shows an etched dot matrix example on an un-deformed and a deformed blank.

Etching of a defined dot matrix on the blank surface
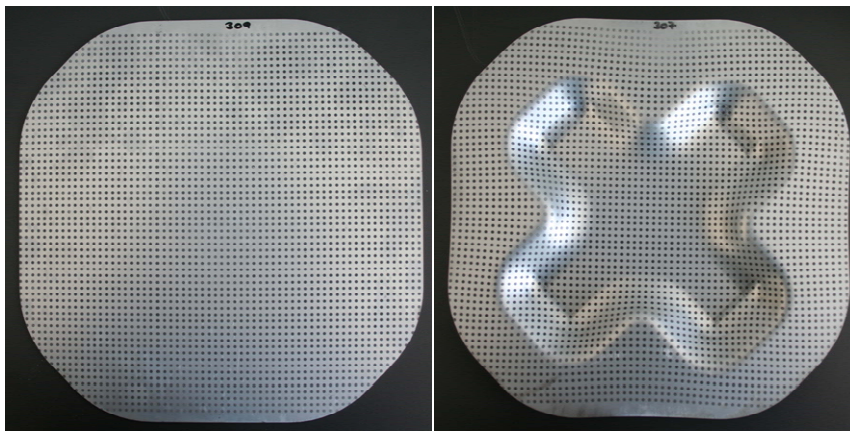
Figure 3-8:   Dot matrix

Through the combination of current, electrolyte and an electric conductive base material, in this case aluminum, the matrix is etched onto the blank surface. Base material, current flow and residence time all influence the etching process in a way that the color, black or white, and also the depth of the etched marks can be modified by changing parameters without the danger of corrosion or other negative effects on the material. Depending on the depth of the points and the blank material, the friction coefficient might increase.

Current, electrolyte and electric conductive base material

The etching unit 300/500 Classic from ÖSTLING, a company specialized on electro-marking systems was used as a marking system. The marking system can diversify the type of current (AC of DC) and as well as the amount of applied voltage. The electrolyte 8090, also from ÖSTLING, was used as conductive element. 8090 is a specialized electrolyte for non-ferrous metal. The material safe data sheet can be found in the appendix.

Marking system

Step by step, the following paragraphs will explain a chronological sequence of work steps to producing a consistent, wear and heat resistant dot matrix on the material EN AA-5182.

The first step is to degrease the blank with a standard degreaser. To prevent any chemical reactions of the combination electrolyte, degreaser residue and possible generation of heat due to current flow, the degreased blanks should be neutralized with warm water.

Next, the membrane with the dot matrix has to be placed on the dried blank. If the membrane is totally dry and/ or used the first time, the blank should be moisturized with electrolyte prior to the placement of the membrane. The adhesion of the membrane to the blank should be kept free from wrinkles, air inclusions and the slipping during the first set of movements with the marking-head. It is important that all wrinkles or air inclusions are eliminated prior to applying the voltage. Once the etching process has started, a shifting or sliding of membrane and blank against each other render the applied dot matrix useless for a following strain and stress measurement. Neither the distance of the points nor the circular form of them could be guaranteed in this case. The strain and stress measurement would already begin with a deviation which would make it impossible to depict a realistic process.

A combination of AC and DC currents showed the best results for the etching process. With respect to heat generation and the capacity overload of the device, lower flow levels of AC and DC have been chosen than suggested by ÖSTLING. For AC current, the recommendation was 8 V, for DC it was 12 V. First tests showed that the application of the two recommended voltages heat up both blank material and electrolyte in a way that bubble formation occurs between blank and membrane. Through the heated up blank material, the electrolyte evaporates under the membrane and starts the formation of blowholes under the membrane. The movement of the marking head and the indicated offset of these bubbles may result in a shifting or sliding of the membrane against the blank. Besides this, it is harmful for health to inhale evaporated electrolyte. After finishing off the first tests, 8V can be suggested for etching with DC and 7V can be suggest for etching with AC.

The application of the two types of current followed a chronological sequence. AC etching is shallow, not very wear resistant and only heat resistant with limitations. Instead, it produces points with high contrast that are easy to illustrate by measuring systems. DC etching goes into the depth of material, is limited wear resistant and heat resistant. Due to the depth of the points the friction coefficient increases. A temporal sequence of DC and AC applications is important since DC etches pits into the material where the following AC application is responsible for the contrast of these pits. This combination of DC and AC application produces a wear and heat resistant dot matrix with a high contrast and enables a stress and strain measurement after several drawing stages and different temper times. The total etching time for DC and AC application amounts 8 minutes for a blank surface of $0.057m^2$.

3.5 The Influence of Lubrication and Blank holder Force

Aside from the deformation characteristic of the material, the tribological relationships in the contact zone between blank surface and tool surface are fundamental for the limits of this deformation process. Friction between the different contact zones influences the material flow inside the tool. Management of the deformation process through controlled friction is possible. The tribological system consists of blank surface, tool surface and lubricant. The lubricant avoids abrasion on both blank- and tool- surface. For aluminum, the lubricant is also needed to prevent adhesion of the material to the tool. Aluminum is susceptible to flaking. Usually, the flakes are generated during the trim operation of the blanks and can be waste material or parts of a protruding flash. Due to the applied pressure, the flakes are cold welded on the tool surface. Depending on the adhesion forces, material can be removed from the tool by a further punch movement. (Ostermann 1998, 342)

Tribology

According to (Lange 1990, 327), the influence of friction increases with increasing part sizes due to the reason that the ratio between surface to volume increases. The best deep drawing results should be reached if the friction under the blank holder is as large as possible and friction in the area of the punch radius as small as possible.

Due to these facts, the influence of lubrication played an important role in the test results. The original plan followed the approach to complete the deformation without the addition of a lubricant. First trial runs without lubrication showed immense distinctions concerning depth and contour accuracy. As the addition of a lubricant increased the drawing depth of the same applications, it degraded contour accuracy and necessitated a variation of the blank holder force.

DU 700 P of RhenusLub GmbH & Co KG was used as a lubricant. This oil is used specifically for the drawing of bars, profiles and tubes in non-ferrous metal. The manufacturer recommends DU 700 P does not have to be removed prior to annealing and leaves no residues or burns following heat treatment. The product has a viscosity of $700 mm^2 \cdot s^{-1}$ at 40°C.

DU 700 P

The lubricant application was intended to represent a repeatable process, close to series. Because of this, the lubricant was only applied to both sides of the blank. A constant lubricant application over the tool surface was impossible due to the tool geometry. The oil volume was measured by a commercial injection syringe used in healthcare. The amount of oil applied to the blank surface was measured in drops. One drop has an average weight of 0.1g. This procedure delivered a repeatable process. A further simplification for the achievement of a repeatable process was that lubrication on the tool can be seen as constant following an average breaking-in lot size of 5 blanks.

Constant application of lubricant

In order to determine the amount of oil necessary for use in the forming process, the oil volume began with 5 drops per blank side and increased up to 15 drops. After a few trials, an average amount of 8 drops per blank side was determined for blanks with unmarked surfaces and 12 drops per blank side for blanks with an electrochemical surface etching for strain and stress measurements. The increase from 8 to 12 drops for blanks with an electrochemical etched dot matrix is a result of the changed surface conditions and the higher friction involved. With an average drop weight of 0.1 g per drop and a blank surface of 0.057m^2, 28.1 g·m^{-2} of lubricant were applied to the blanks in the initial state and 42.1 g·m^{-2} on etched blanks. In the 1st and 2nd drawing stages, the same amount of lubrication was applied. The only difference was that a constant spreading of lubricant over the part's surface was more difficult in the second stage due to the contour of the part compared to the flat blank in the first stage.

With the variation of the amount of oil in the process, the maximum drawing depth varied as well. A correlation of the applied oil amount to the drawing depth can be assumed. An increase of drawing oil does indeed increase the drawing depth, but decreases the contour accuracy in a way that the material does not follow the punch contour at the inner radius (Figure 3-9) of the cross die any more. As a general standard, in order to validate the contour accuracy of the formed cross parts, it could not be confirmed that all interpretations regarding contour accuracy are primarily subjective. The practical results showed that, for an average drawing depth up to 25mm, the blank was able to copy the contour of the punch in all areas. This is equal to with the AutoForm simulation results.
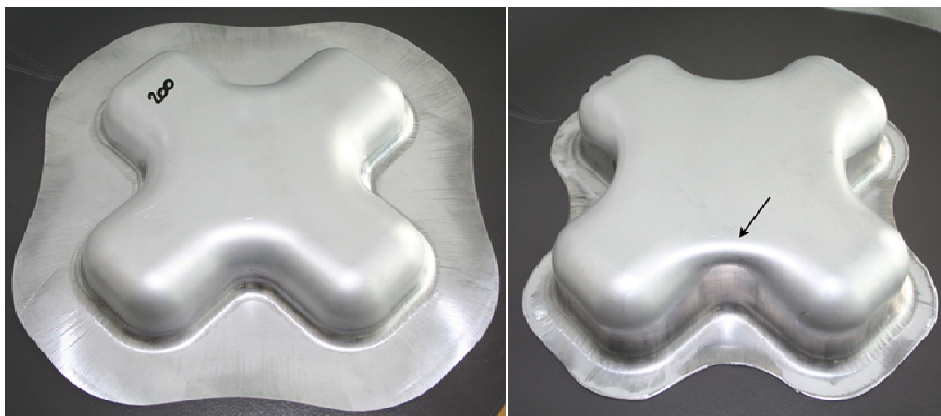
Figure 3-9:   Accuracy of shape; right: h=20mm; left: h=40mm

The maximum drawing depth in the first stage was limited to 26mm without lubrication. The addition of a lubricant increased the drawing depth at the expense of contour accuracy. A further increase of lubrication up to 15 g per blank side indeed delivered an increased drawing depth (up to 40 mm), yet the contour accuracy as a quantitative criterion was no longer fulfilled. To incorporate the positive

effects of lubrication but still achieve an adequate contour accuracy, a variation of the blank holder force was necessary. As the forming process began with a blank holder pressure of 5,5 MPa, it was increased with additional oil amounts involved in the process, and was a measure necessary because of the loss of contour accuracy, particularly when bulging at the bottom of the cross part in the area of the inner radius became apparent. The final parameters for the blank holder pressure following the trials were 11MPa.

3.6   Forming Parameters

The definition of forming parameters can be seen as one of the most important steps prior to the actual deformation process. The previous search for an optimum amount of lubricant, blank holder force, contour accuracy and drawing depth showed that restrictions were necessary to contain the required effort within reasonable bounds. By changing a single input variable, all other variables in the process are influenced and might change their behavior to each other. Because of this, the variation of forming parameters had to be limited to desirable yet reasonable values. (Table 3-4) shows a list of all defined forming parameters and their values.

Stroke force	1000 kN
Drawing speed	10 mm·s^{-1}
Blank holder pressure	11 Mpa
Lubrication	25,2 g·m²

Table 3-4:   Forming Parameters

3.7   Determination of Deformation Limitations

The determination of deformation limitations was done by the estimation of the maximum drawing depth and an enclosed stress and strain analysis.

In the first step, the maximum drawing depth was determined. From here, the drawing depth was successively increased until a material failure took place. The first signs of necking were observed at a depth of 28 mm in the vicinity of the punch's edge radius in Section 1 (Figure 3-10).

Maximum drawing depth
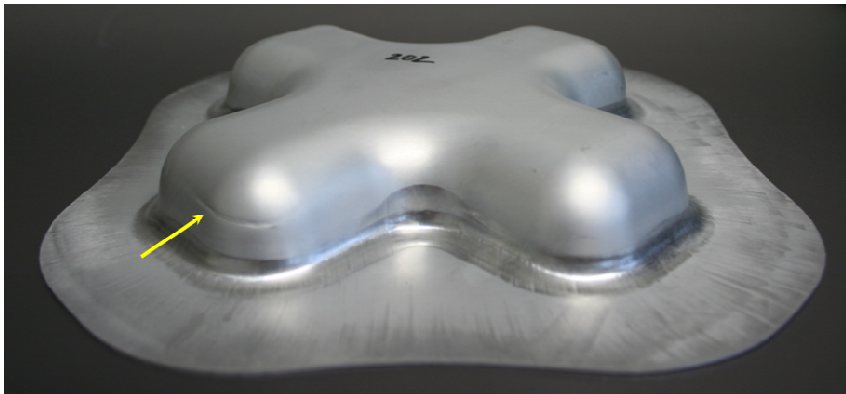
Figure 3-10: Material failure; 1st stage; h=28 mm

Next, blanks with an etched dot matrix were deformed to various drawing depths, in order to find the optimum drawing depth according to the FLD criteria. The analysis was carried out with ARGUS (2.5.3). To remain within the criteria of FLD, the optimum drawing depth of EN AA-5182 is 18 mm, in combination with the x-shaped cross tool and using the predetermined forming parameters (3.6.). In contrast, the AutoForm simulation predicted the optimum drawing depth at 20 mm.

ARGUS measurement
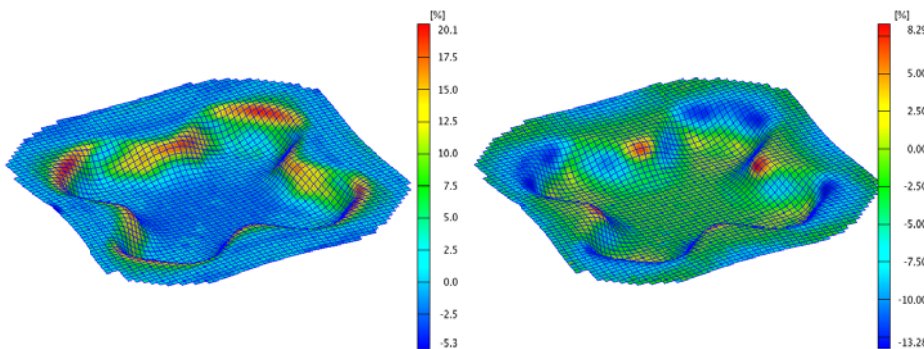
Figure 3-11: Right: Major Strain; left: Minor Strain
1st stage; h=18 mm
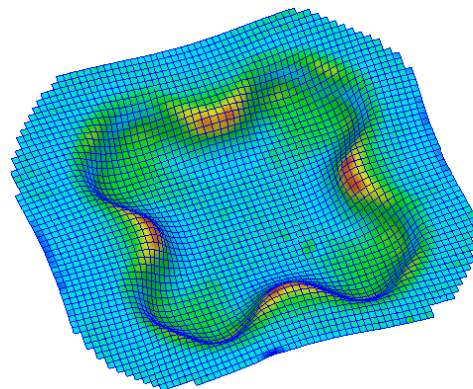
Figure 3-12: Critical areas according to FLD; 1st stage; h=18mm

31
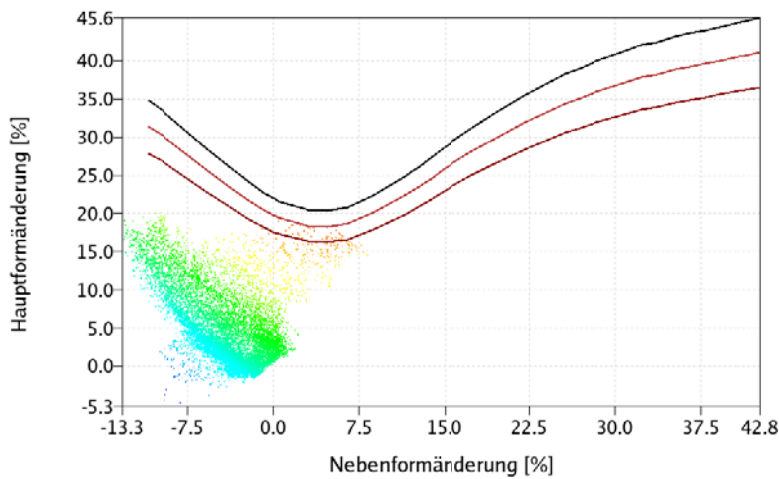
Figure 3-13:   Forming Limit Diagramm AW EN-5182; 1st stage;
                h=18mm

According to 2.5.4, the detailed analysis of the deformed part showed that in Section 1, deformation primarily occurred in the area of deep drawing. In Section 2 the deformation occurred in the area of stretch forming, here the highest thinning and minor strain took place (Figure 3-11, Figure 3-12, and Figure 3-13).

FLD application
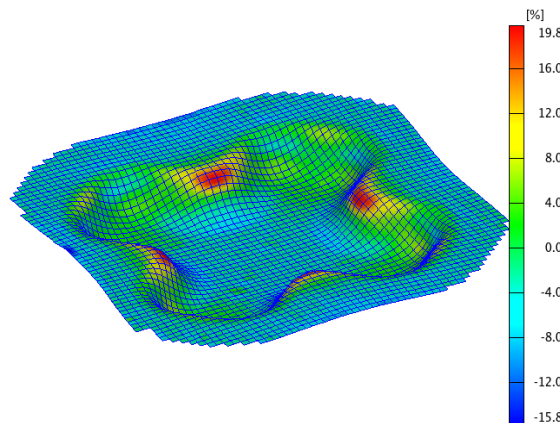
Figure 3-14:   Thinning; 1st stage; h=18 mm

The highest degree of thinning (Figure 3-14) was found in Section 2 at 19.8 %, resulting in a minimum material thickness of 0.96mm.

Further experiments have been carried out with parts at a drawing depth of 18 mm, as this was the depth where produced parts stayed within the FLD criteria.

3.8   Recovery and Recrystallization

The heat treatment aimed to reach recovery and/or recrystallization of the deformed microstructure. The recrystallization diagram shows

the recrystallization temperature and time depending on the degree of deformation. For EN AA-5182, a recrystallization diagram could not be found in various literature or be provided by the manufacturer. Instead of a recrystallization diagram, the temperature area of a possible recovery/ recrystallization was found.

According to (Ostermann 2007, 60), the recrystallization temperature of wrought aluminum alloys lies between 300°C and 400°C, depending on the degree of deformation, material composition and duration of heat treatment. Ostermann only provides information regarding the temperature region in which recovery / recrystallization may take place, more detailed information about the relationship between degree of deformation, temper temperature and holding time is not included in his work.

The chamber oven at the Institute of Tools and Forming was used for completion of the heat treatment. For the thermal treatment, a temperature level of 350°C was chosen. The temperature difference from top to bottom in this oven at an adjusted temperature of 350°C is 30°C. Due to the reason that the temperature measurement inside the chamber takes place at the top of the chamber, the temperature at the bottom only reaches 320°C.

The process followed the assumption that the deformed blanks are exposed to a heat treatment for various periods of time at constant temperatures. The heat treatment itself can be divided into heating time and holding time. The holding time separated all heat treated parts into five groups. The proposal was to hold the deformed parts 5 min, 15 min, 30 min, 60 min and 120 min at a constant temperature. The cooling of the parts took place at ambient air temperature without any further control. Each group consisted of 13 samples, with one part of each group being used for a temperature measurement with a thermocouple. Another sample of each group was used for a stress and strain analysis following the second drawing stage. Figure 3-15 shows the temperature gradients of group 1 with a holding time of 5 min and an average heating time of 20 min. The temperature gradients for group 2 (15 min), group 3 (30min), group 4 (60min) and group 5 (120 min) can be found in the appendix.
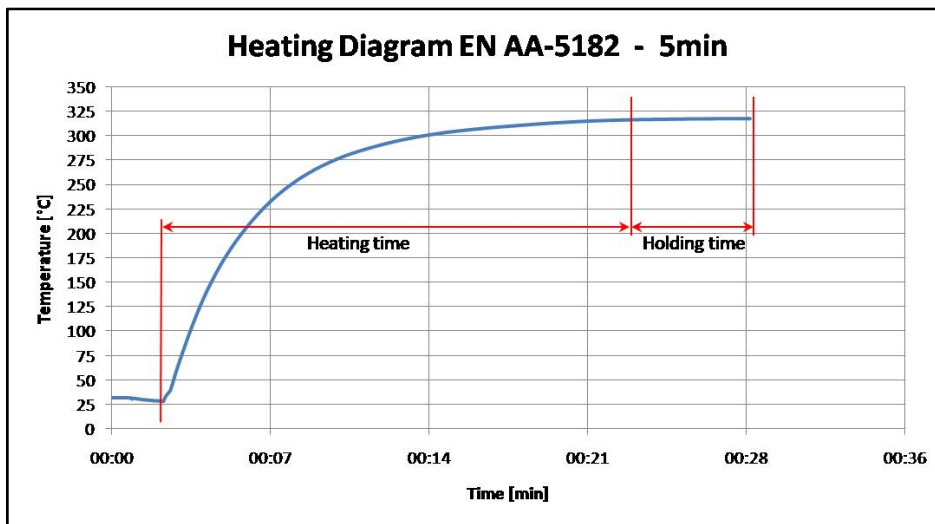
Figure 3-15:   Heating Diagram Group 1

3.9   2nd Drawing Stage

In the second drawing stage, the pre-formed and heat treated parts were formed further to the point where material failures occurred. The approach was to find the maximum drawing depth and reduce it until no lateral contraction (optical validation) could found. Usually the depth at which adequate parts were produced, according to criteria of being optically error-free, were only one or two millimeters below the maximum drawing depth.

For all holding times, the drawing depth of the 2nd stage was 32 mm. Presumably, the holding time and the differentiation between recovery and recrystallisation had no influence on the formability behavior of the material in the 2nd drawing stage.

4   Metallography

The metallography was completed in order to evaluate effects of the thermal treatment. Since there was no recrystallisation diagram available for EN AW-5182, the recrystallisation temperature at a defined degree of deformation was unclear. Because of this, a microstructure analysis was necessary to evaluate the deformation in the 2nd stage in relation to heat treatment and microstructure.

Evaluation of thermal treatment

For the structural analysis, 2 defined sections of the cross parts have been cut out. (Figure 4-1) shows the planes in which the microstructure analyze was done. The degree of deformation was most important for the selection of the material samples. According to (Ostermann 1998, 60), the number of nuclei increases with an increase of the degree of deformation. The result of this was that the cutting samples were selected from the two sections with the highest deformation in the finished part.

Arrays of microstructure analyzation
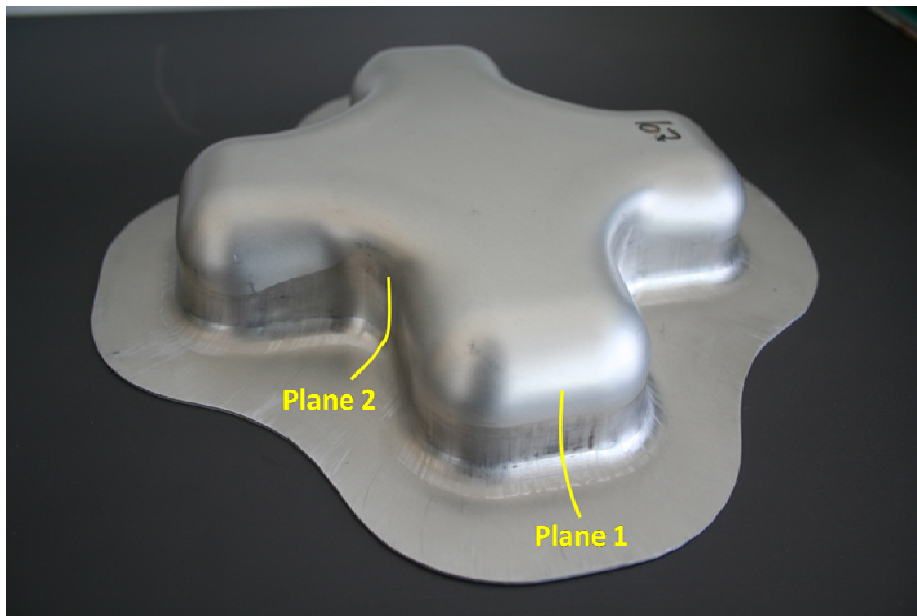
Figure 4-1:   Planes of microstructure analysis

After the samples were cut out of the deformed cross parts, they were embedded in synthetic resin at the Institute of Tools and Forming. Further sample preparation was completed at the Institute of Material Science and Welding. A process of grinding and polishing with various sand-and polishing-disks with different additives was used for sample preparation. (Table 4-1) shows the chronological sequence of all work steps of the sample preparation. Due to the different sample conditions, concerning the quality of the embedding, the duration of each step cannot be specified at this point exactly. Usually, it varied between two and five minutes and had to be repeated if proper results were not achieved in the first attempt.

Sample preparation

	GRAIN SIZE	*ADDITIVE*
GRIND	500	Water
	1200	Water
	2400	Water
	4000	Water
POLISH	3 μm	Water
	1 μm	Water
	< 1 μm	OP-S Suspension
ETCH	100 ml destilled water	
	4 ml hydrogen fluorid	
	acid temperature 150° C	
	residence time 60 sec.	

Table 4-1:   Chronological sequence of sample preperation

After the final polishing step, the samples were cleaned under running water. The formed surface was covered with alcohol and dried by a commercial hair dryer. The etching process was also completed using dehydration with alcohol and a commercial hair dryer. According to the Institute of Material Science and Welding, this was necessary in order to prevent the samples from building up moisture, which could cause unpleasant effects during inspection under the light microscope.

4.1   Microstructure

The pictures of the material microstructure were taken by a light microscope at the Institute of Material Science and Welding. A focus of 2.5 mm was used, allowing for a differentiation between grain boundaries.

In the following, the microstructure diagrams of all different temper states, as well the initial microstructure, are discussed. In all of the groups, the grain size of the recrystallized microstructure is bigger than that of the initial microstructure. The dispersed microstructure of the initial state is a result of the high degree of deformation during the milling process and the enclosed thermal treatment.

Microstructure diagrams

Even if the deviation of the degree of deformation between Sections 1 and 2 is only marginal, it shows differences in the recrystallization progress. If necessary, Section 1 and Section 2 are explained separately. (Table 4-2) gives an overview of different temper groups.

Group	Section	Holding time [min]	Recrystallization	Note
Group 1	S 1	0	no	
	S 2		no	
Group 2	S 1	5	no	neutral phase
	S 2		yes	neutral phase
Group 3	S 1	15	yes	neutral phase
	S 2		yes	neutral phase
Group 4	S 1	30	yes	neutral phase
	S 2		yes	neutral phase
Group 5	S 1	60	yes	
	S 2		yes	
Group 6	S 1	120	yes	
	S 2		yes	

Table 4-2:   Temper Groups

Group 1 – initial state, deformed

Group 1 can be viewed as the reference for all other states. The parts of Group 1 have been drawn in a single step to the point of material failure. No thermal treatment was applied. The microstructure of this sample is very similar to that of the initial state microstructure. The grains are elongated and deformed and show no variation between Sections 1 and 2.

Group 1

(Figure 4-2) shows a stretched and deformed initial state microstructure. The white band in the middle of the cross section is presumably the neutral phase, where the grains in this area have the lowest or no deformation at all. Samples of Group 1 reached a drawing depth of 27 mm in a single draw.
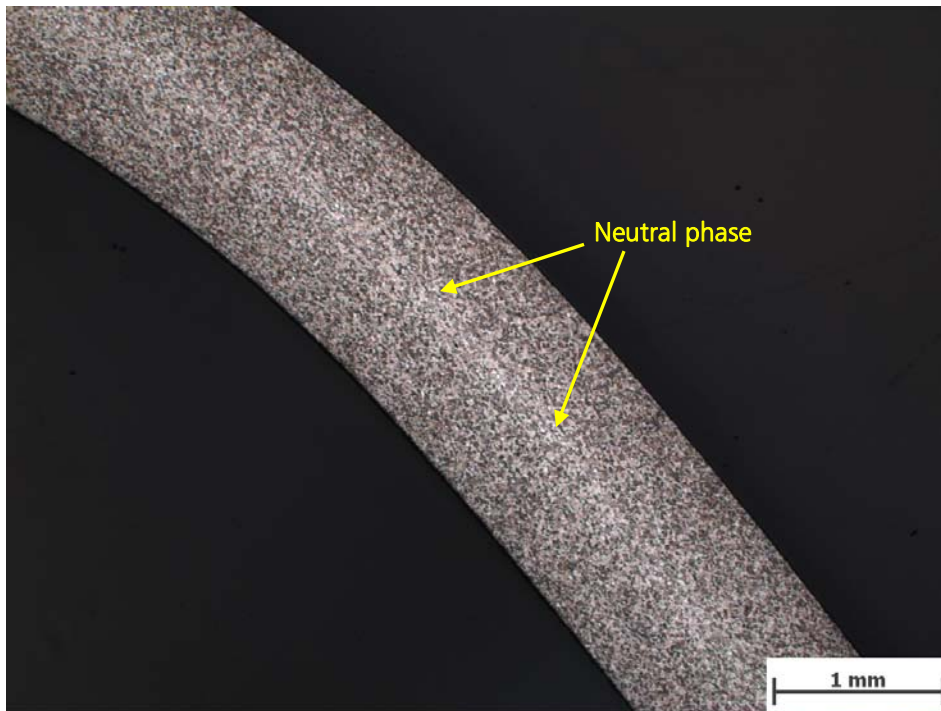
Figure 4-2:   Recrystallization Diagram Group 1 – 1311w064

Group 2 – 5 minutes

Group 2

For the parts produced in this group, the holding time for recovery/ recrystallization was 5 minutes. In (Figure 4-3), the beginning of recrystallization can be seen. Due to the short holding time, recrystallization occurred only in areas of strong deformation and a high concentration of nuclei. In Group 5, this took place at the material border. The holding time of 5 minutes at a temperature of 320°C is too short to reach recrystallization throughout the entire cross section.

Recrystallization
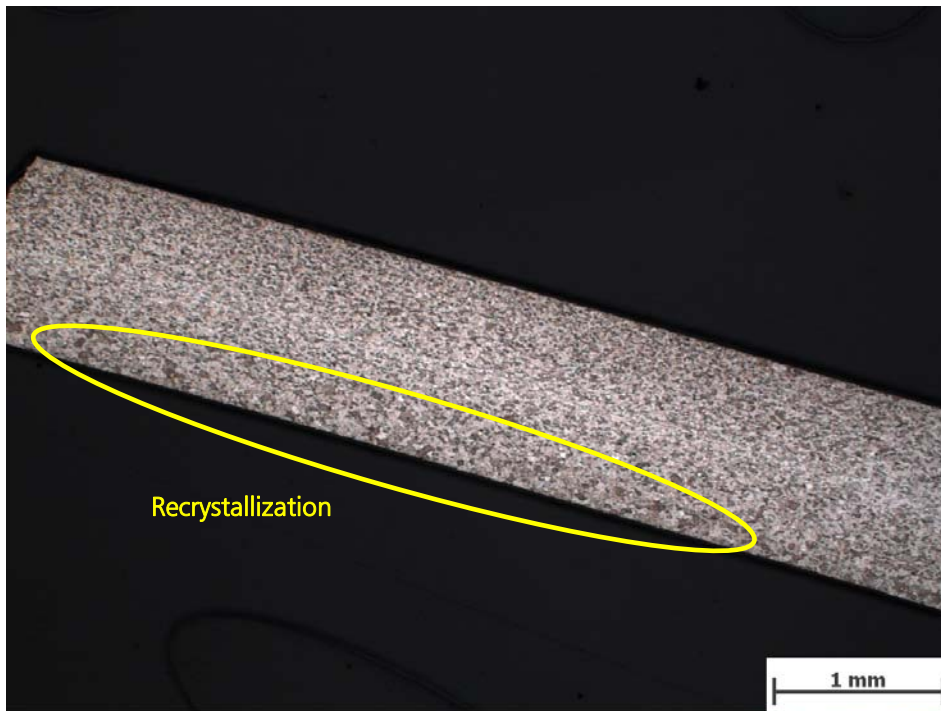
Figure 4-3:   Recrystallization Diagram Group 2 – 1311w049

Group 3 – 15 minutes

Group 3 was held on temperature for 15 minutes. In Section 1 *Group 3*
(Figure 4-4 and Figure 4-5), the recrystallization originated at the
outer radius, where the highest natural strain was present. A neutral
phase in the middle of the material can be interpreted, where the
grains were neither stretched nor compressed. At 15 minutes hold-
ing time, recrystallization ended at the beginning of the neutral
phase. On the inner radius, recrystallization is partially visible.
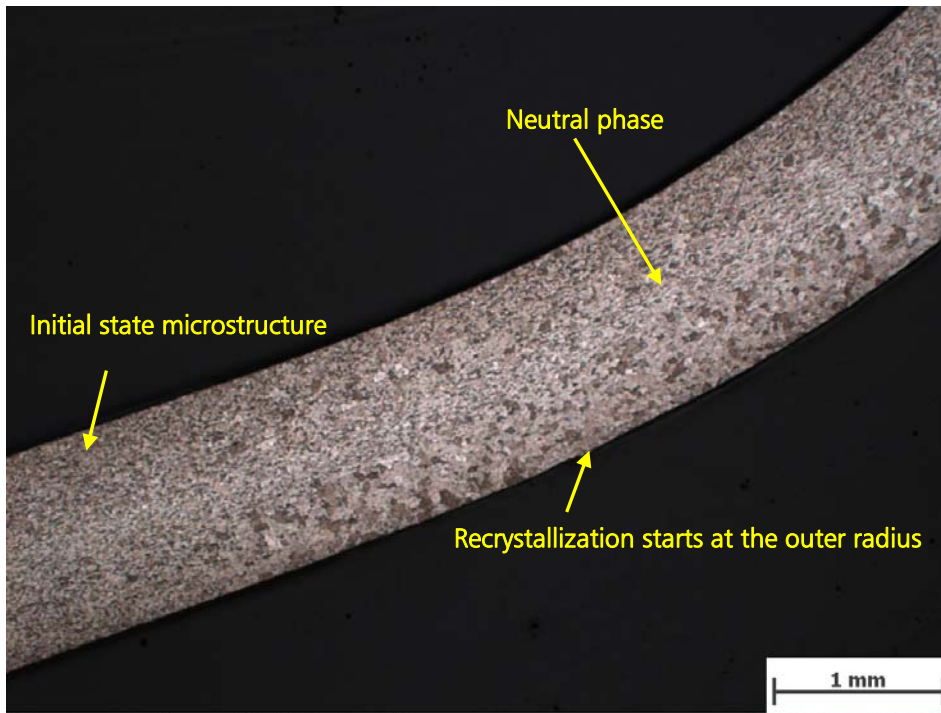
Figure 4-4:   Recrystallization Diagram Group 3 – 1311w038

Figure 4-5:   Recrystallization Diagram Group 3 – 1311w039

Section 2 has a higher degree of deformation and a higher number of nuclei and inner energy. Due to this, a continuous neutral phase is not determinable. The grain size varies from larger to smaller grains in the center of the radius. Conspicuously, the recrystallization appears to travel from the outer radius to the inner one where no re-

crystallization took place on the border of the inner radius (Figure 4-6, Figure 4-8 and Figure 4-7).
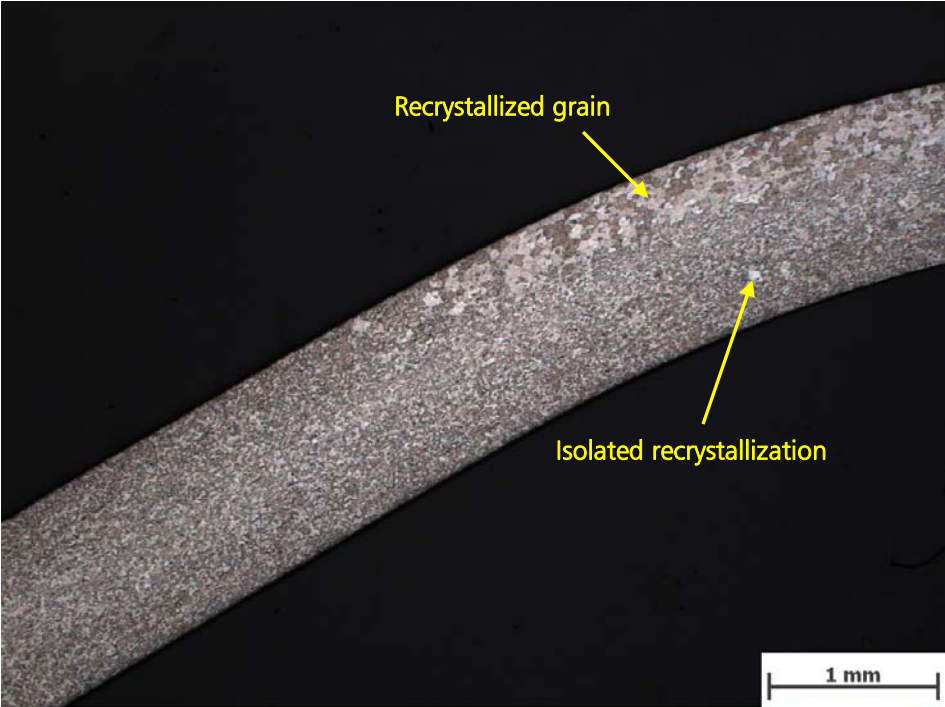
Figure 4-6:   Recrystallization Diagram Group 3 – 1311w041

Figure 4-7:   Recrystallization Diagram Group 3 – 1311w043
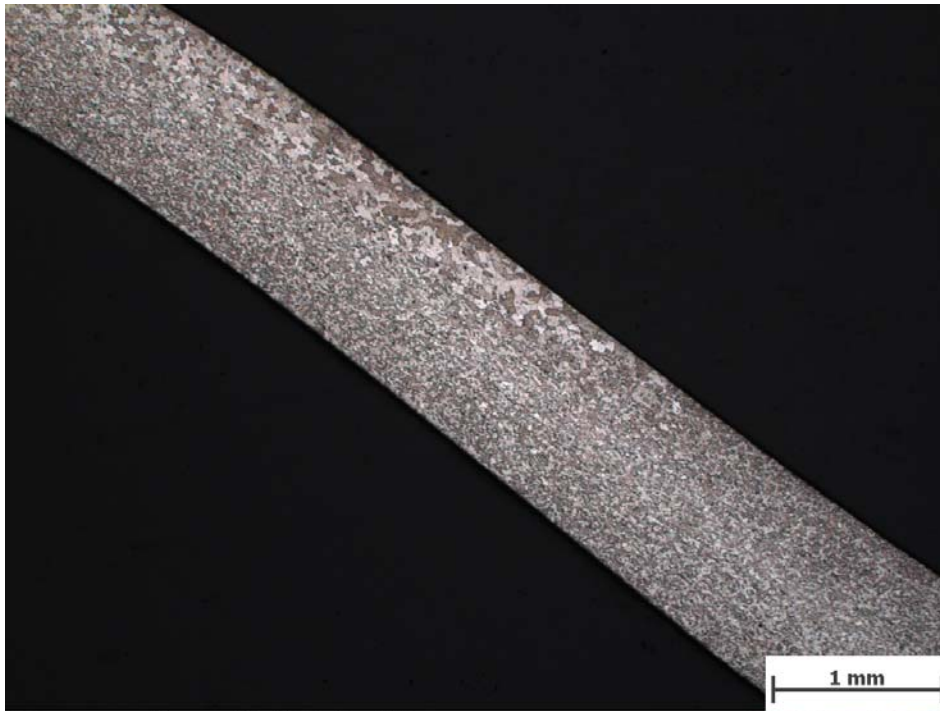
Figure 4-8:   Recrystallization Diagram Group 3 – 1311w044

Group 4 – 30 minutes

Group 4

Group 4 had a holding time of 30 minutes. A higher degree of recrystallization than in groups 2 and 3 can be expected. In Section 1, a discontinued neutral phase can be interpreted. Recrystallization again begins at the outer radius; an isolated recrystallization can be found at the inner radius as well. (Figure 4-9 and Figure 4-10)
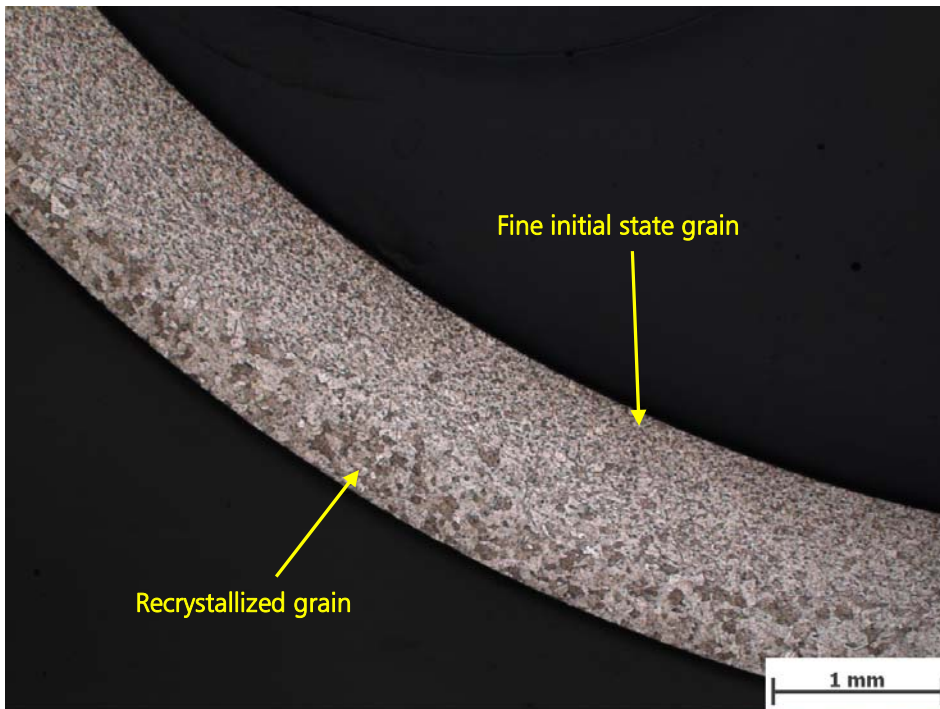
Figure 4-9: Recrystallization Diagram Group 4 – 1311w057

Figure 4-10: Recrystallization Diagram Group 4 – 1311w058

In Section 2, recrystallization occurred for the first time over the entire cross section. Recrystallization began at the outer radius of the cross section, which had the highest degree of deformation. According to the higher number of nuclei in the area of the outer radius, a

finer recrystallized microstructure was found than in all other areas (Figure 4-11 and Figure 4-12).
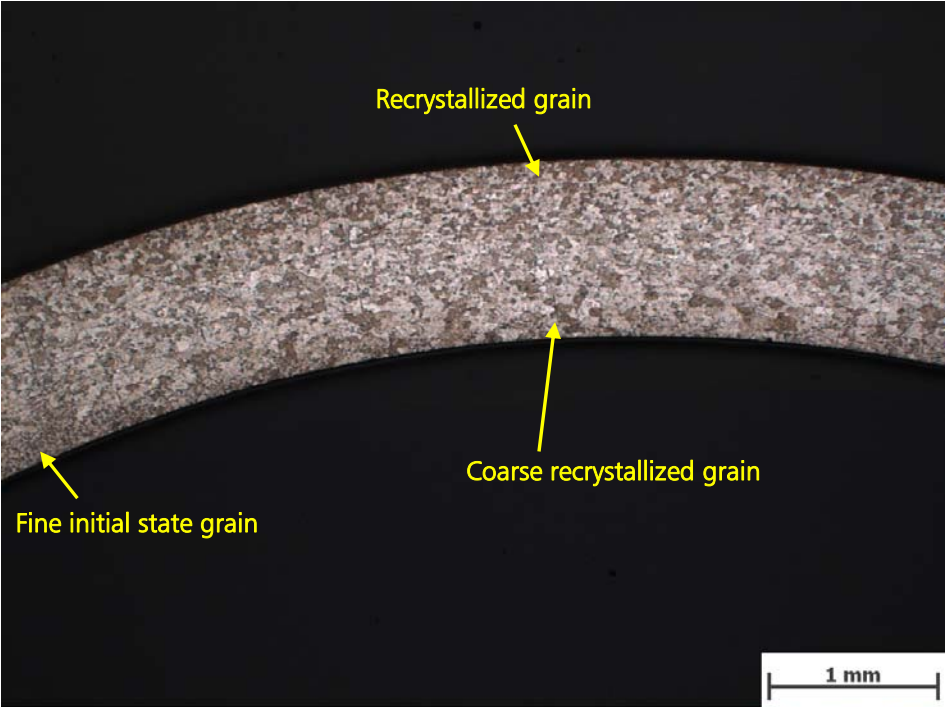
Figure 4-11:   Recrystallization Diagram Group 4 – 1311w074

Figure 4-12:   Recrystallization Diagram Group 4 – 1311w075

Group 5 – 60 minutes

For Group 5, the holding time for recovery/ recrystallization was set at 60 minutes. Section 1 still shows an interrupted neutral phase through partial recrystallization. According to the number of nuclei and the duration of holding time, (Figure 4-13) and (Figure 4-14) display both a larger grain size at the entry of the radius, compared to the size of the grains in the rest in the radius.
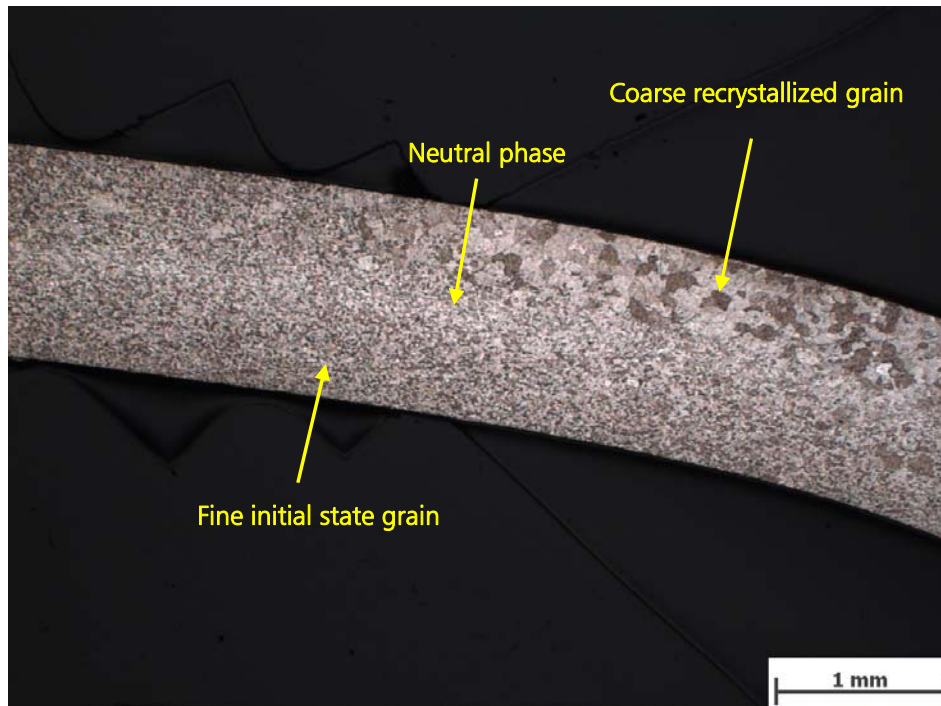
Figure 4-13:   Recrystallization Diagram Group 5 – 1311w052
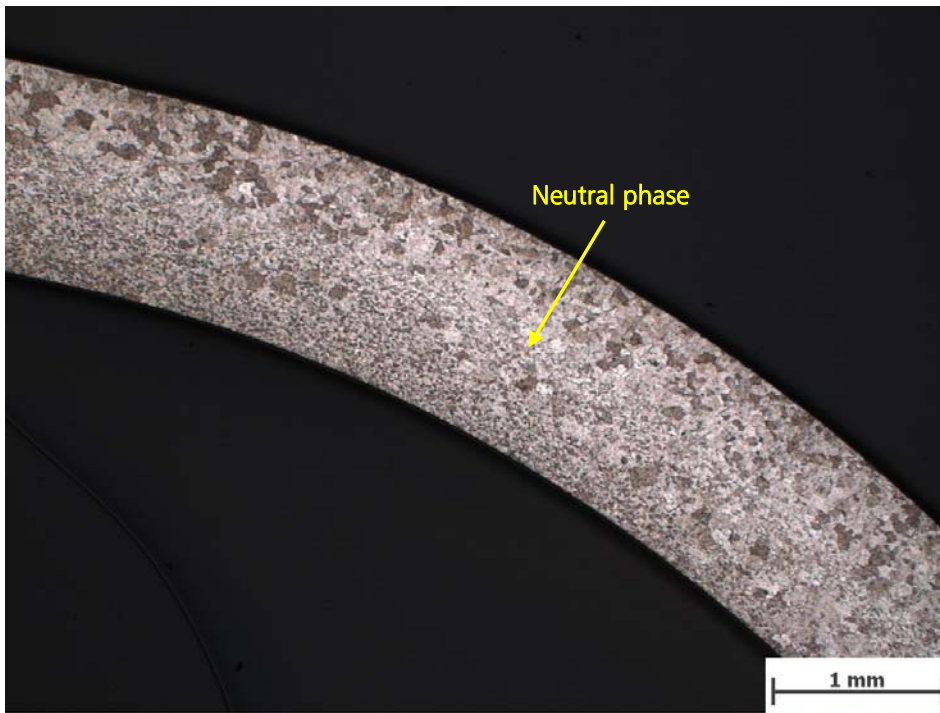
Figure 4-14:   Recrystallization Diagram Group 5 – 1311w053
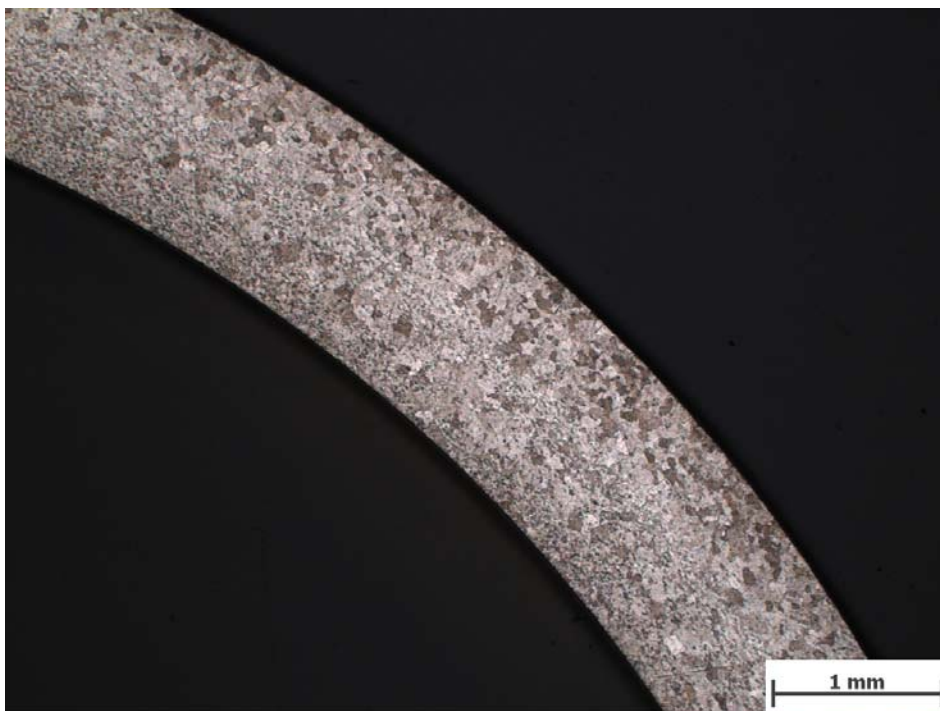
Figure 4-15:   Recrystallization Diagram Group 5 – 1311w054

In (Figure 4-16) and (Figure 4-18) of Section 2, the beginning of re-crystallization on the outer radius is visible. In (Figure 4-18), the re-mains of a neutral phase can be seen as a light, fine-grained band in the middle of the cross section. (Figure 4-17) shows recrystallization

over the whole cross section with a finely recrystallized microstructure on the outer to a coarser one on the inner radius.
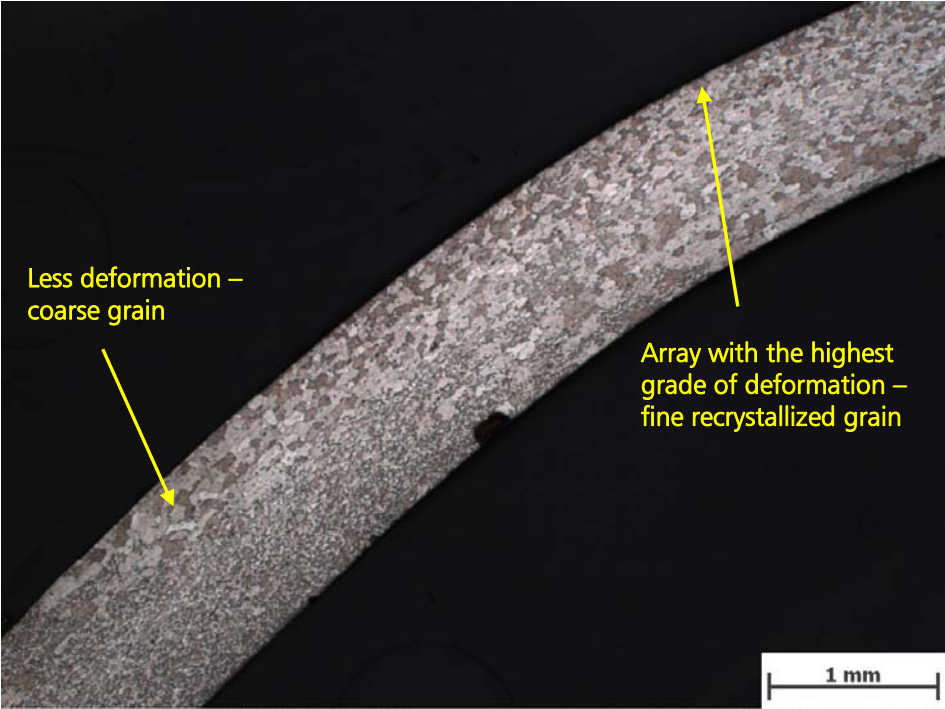
Figure 4-16:   Recrystallization Diagram Group 5 – 1311w025
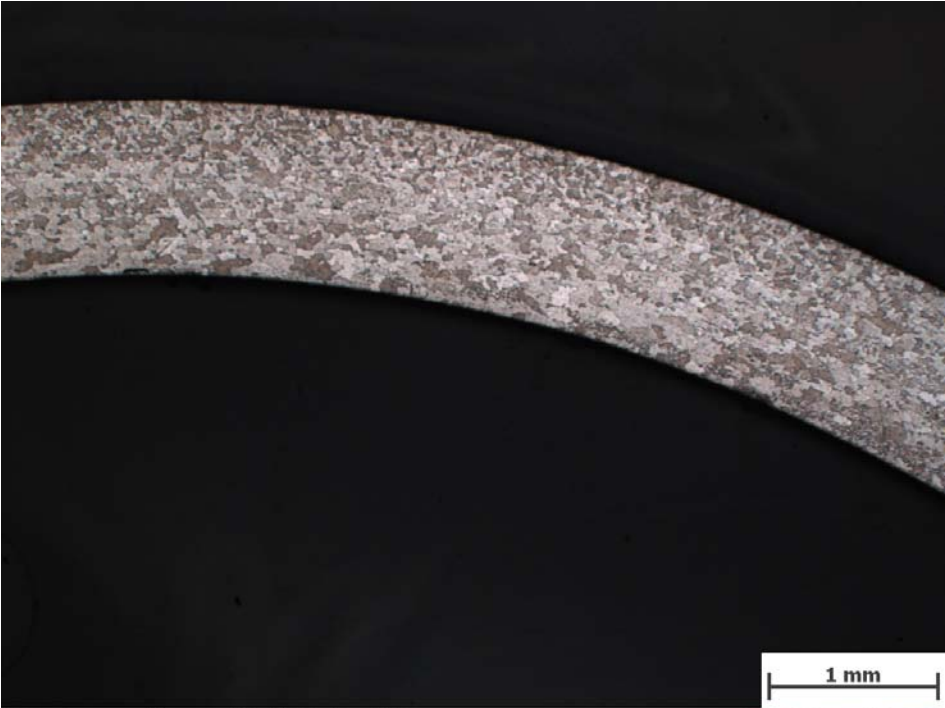
Figure 4-17:   Recrystallization Diagram Group 5 – 1311w026

Figure 4-18:   Recrystallization Diagram Group 5 – 1311w027

Group 6 – 120 minutes

Group 6 underwent a holding time of 120 minutes. Due to the long holding time, total recrystallization can be found in Sections 1 and 2. (Figure 4-19) and (Figure 4-20) were taken of Section 1, whereas (Figure 4-21) to (Figure 4-24) show the recrystallization in Section 2.

Group 6
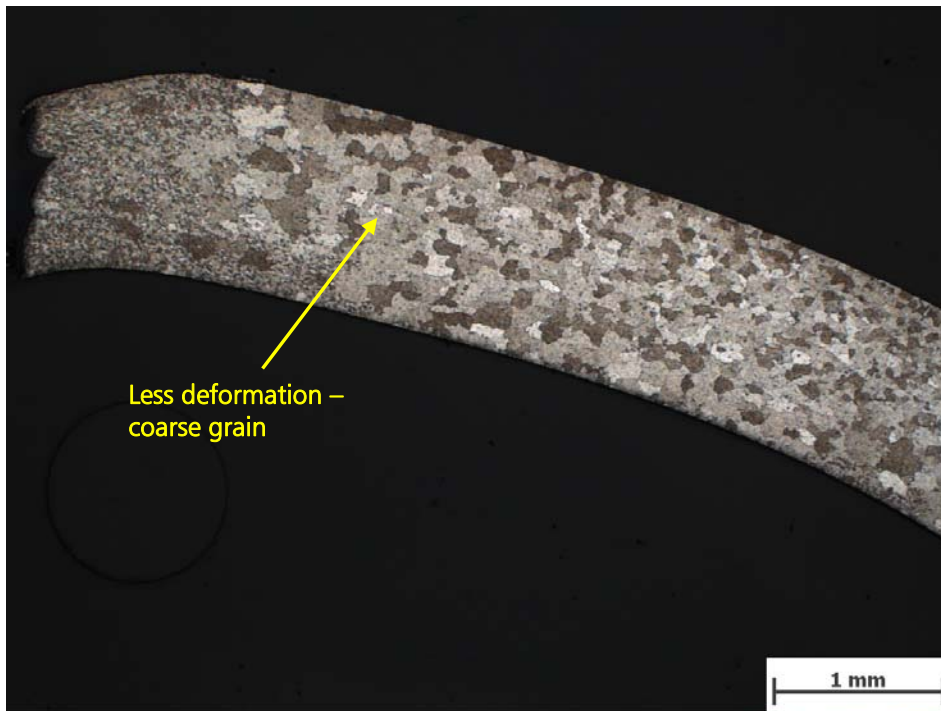
Figure 4-19:   Recrystallization Diagram Group 5 – 1311w099
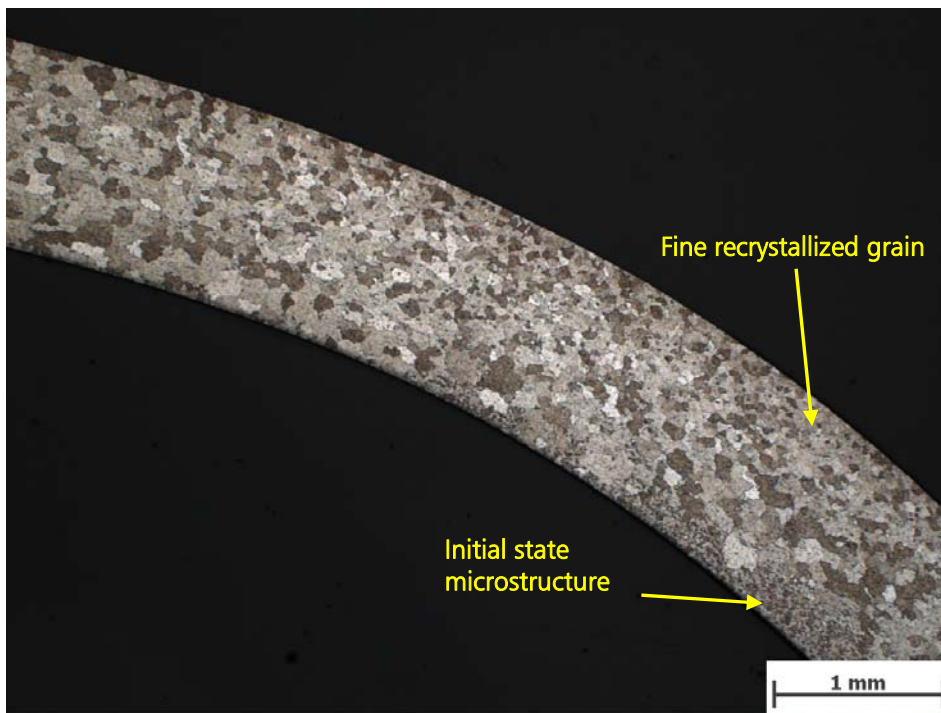
Figure 4-20:   Recrystallization Diagram Group 5 – 1311w100
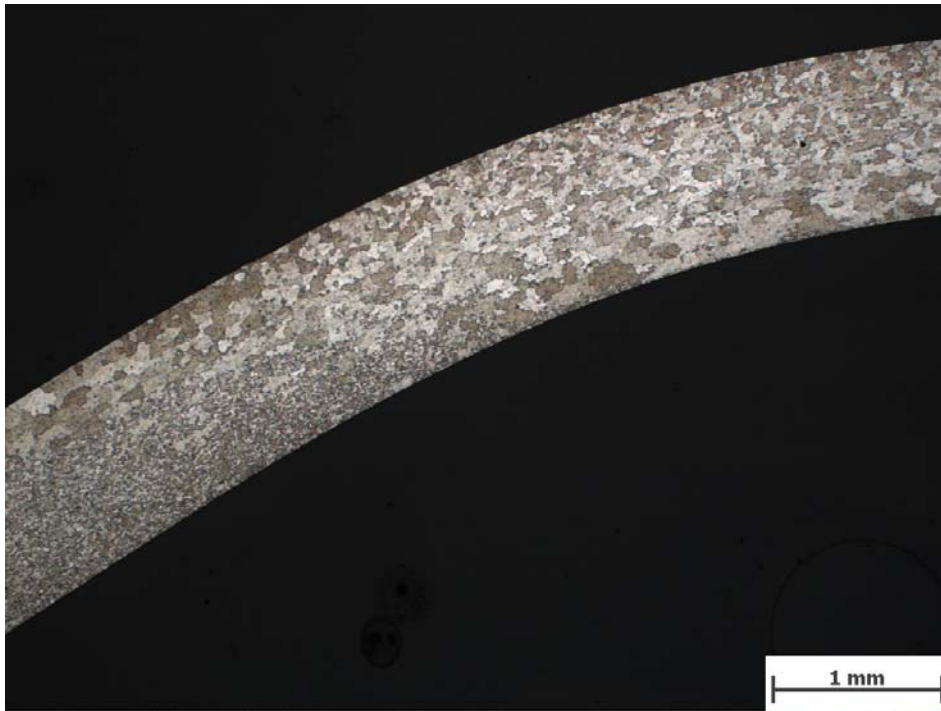
Figure 4-21:   Recrystallization Diagram Group 5 – 1311w105
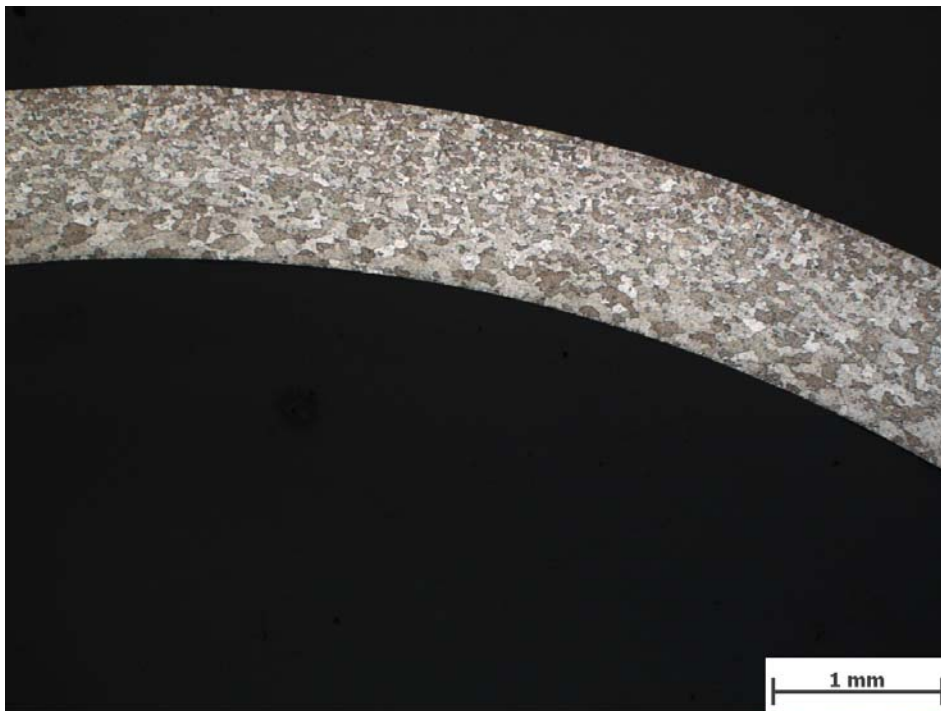
Figure 4-22:   Recrystallization Diagram Group 5 – 1311w107

Figure 4-23: Recrystallization Diagram Group 5 – 1311w108
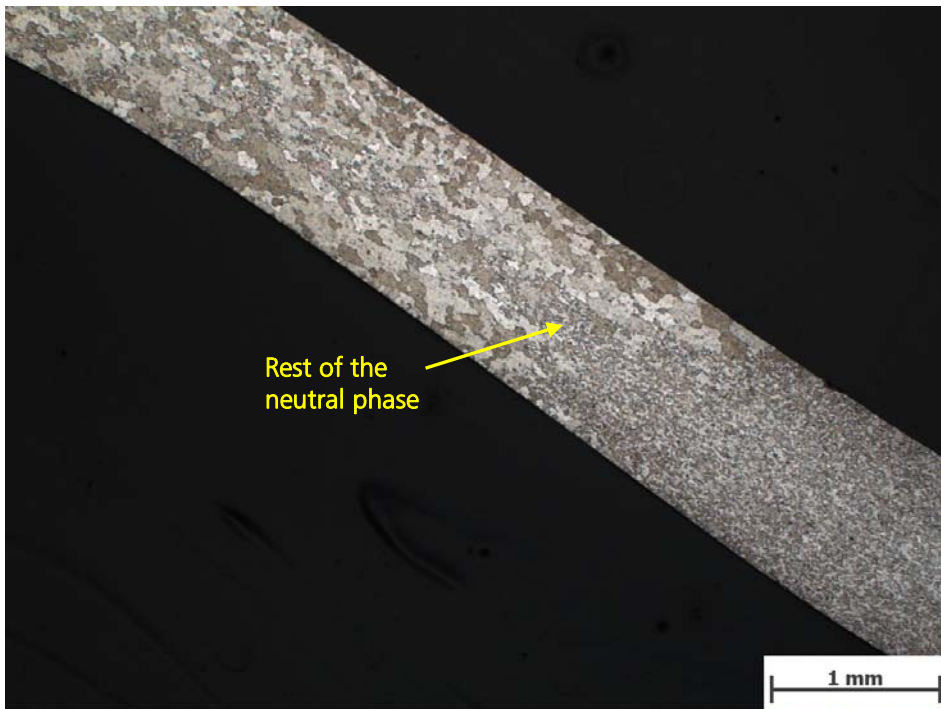
Figure 4-24: Recrystallization Diagram Group 5 – 1311w109

5 Conclusion

In general, it can be noted that the original objective, to increase the degree of deformation of the aluminum alloy EN AW-5182 through a double staged deep drawing process involving an intermediate thermal treatment was achieved. The drawing depth was increased by 18.5 %, from 27 mm to 32 mm.

Contrary to expectation, the duration of the holding time and the level of recrystallization do not have any influence on the achievable degree of deformation in the 2nd drawing stage. All tempered groups reached a maximum drawing depth of 32 mm.

According to Group 2 with a holding time of 5 minutes (Figure 4-2), the material's recovery is adequate to increase the degree of deformation in the 2nd drawing stage. The effects of strain hardening (2.4.1) produced through the movement of dislocations (2.3) during the deformation process are partially abolished. As from Group 2 to Group 6, the percentage of recrystallized microstructure increases up to a total recrystallization over the entire cross section, the depth of draw and further the degree of deformation did not increase with the fraction of recrystallized material.

The location of material failures was altered following thermal treatment. For parts drawn with no thermal treatment involved, a drawing depth of 27 mm was realized and material failure occurred in Section 1 in the area of the punch edge radius (Figure 5-1). According to (Lange 1990, 325), the material failure in the first drawing stage occurred due to the reason that the maximum drawing ratio β_{max} was exceeded. The transmission of the drawing force from the punch into the deformation zone stopped. Necking and material failures occurred along the punch edge radius as well.

Figure 5-1:   Material failure; without thermal treatment

For those parts involving a thermal treatment and achieving drawing depths of up to 32 mm, the material failure appeared in Section 2. The crack expansion of thermally treated parts is parallel to the direction of the punch movement (Figure 5-2). The high thinning in Section 2 is the reason for the material failures that ultimately limit the 2nd drawing stage.

Figure 5-2:   Material failure; with thermal treatment

(Figure 5-3) compares the material thinning to the annealing time. A tendency of the material thinning in relation to the annealing time could not directly be identified (Figure 5-3).
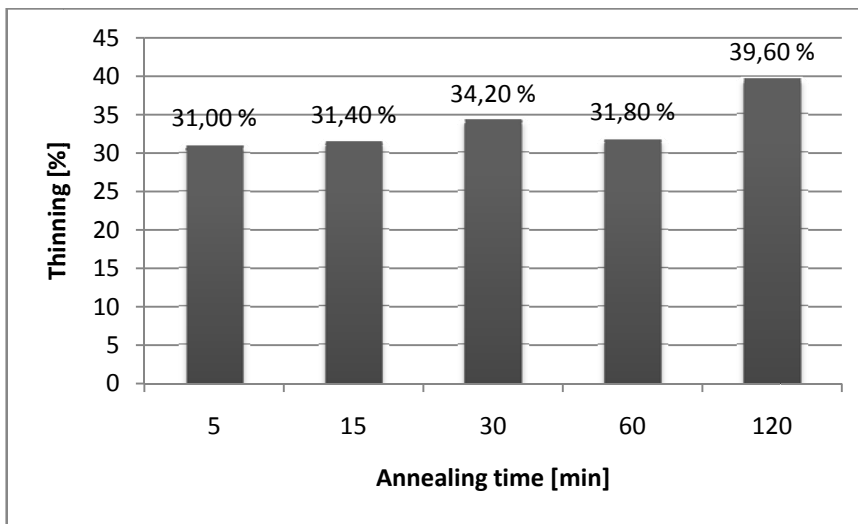
Figure 5-3: Thinning 2ⁿᵈ stage

Based on Group 2, with an annealing time of only 5 minutes, the maximum thinning increased from 19.8 % following stage 1 up to 31 % in the second stage. The minimum material thickness after the 2ⁿᵈ drawing stage in Section 2 is 0.8 mm (Figure 5-4).
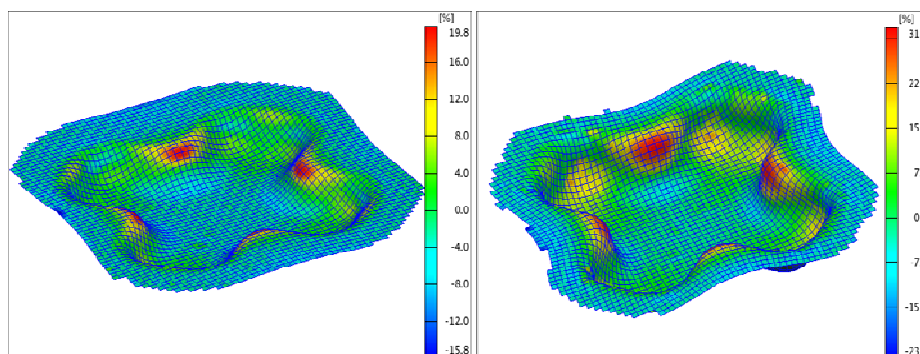
Figure 5-4: Thinning 1ˢᵗ and 2ⁿᵈ stage; left: 1ˢᵗ stage, h=18mm; right: 2ⁿᵈ stage, h=32mm, annealing time=5 min.

With the exception of Group 6 (120 minutes), major strain (Figure 5-6) and minor strain measurements (Figure 5-7) following the 2ⁿᵈ drawing stage did not show a correlation with the annealing time.

Group 6 with an annealing time of 120 minutes displayed the highest major strain, minor strain and thinning. It can be assumed that, due to the annealing time of 120 minutes, a total recrystallization over the entire cross section is delivered; the change of material properties through recrystallization has an influence on the formability behavior. The initial microstructure had a smaller grain size than the recrystallized microstructure, and aside from this, it can also be assumed that it possessed more strength and ductility. According to (Krammer 2009, 301), a recrystallized microstructure with bigger

grains is accompanied by a reduction in strength and ductility (Figure 5-5).
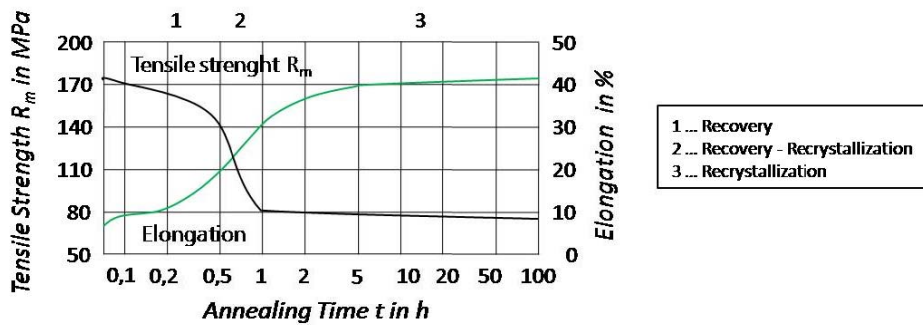
Figure 5-5:   Softening of Aluminum (Krammer 2009, 302)

Ultimately, annealing above the recrystallization barrier led to a softening of the material. According to (Figure 5-5) the recovered material has a higher tensile strength than the recrystallized material does, the main part of the deformation force affects the recrystallized material and is not constant over the entire cross section. Accordingly, it can be explained that the major strain (Figure 5-6), minor strain (Figure 5-7) and also the material thinning (Figure 5-3) all show the highest rates in Group 6, which underwent an annealing time of 120 minutes.
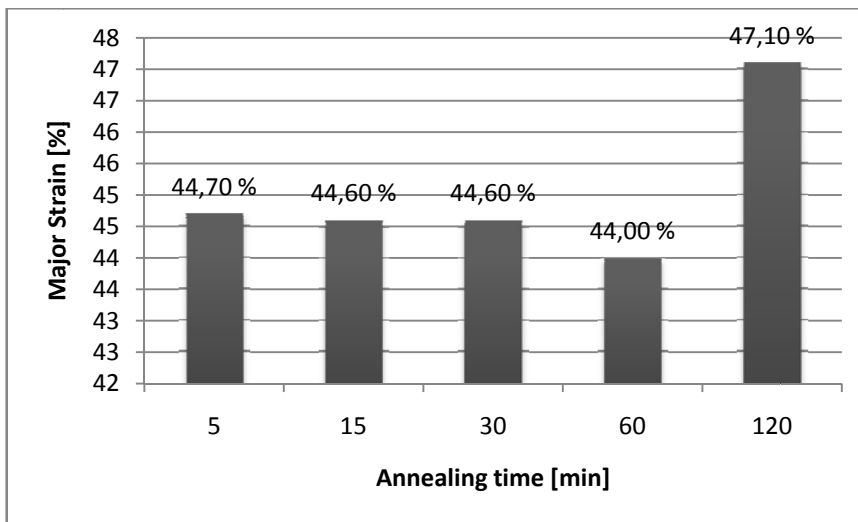
Figure 5-6:   Major Strain 2nd stage
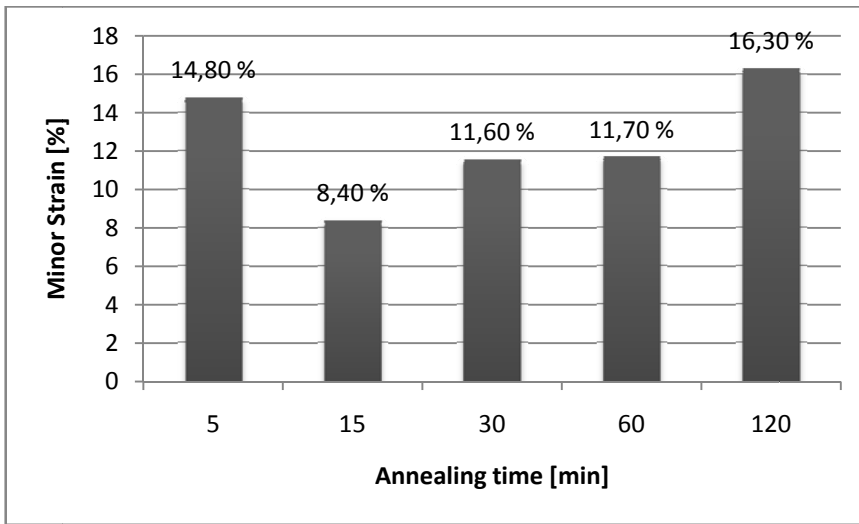
Figure 5-7:   Minor Strain 2nd stage

6 Technological Outlook

In order to build up on the results of this work, the application of an adequate recrystallization diagram for the EN AW-5182 material is recommended for further tests. The knowledge of the specific degree of deformation could more accurately define the process parameters annealing temperature and holding time. As a result, a variation of holding time and microstructure analysis could be skipped.

The existing project followed the approach to apply a thermal treatment to the entire part. Due to this, areas with a high degree of deformation achieved partial or total recrystallization, whereas areas where lesser deformations occurred, only recovery took place (2.4.4). The effects of work hardening were totally or partially undone. It is helpful to soften the material at the flange and in the area of the die radius for further deformation; the effect of work hardening is an advantage used in the part bottom and flanges in order to achieve a better force transmission into the deformation zone and bending zone (2.5). Through the increased strength of material in these areas, a lateral contraction and material failure will begin at higher stress levels and increase the drawing ratio. The partial thermal treatment could be carried out using induction, conduction or thermal radiation. The responding behavior of aluminum for induction, conduction and thermal radiation has to be confirmed.

According to (Lange 1990, 325), a targeted lubrication should have a positive effect on the drawing performance. As a result, the targeted lubrication of tool and blank will increase the drawing depth. As mentioned in Chapter 3.5, the friction coefficient ideally would be as high as possible in the area of the blank holder and as low as possible in the area of the punch edge radius. The result would be an application of lubricant to both the punch and the drawing radius of the lower tool. The upper tool and especially the contact surface of the lower tool should remain free of lubricant. It could pose a problem to achieve a constant lubrication of all sample parts, making it difficult to repeat this process. As was clearly shown in this project, a constant application of lubricant to a flat blank (1st stage) is easier and more economical than the application of lubricant to the pre-formed part geometry in the 2nd stage. Beside the difficulties in the application of a constant lubricant film to complex forms, the deformation of blanks used for electrochemical etching require different amounts of lubricant than blanks in the initial state. In the existing solution, this was considered by a higher amount of lubricant spread over the blank surface.

List of Figures

List of Tables

Bibliography

Bargel, Hans-Jürgen, Hermann Hilbrans, Karl-Heinz Hübner, Oswald Krüger, and Günter Schulze. *Werkstoffkunde.* Berlin Heidelberg: Springer-Verlag, 2008.

European Aluminium Association, MATTER and the University of Liverpool. *alumatter.* 2001-2010. http://aluminium.matter.org.uk (accessed 02 25, 2011).

Friebe, Klein, and Galanulis. *Numerical comparision and verification of FEA in sheet metal forming by optical measurements of largen and complex parts.* Graz: International Deep Drawing Research Group, 2010.

GeoScienceWorld. 2011. www.geoscienceworld.org (Zugriff am 19. 05 2011).

Hirth, John Price, and Jens Lothe. *Thory of Dislocations.* Malabar, Florida: Krieger Publishing Company, 1991.

Huda, Zainul. *Effects of Degrees of Cold Working and Recrystallisation on the Microstructure and Hardness of Commercial-Purity Aluminum.* Paper, European Jounal of Scientific Research, 2009.

Klocke, Fritz, und Wilfried König. „Fertigunsverfahren 4." In *Grundlagen*, von Fritz Klocke und Wilfried König, 183. Berlin: Springer, 2006.

Krammer, Catrin. *Aluminium Taschenbuch 1.* Duesseldorf: Aluminium-Verlag Marketing & Kommunikation GmbH, 2009.

Lange, Kurt. *Umformtechnik, Band 1: Grundlagen.* Berlin: Springer, 2002.

Lange, Kurt. *Umformtechnik, Band 3: Blechbearbeitung.* Berlin: Springer, 1990.

Miller, W.S., et al. *Recent development in aluminium alloys for the automotive industry.* Paper, Material Science and Engineering, 2000.

Ostermann, Friedrich. *Anwendungstechnologie Aluminium.* Berlin: Springer, 2007.

Ostermann, Friedrich. *Anwendungstechnologie Aluminium.* Berlin: Springer Verlag, 1998.

Röhr, Caroline. *ruby.chemie.uni-freiburg.* 2011. http://ruby.chemie.uni-freiburg.de/ (Zugriff am 19. 05 2011).

*Umformtechnik, Band 3: Blechbearbeitung*BerinSpringer1990

Wen, Wei, and J.G. Morris. *The effect of cold rolling and annealing on the serrated yielding phenomenon of AA5182 alluminum alloy.* Paper, Lexington, Kentucky, USA: Material Science and Engineering, 2004.

Appendix

ARGUS Analyze

Nr. 300   Major Strain   h=18mm

Nr. 300   Minor Strain   h=18mm

Nr. 300   Forming Limit Diagram   h=18mm
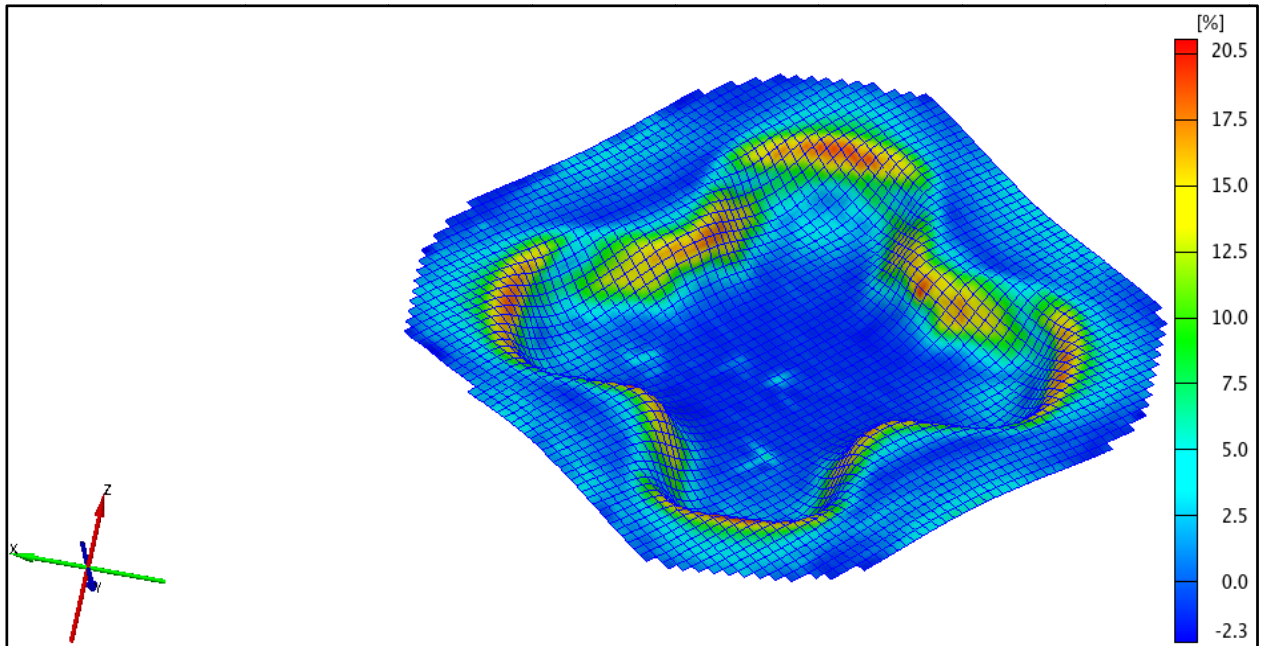
Nr. 300   Thinning   h=18mm
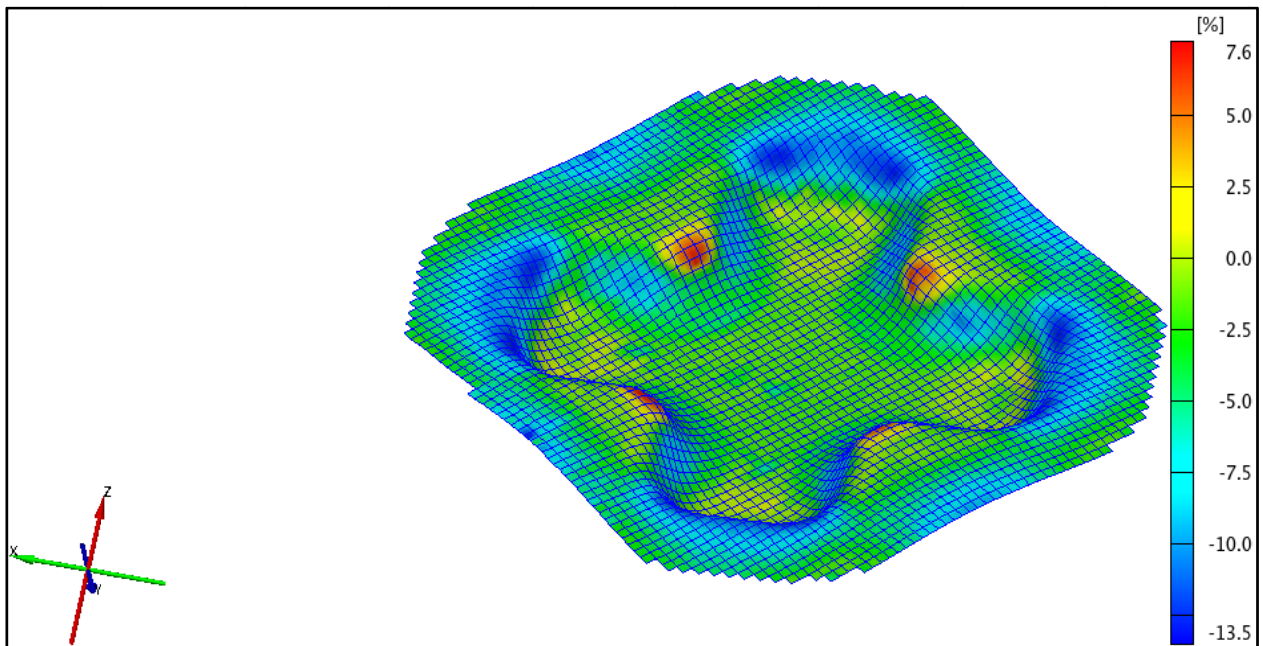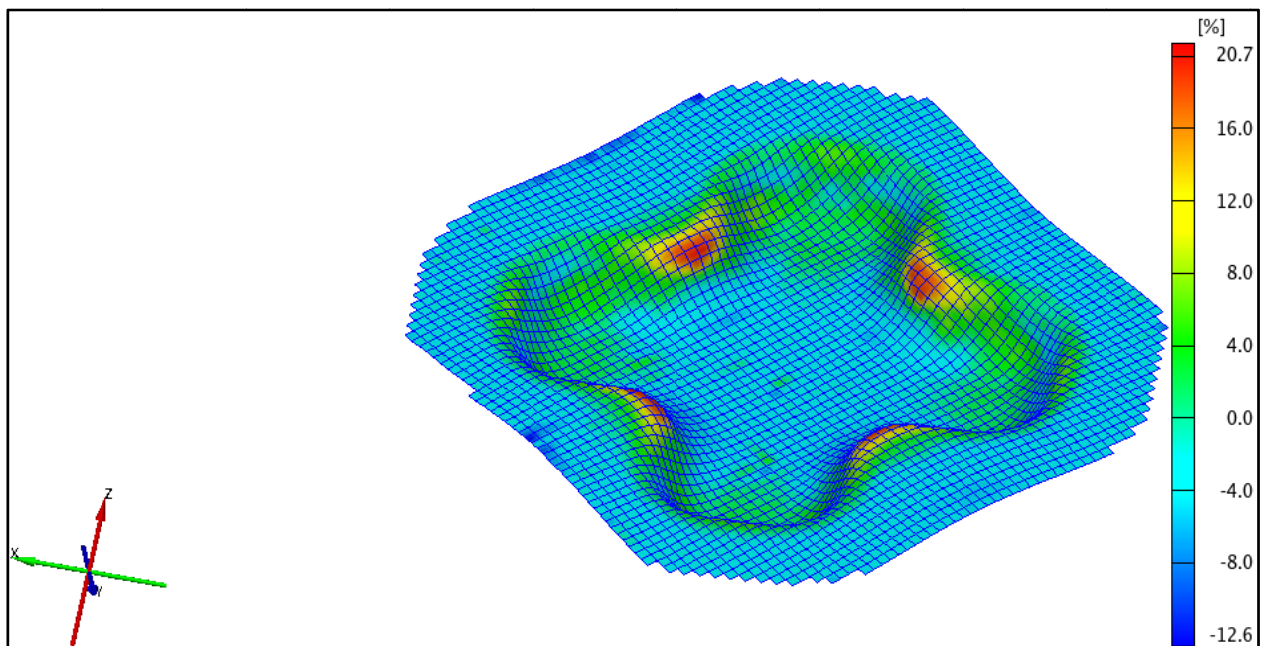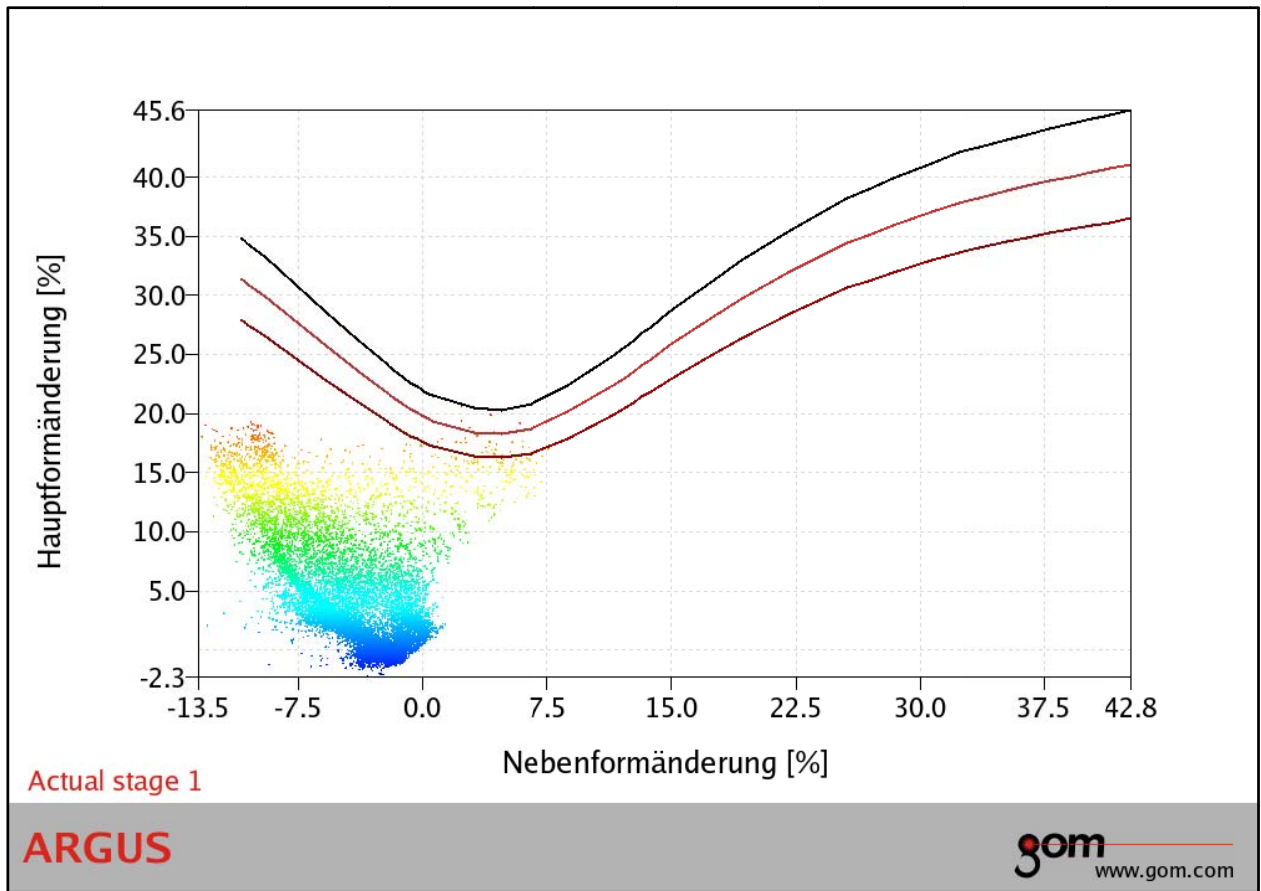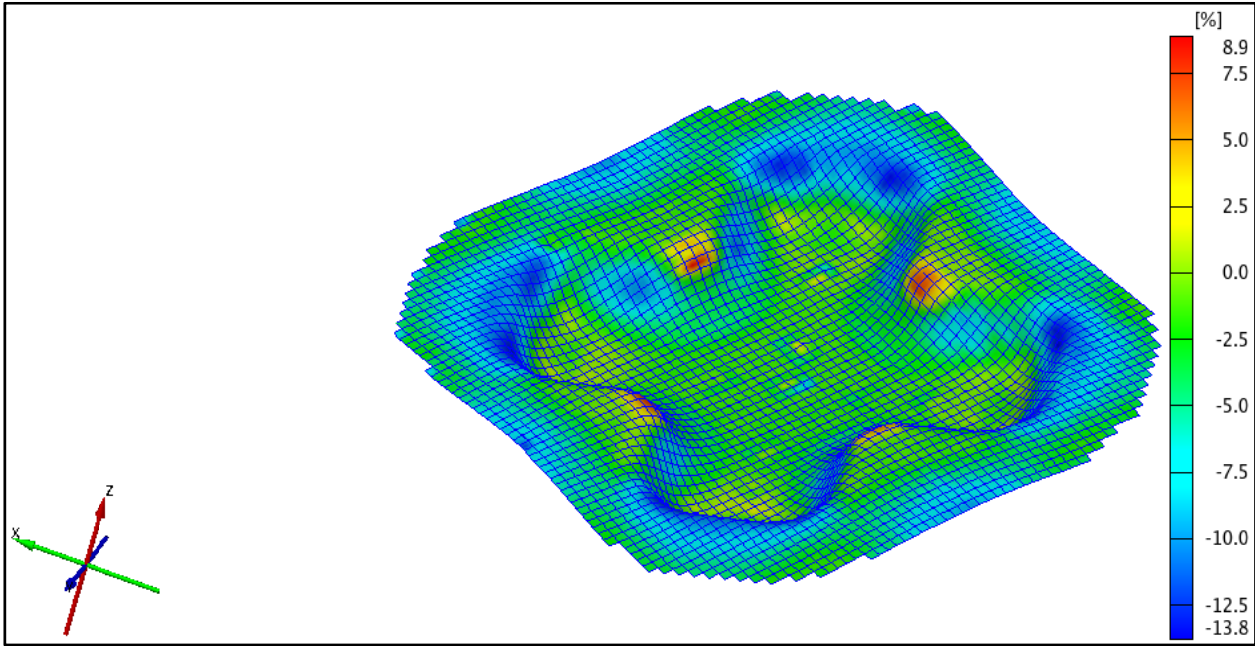
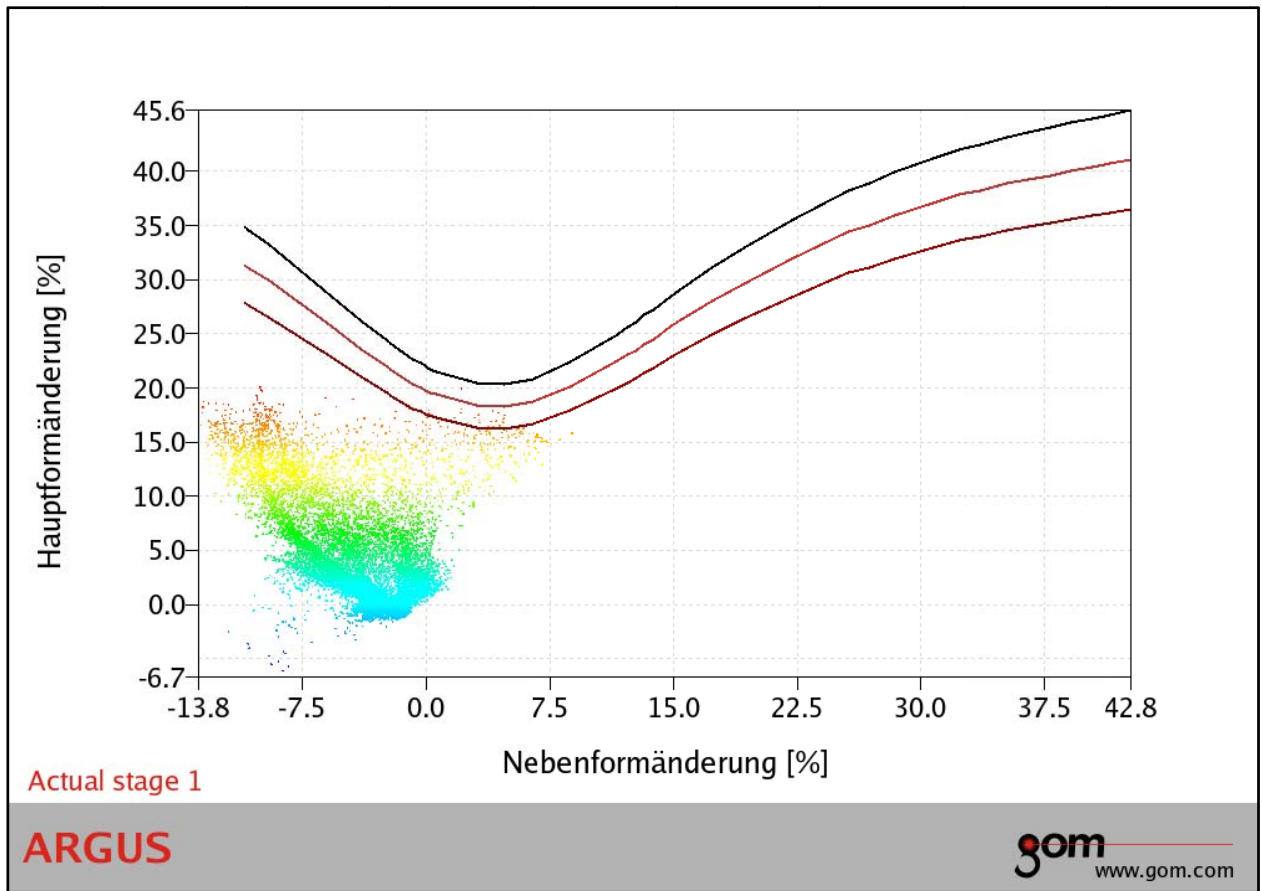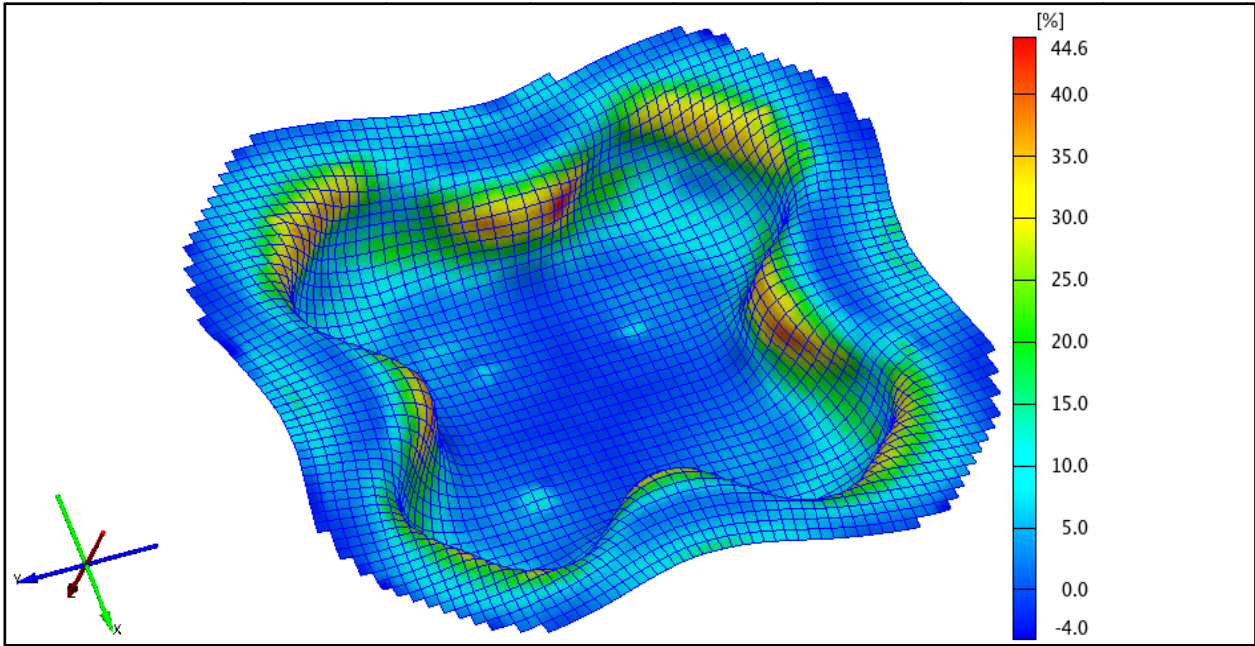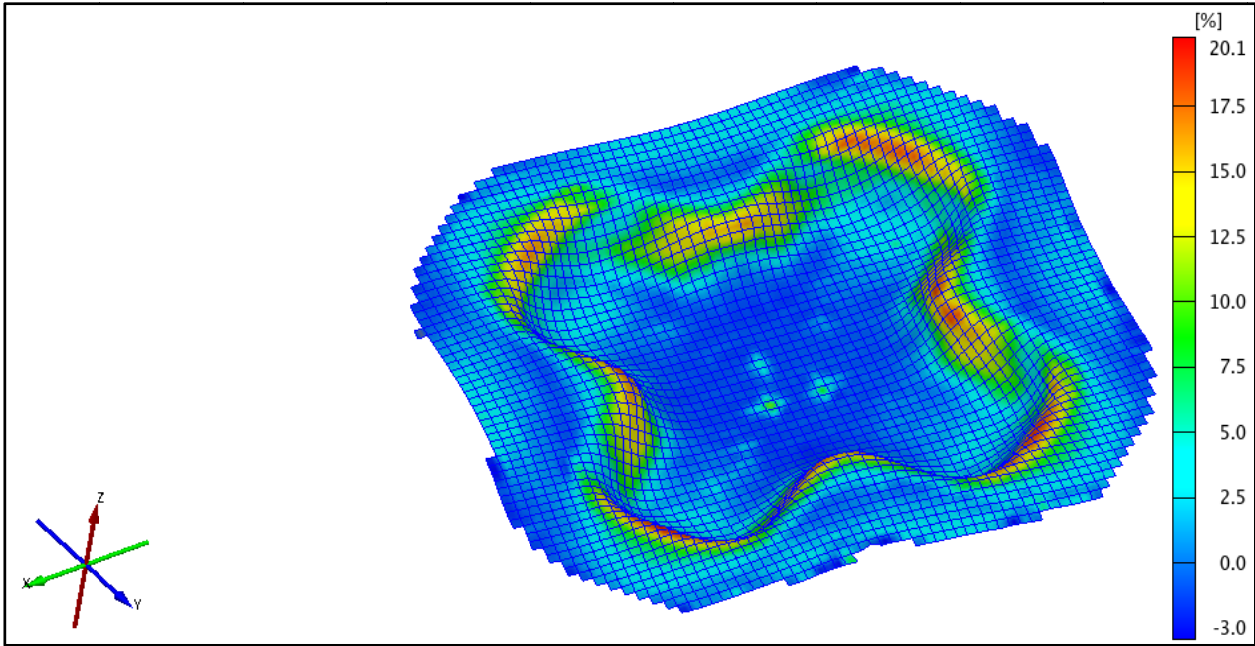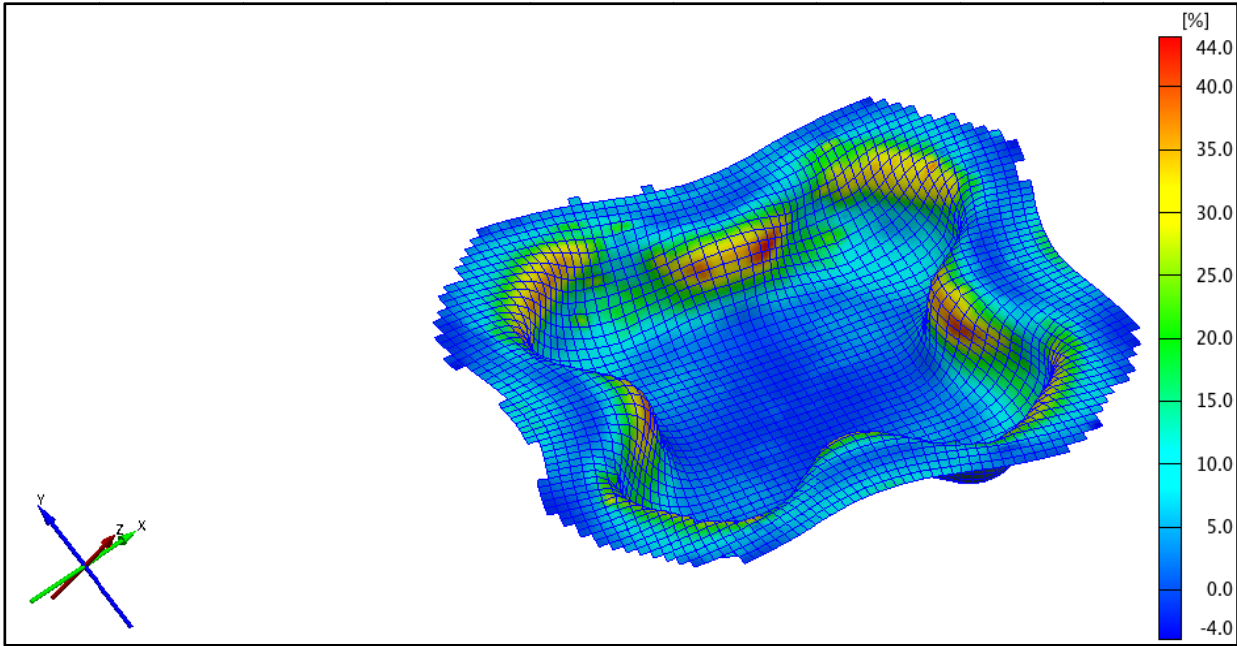Nr. 300   Major Strain   h=32mm
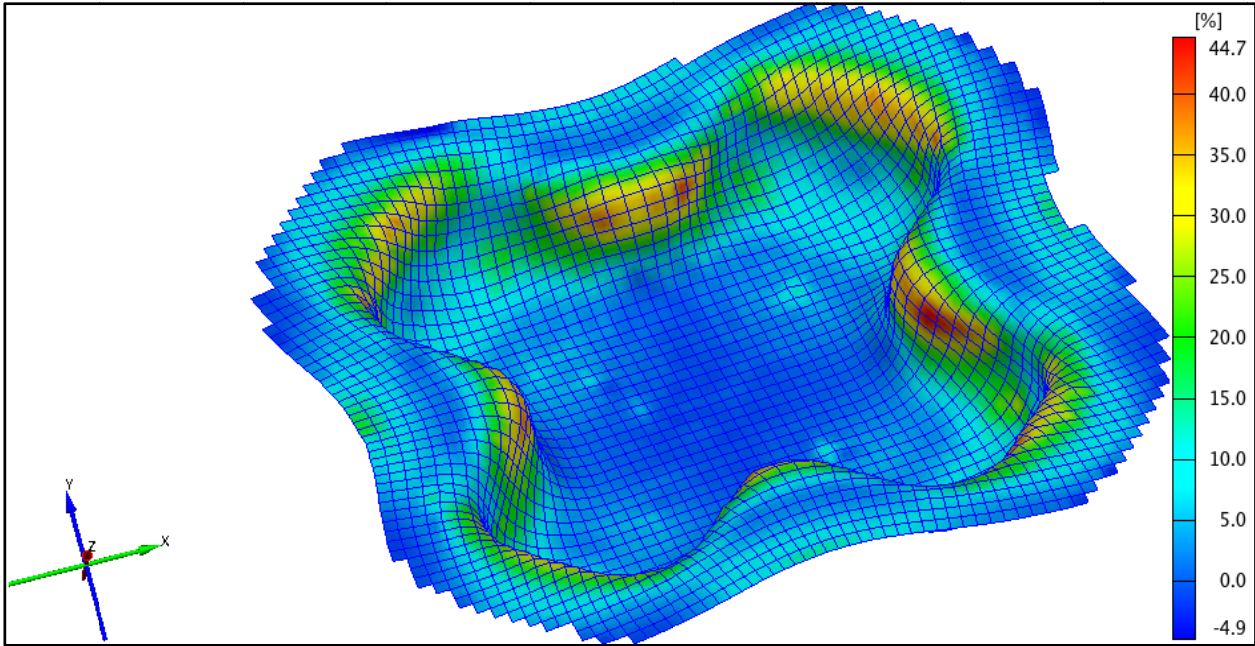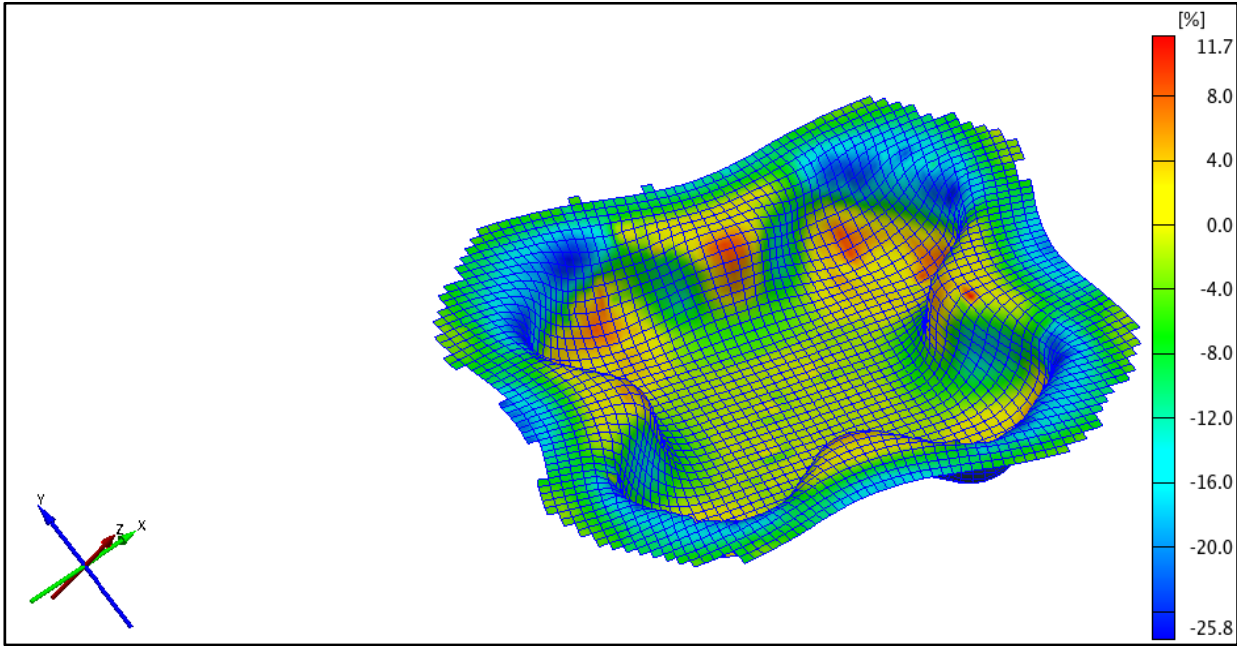

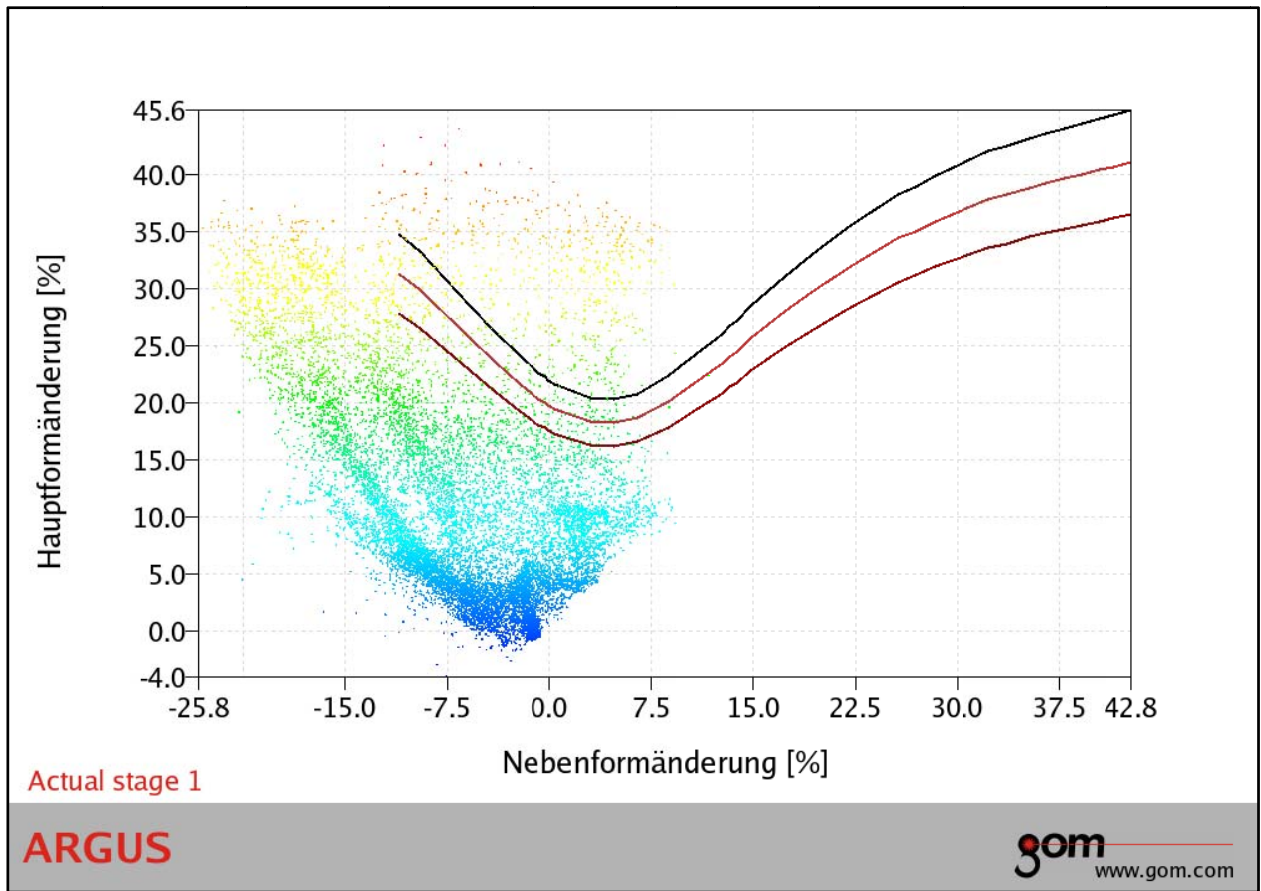Nr. 300   Minor Strain   h=32mm
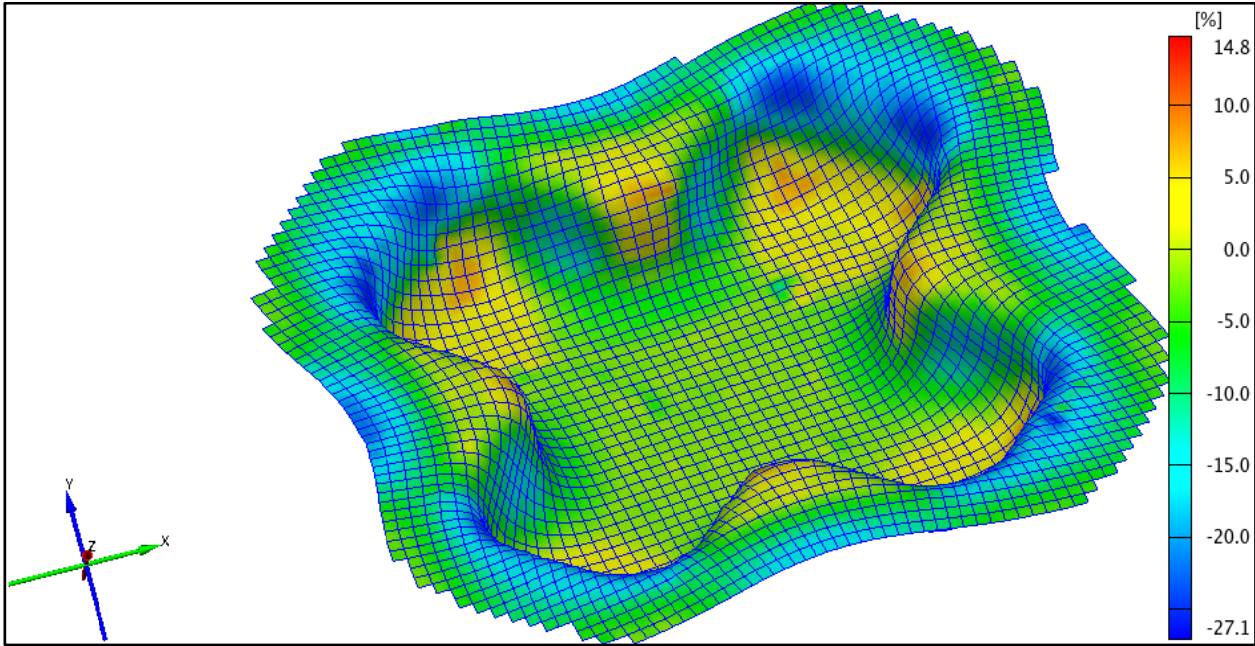
Nr. 300   Forming Limit Diagram   h=32mm
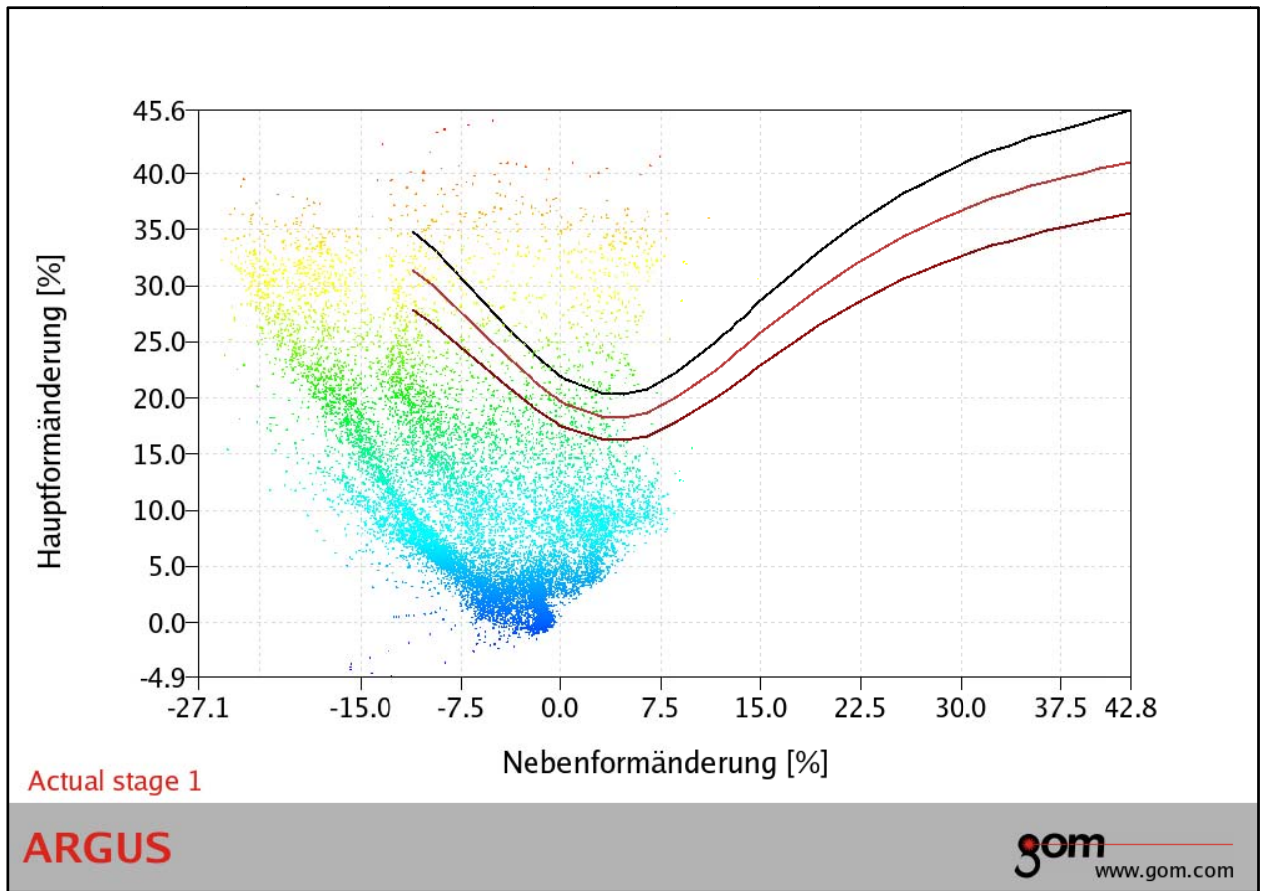
Nr.300   Thinning   h=32mm
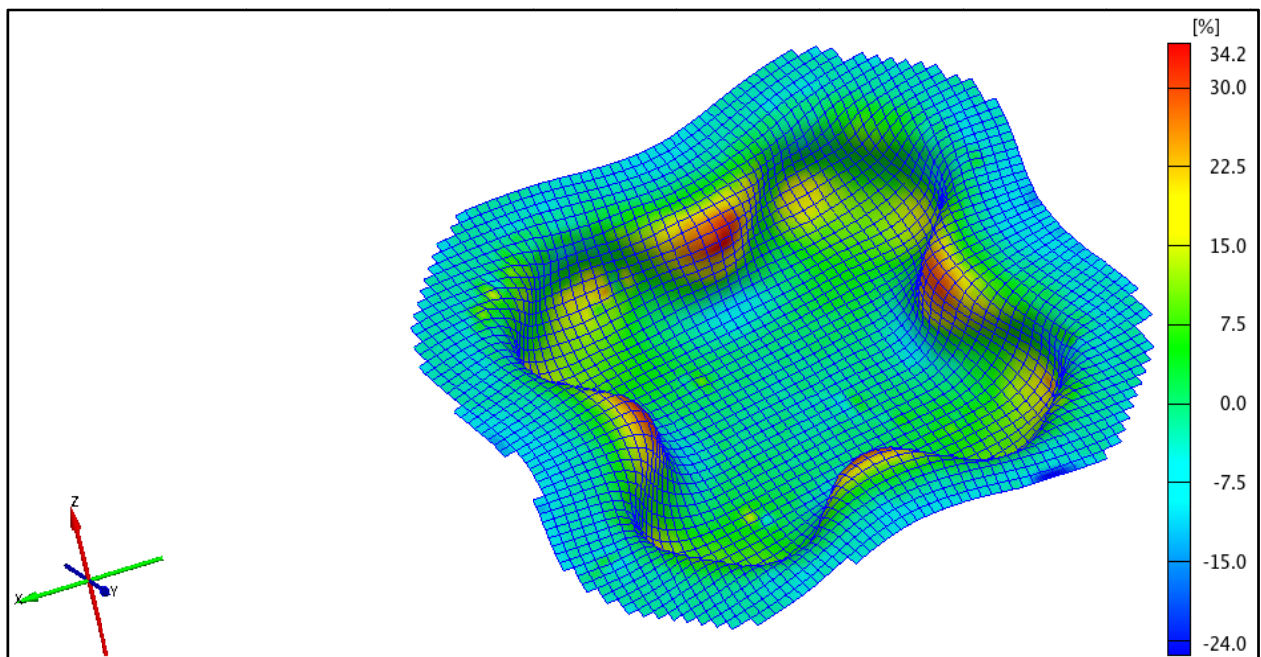
Nr.301   Major Strain   h=18mm
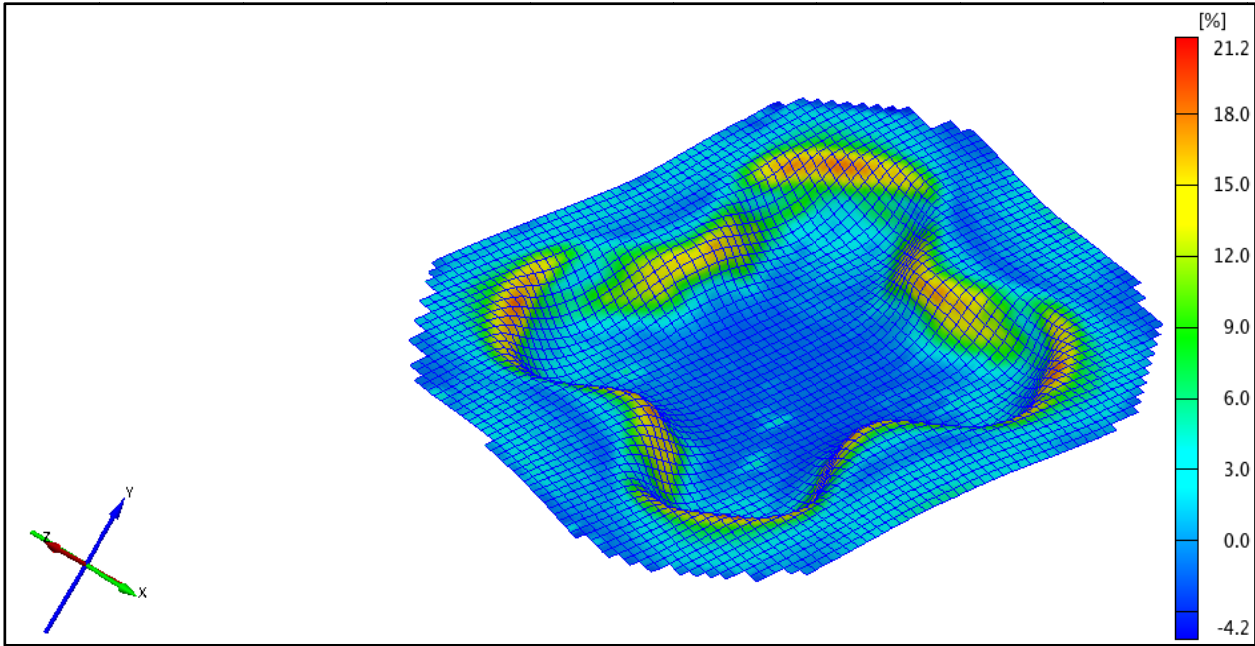
Nr.301   Minor Strain   h=18mm

Nr.301   Forming Limit Diagram   h=18mm

Actual stage 1

ARGUS

gom
www.gom.com
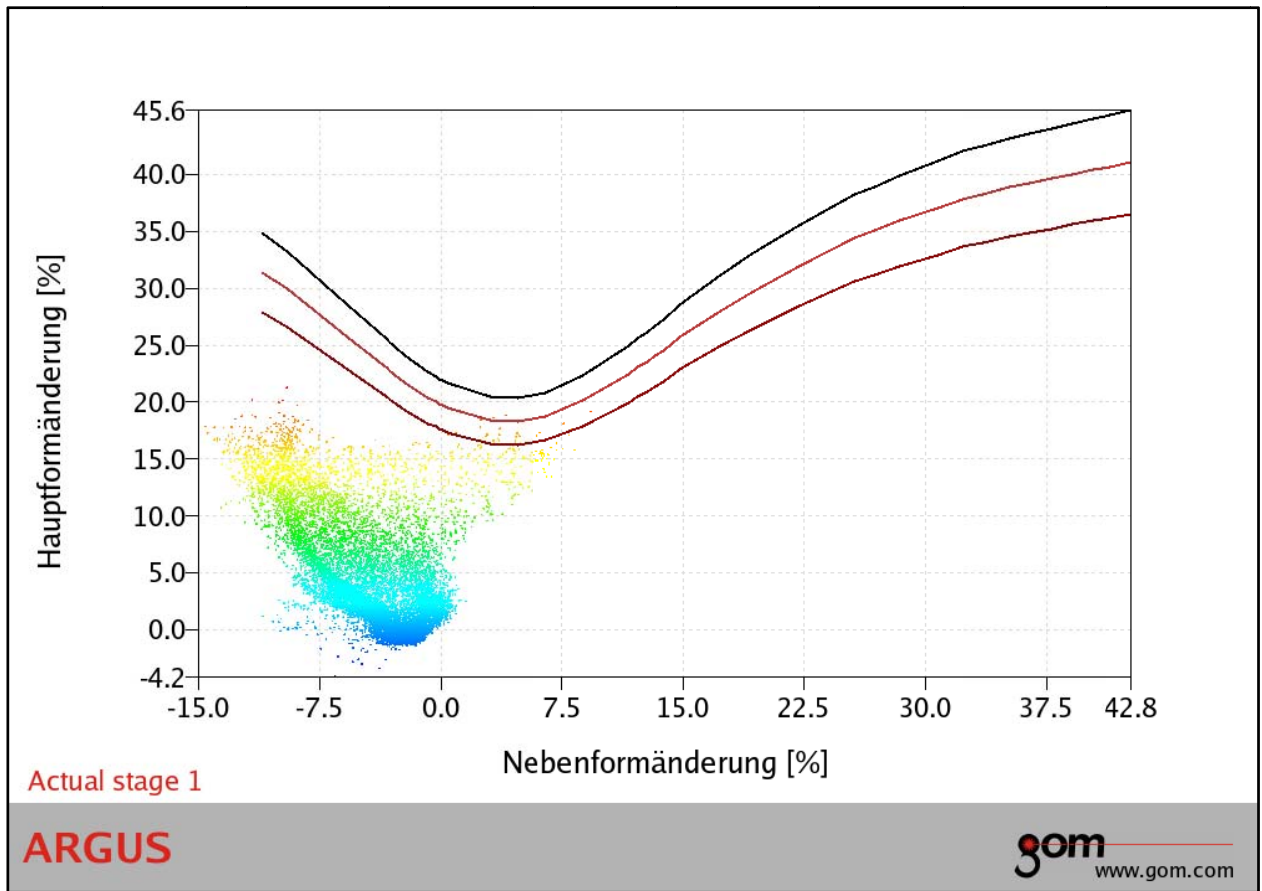
Nr.301   Thinning   h=18mm
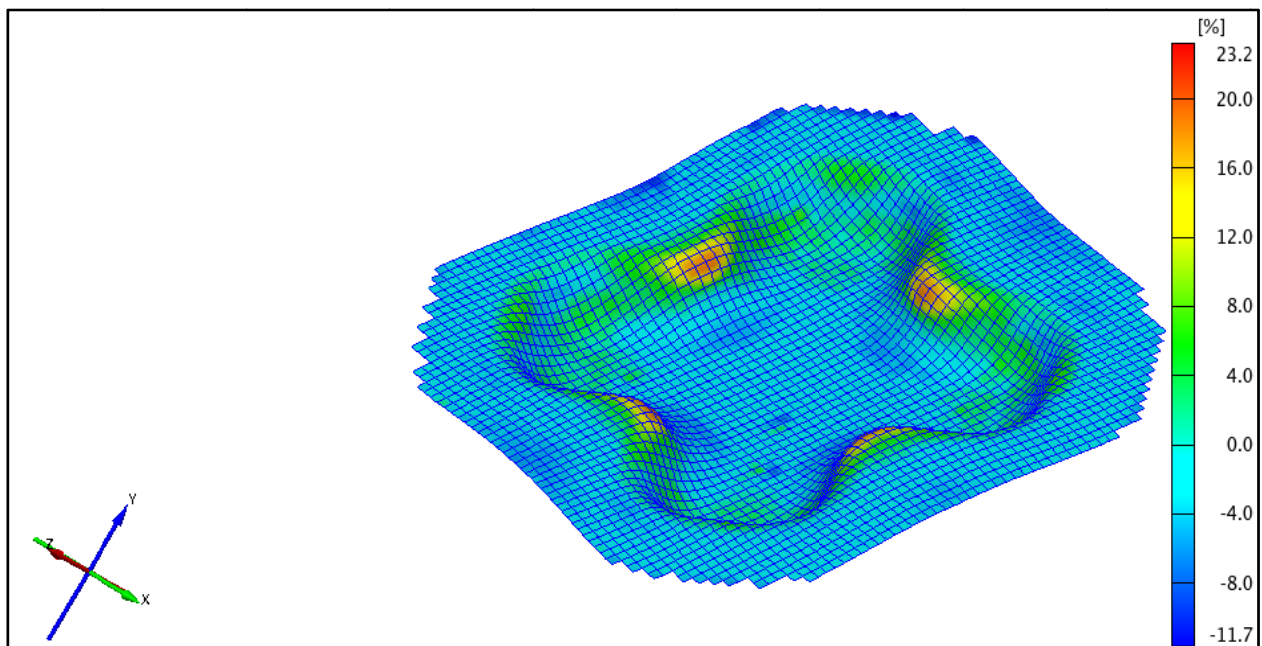
Nr.301   Major Strain   h=32mm
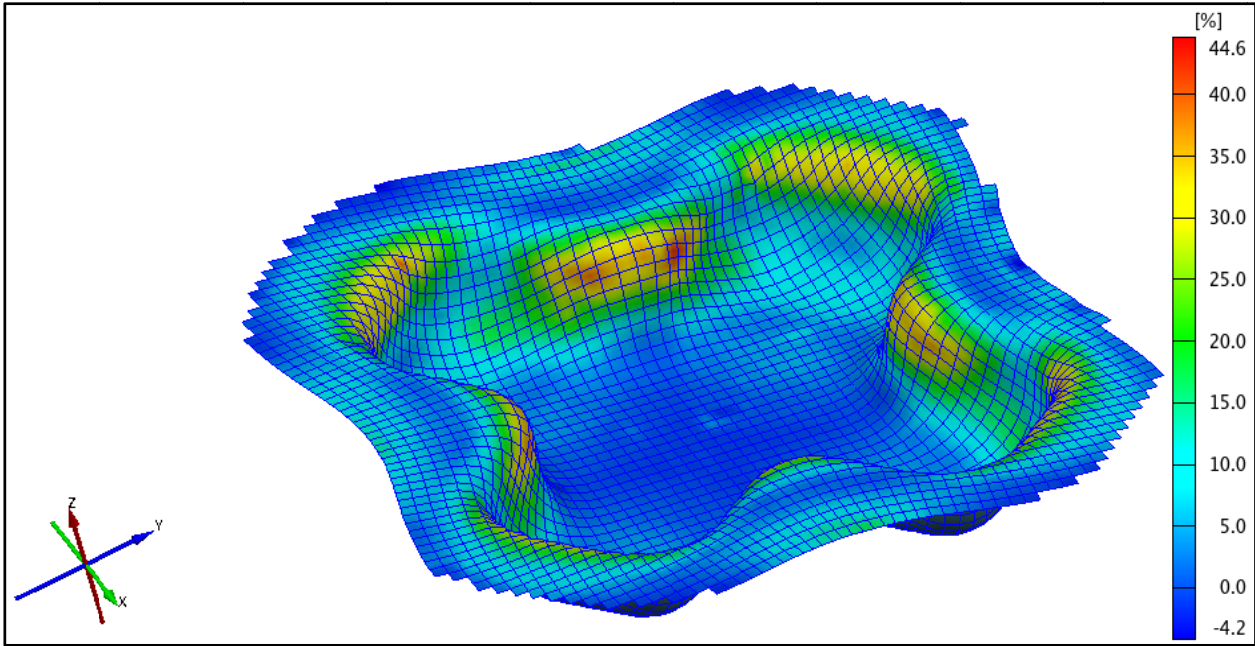
Nr.301   Minor Strain   h=32mm
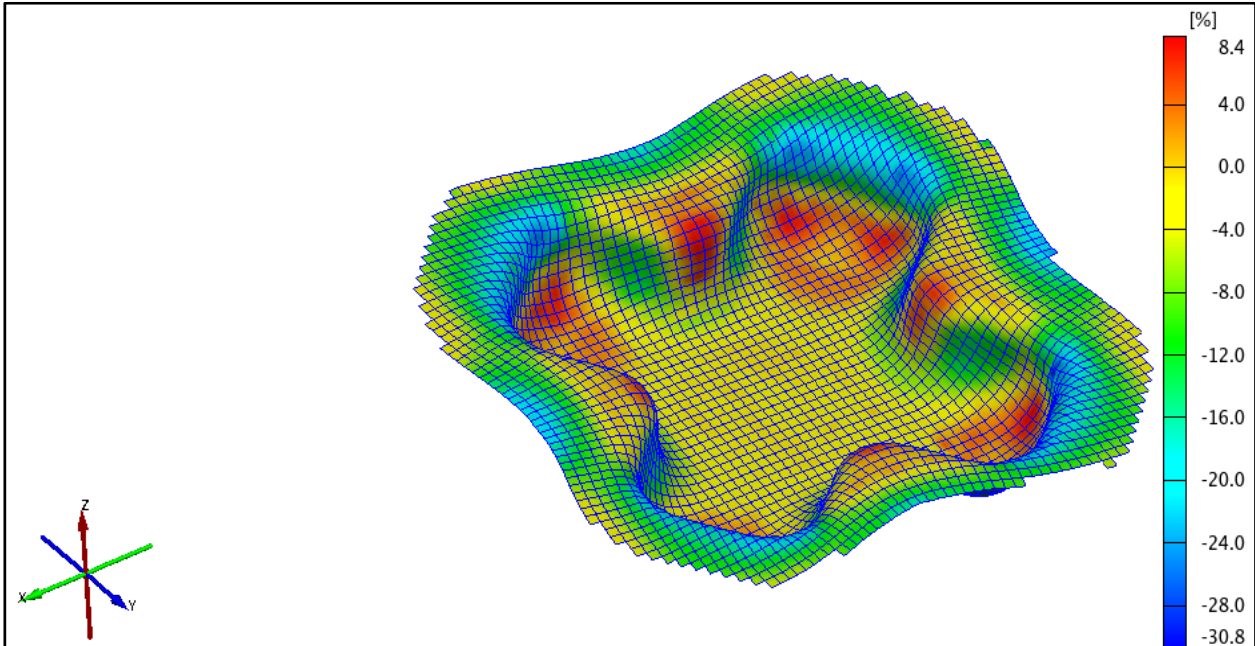
Nr.301   Forming Limit Diagram   h=32mm
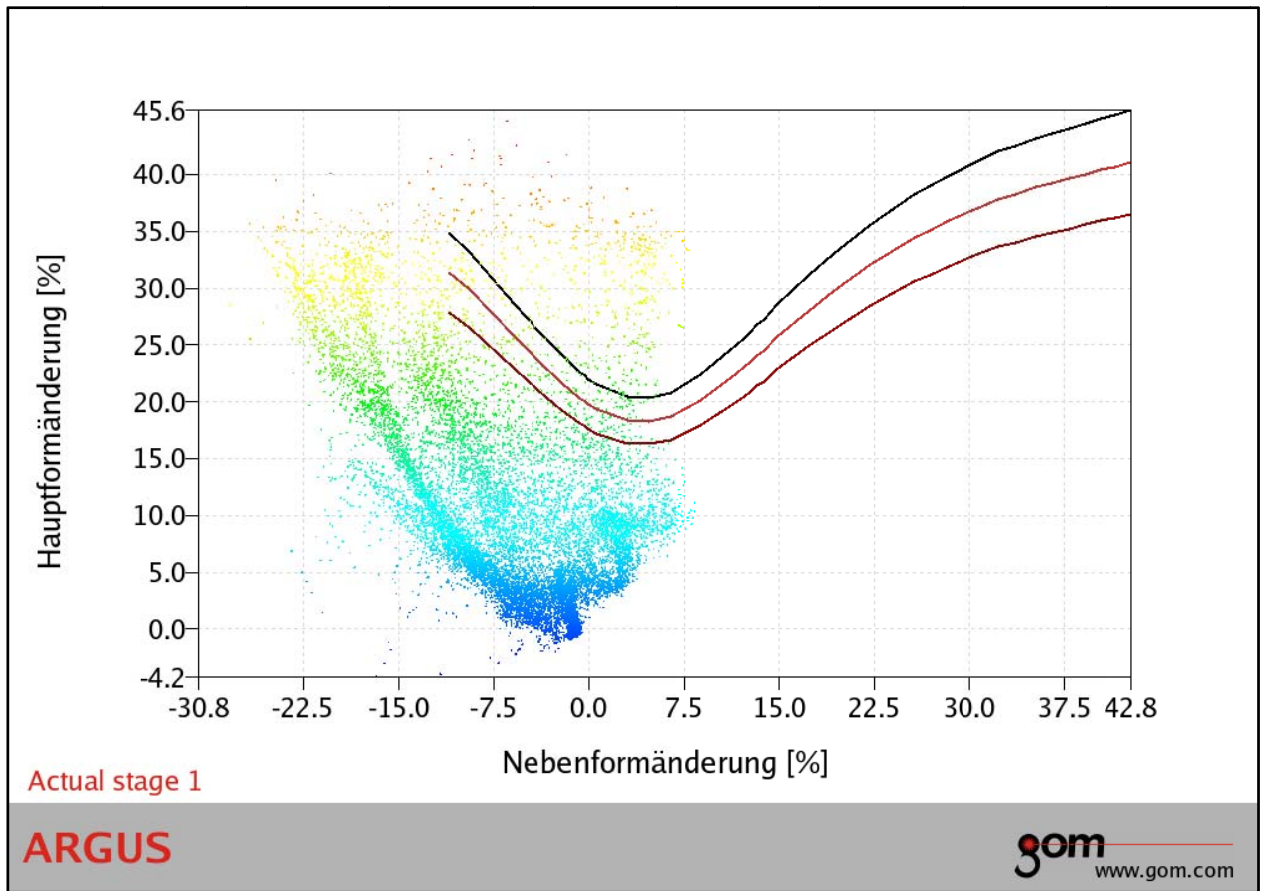
Nr.301   Thinning   h=32mm
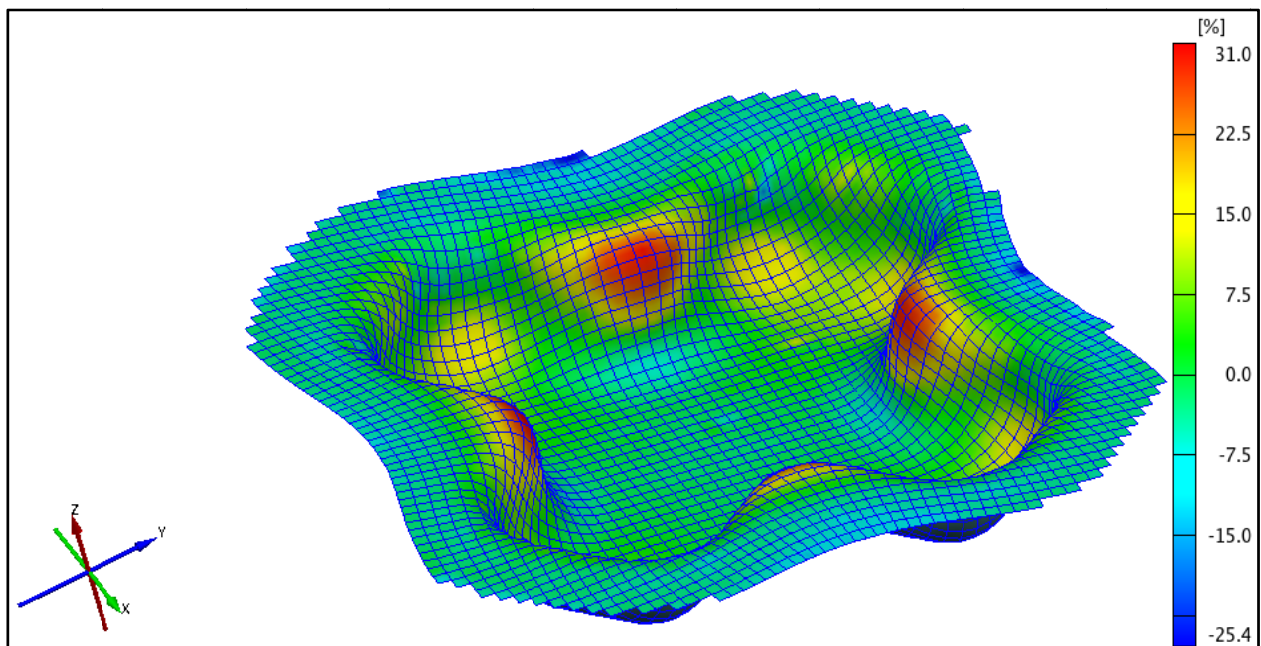
Nr.302   Major Strain   h=18mm


Nr.302   Minor Strain   h=18mm

Nr. 302   Forming Limit Diagram   h=18mm
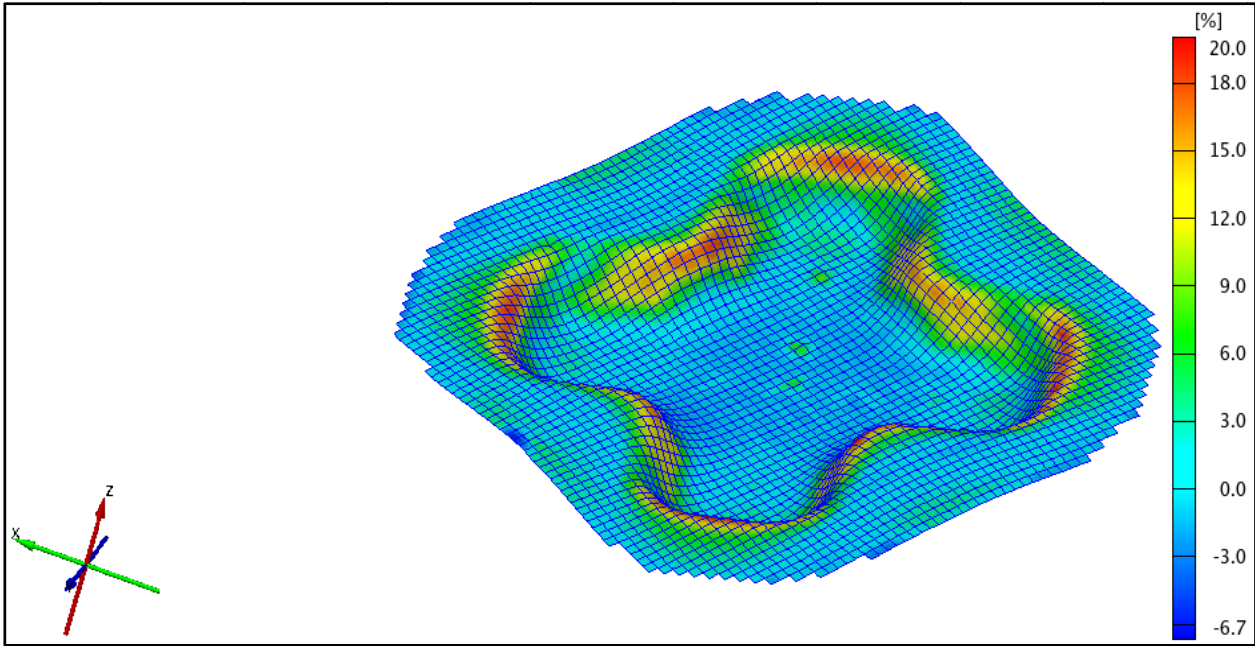
Nr.302   Thinning   h=18mm
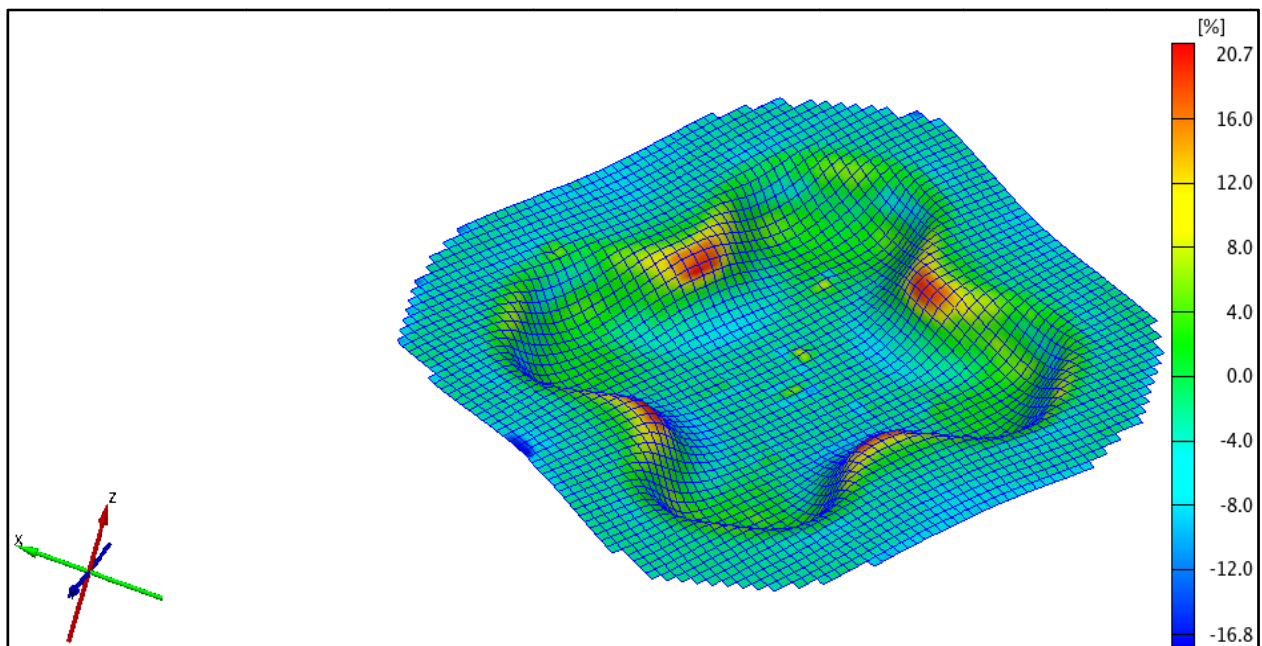
Nr.302   Major Strain   h=32mm

Nr.302   Minor Strain   h=32mm

Nr.302   Forming Limit Diagram   h=32mm

Nr.302   Thinning   h=32mm
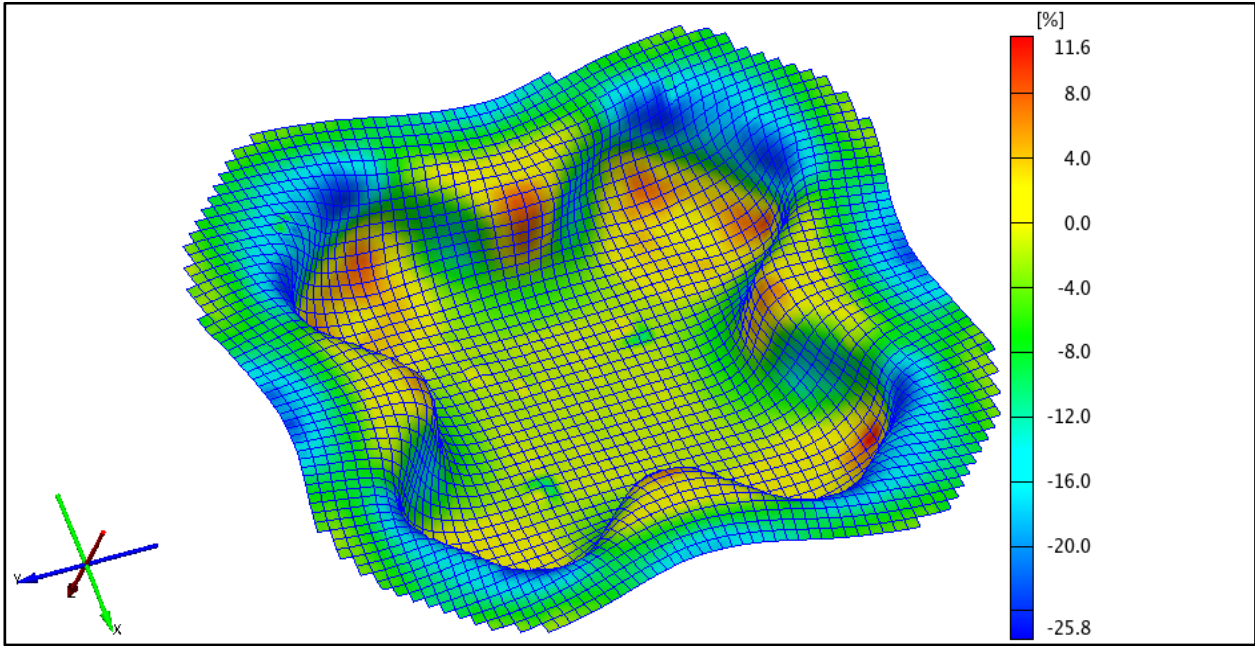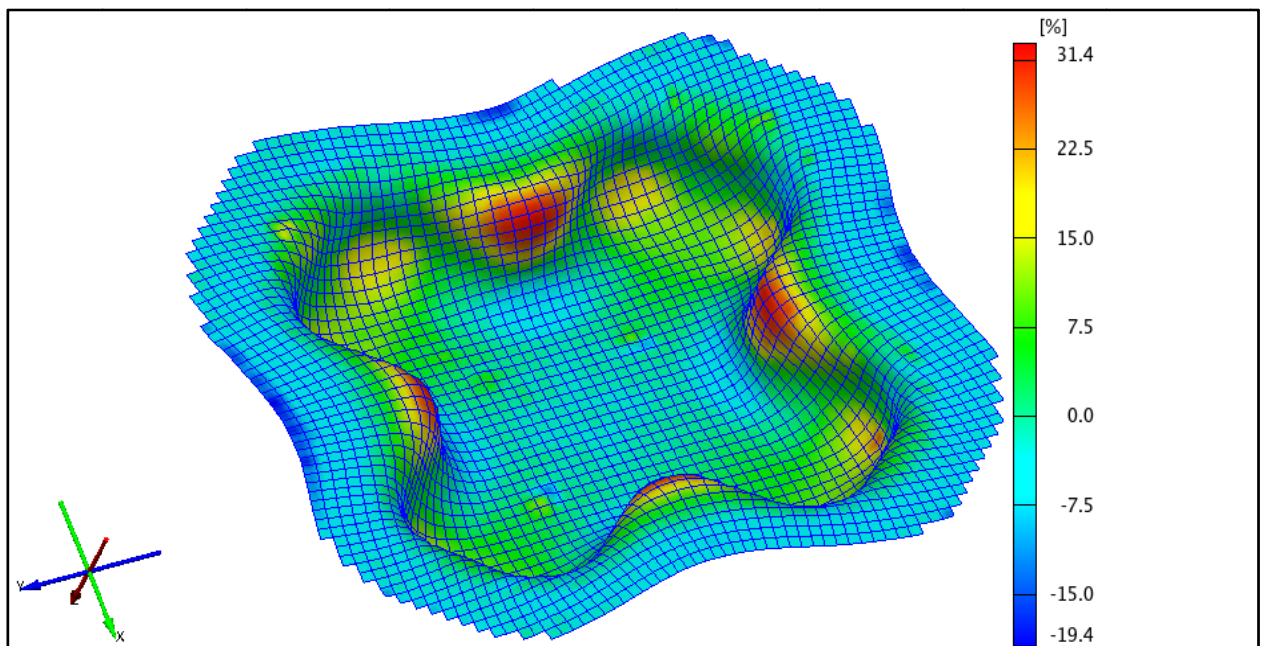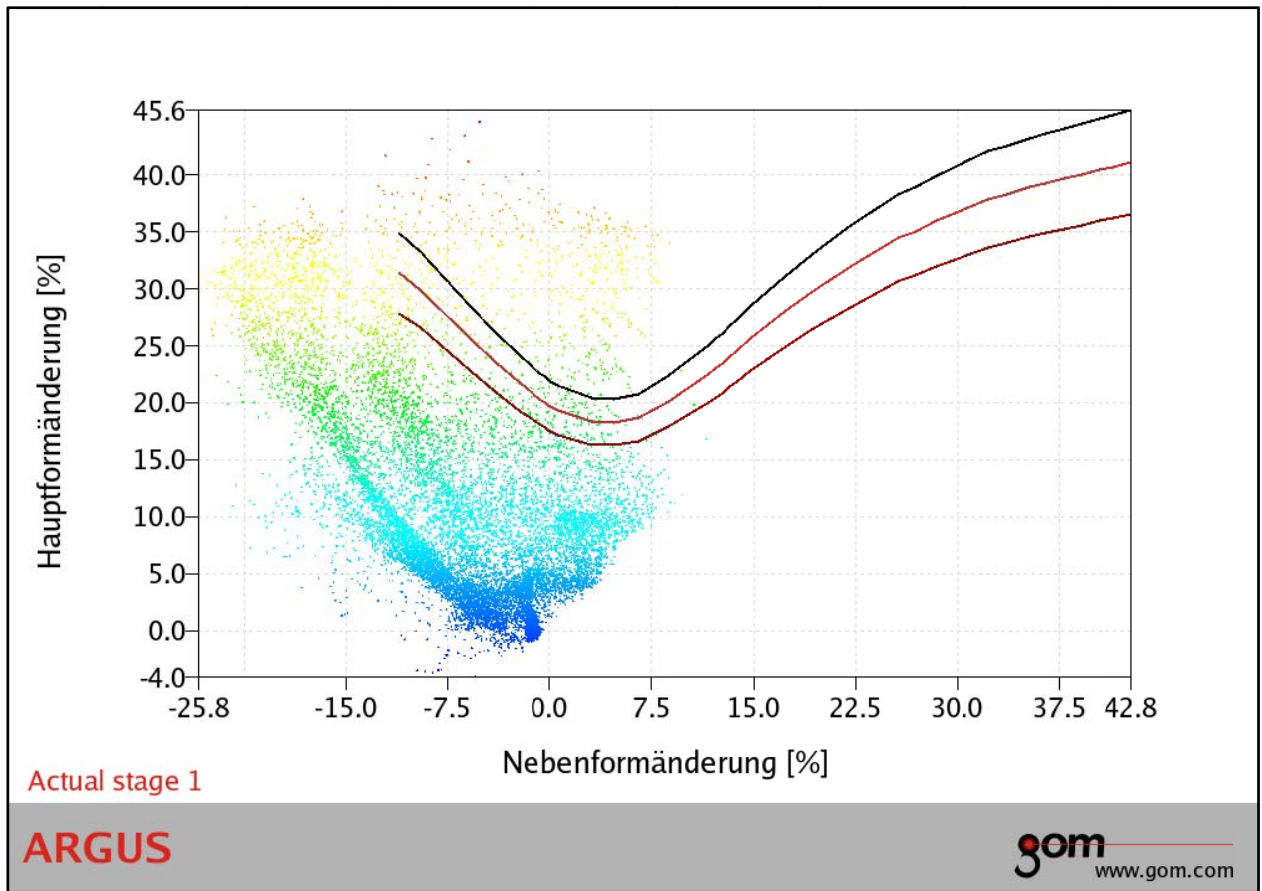
Nr.303   Major Strain   h=18mm

Nr.303   Minor Strain   h=18mm

**Nr.303 Forming Limit Diagram h=18mm**
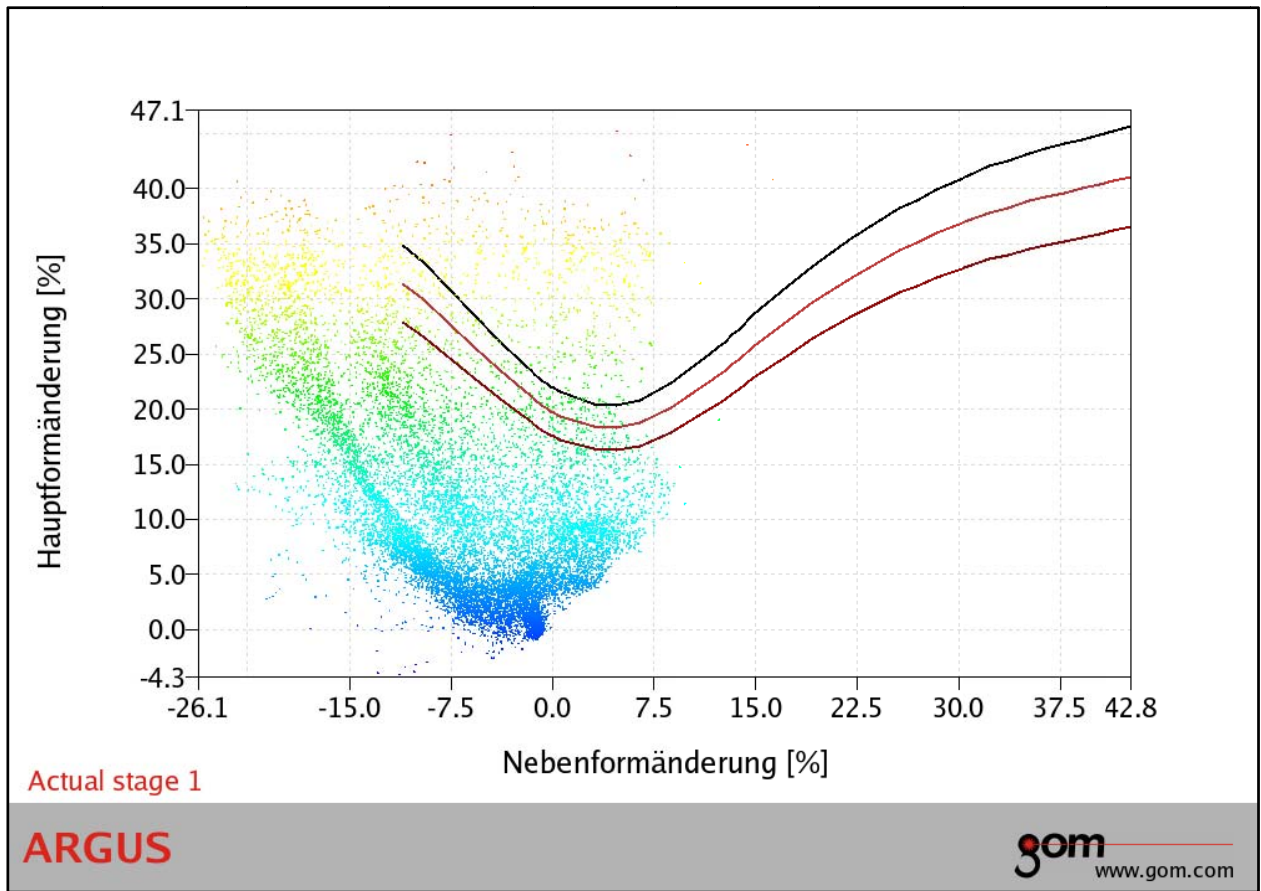

Nr.303 Thinning h=18mm
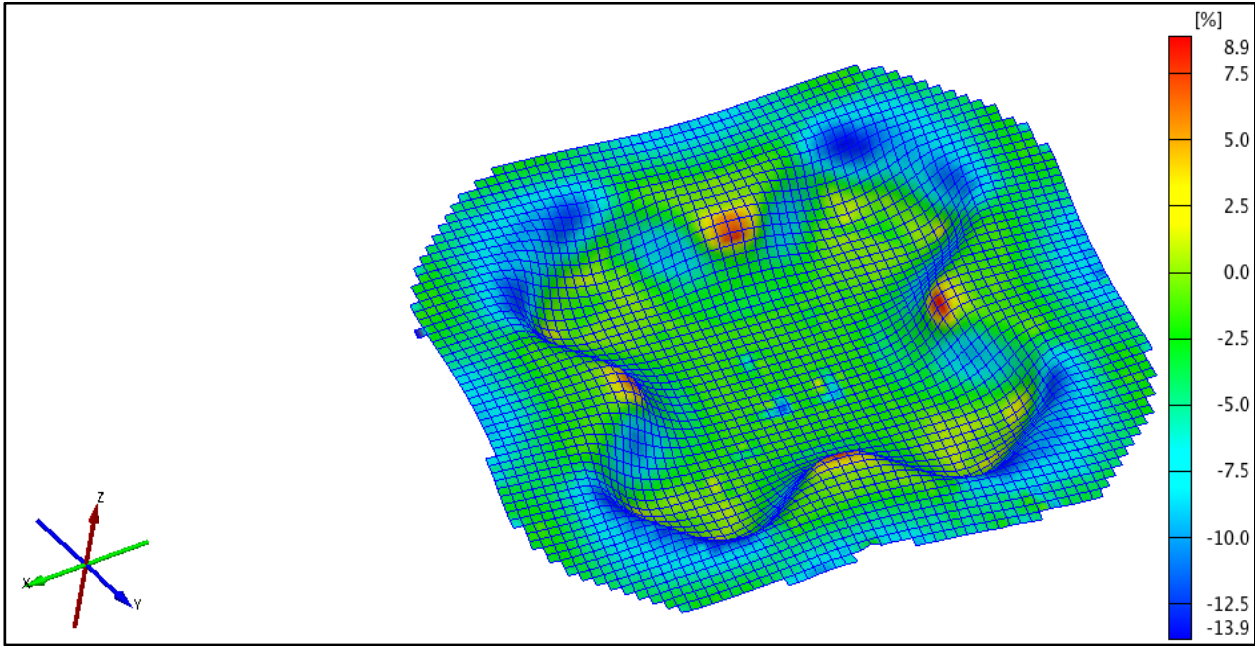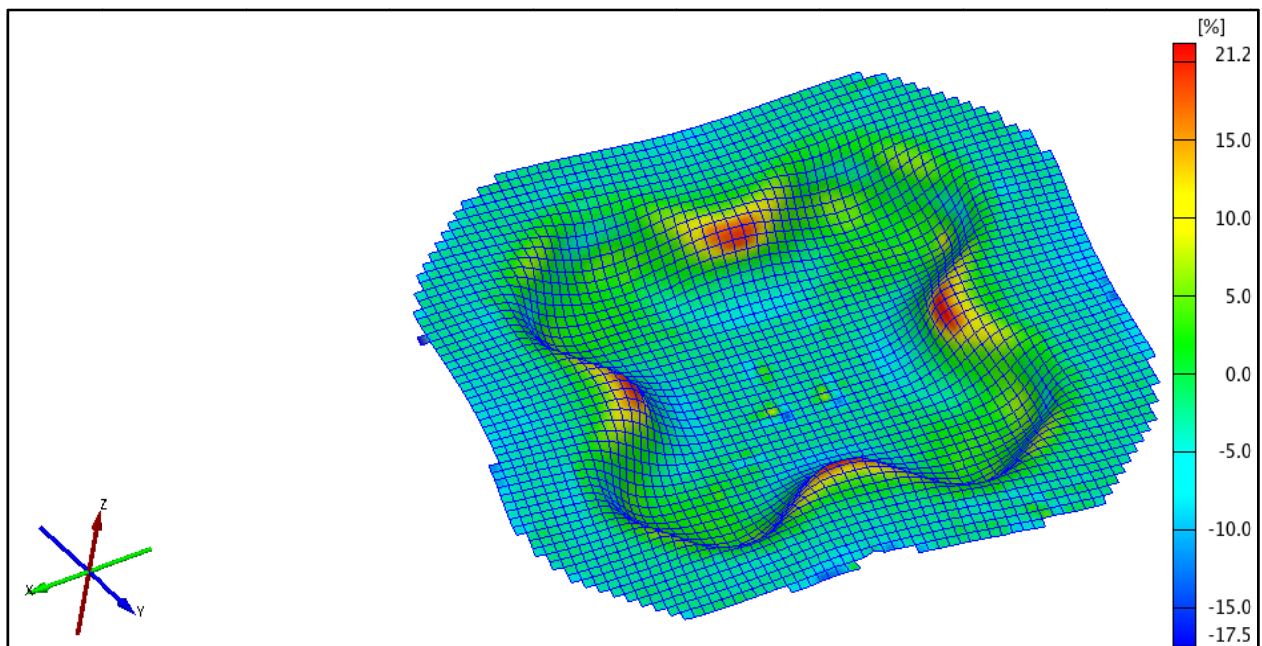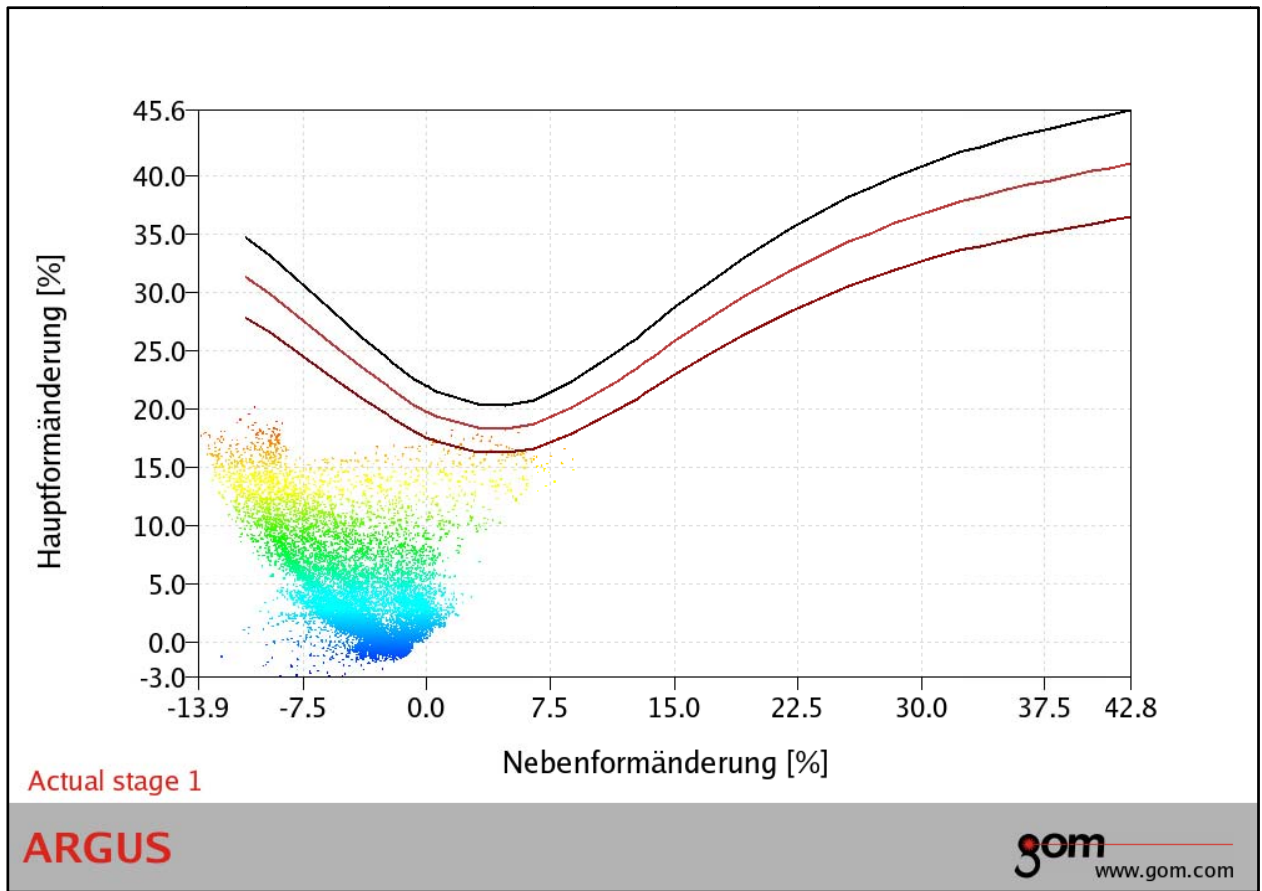
Nr.303　　　Major Strain　　　　　　h=32mm

Nr.303　　　Minor Strain　　　　　　h=32mm

Nr.303　　　　Forming Limit Diagram　　　h=32mm

Nr.303　　　　Thinning　　　　　　　h=32mm

77
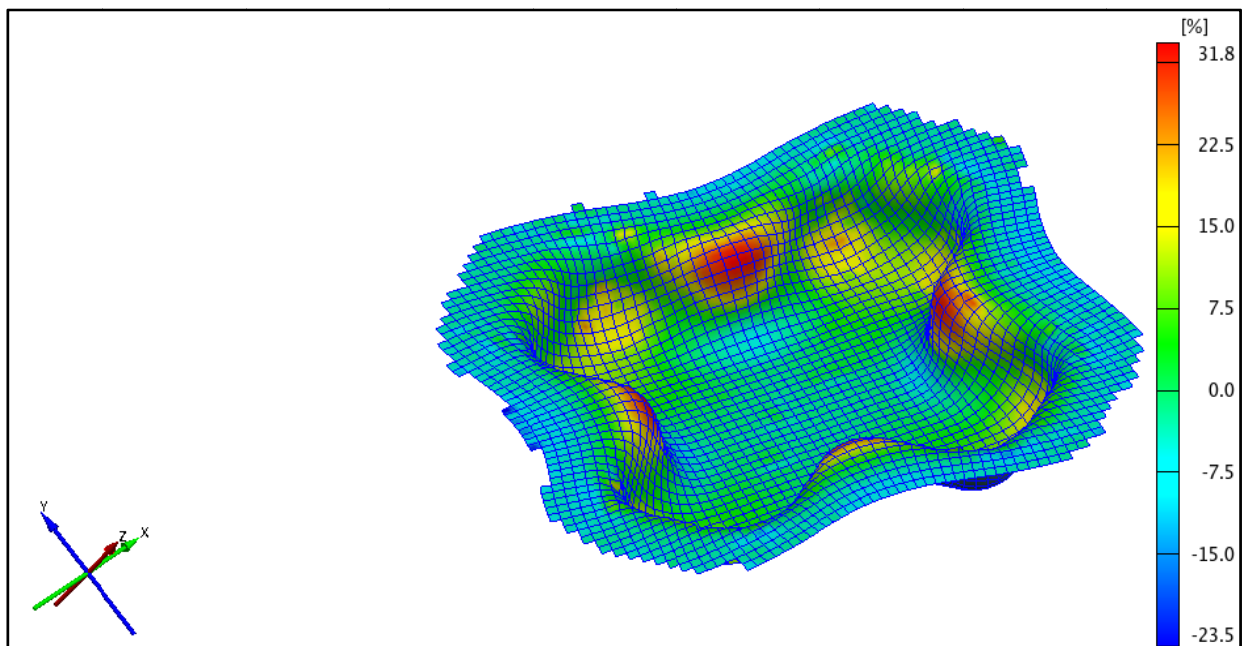
Nr.304   Major Strain   h=18mm

Nr.304   Minor Strain   h=18mm

Nr.304   Forming Limit Diagram   h=18mm
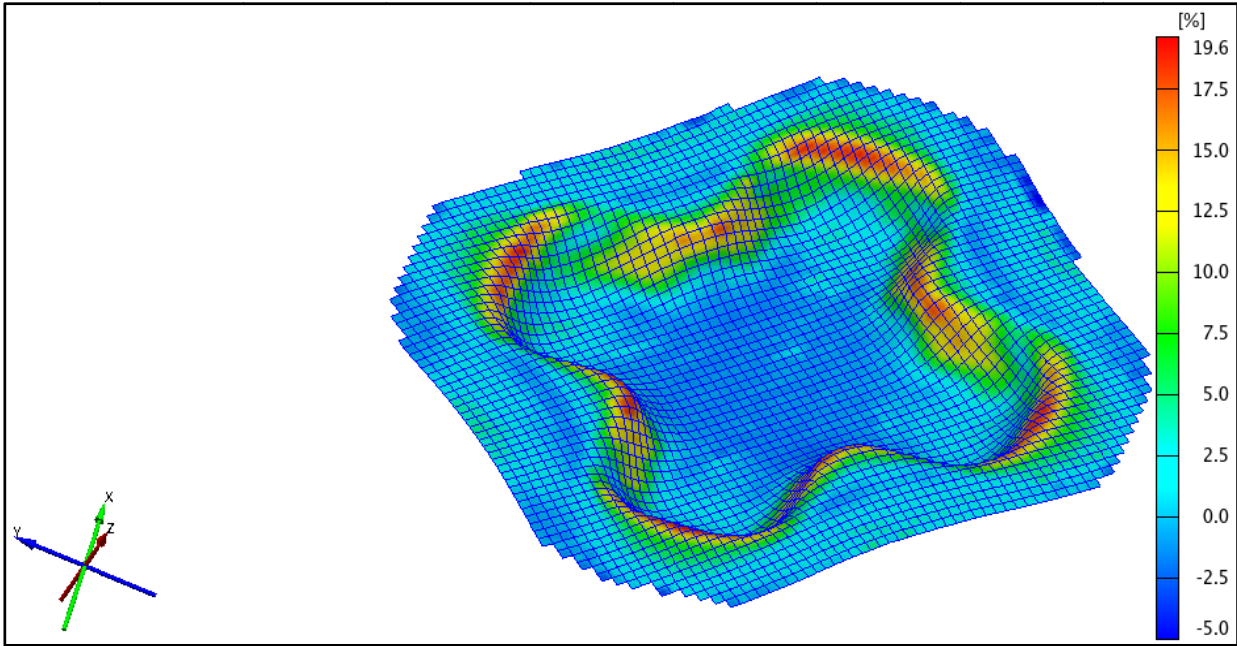
Nr.304   Thinning   h=18mm
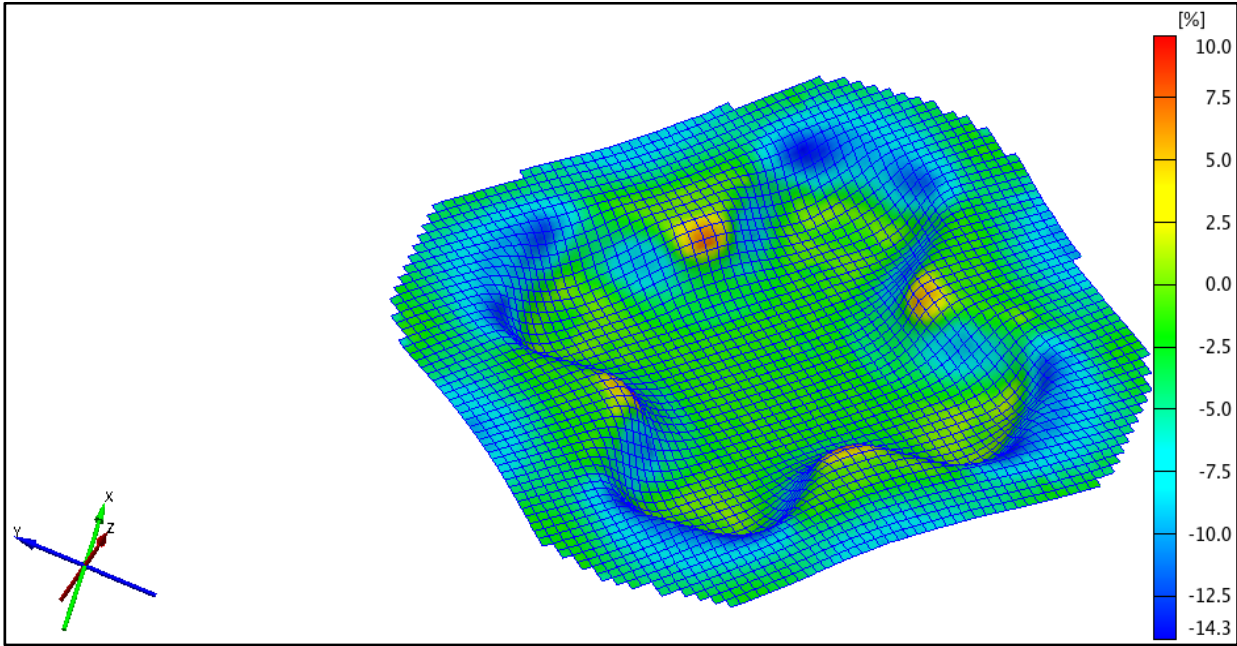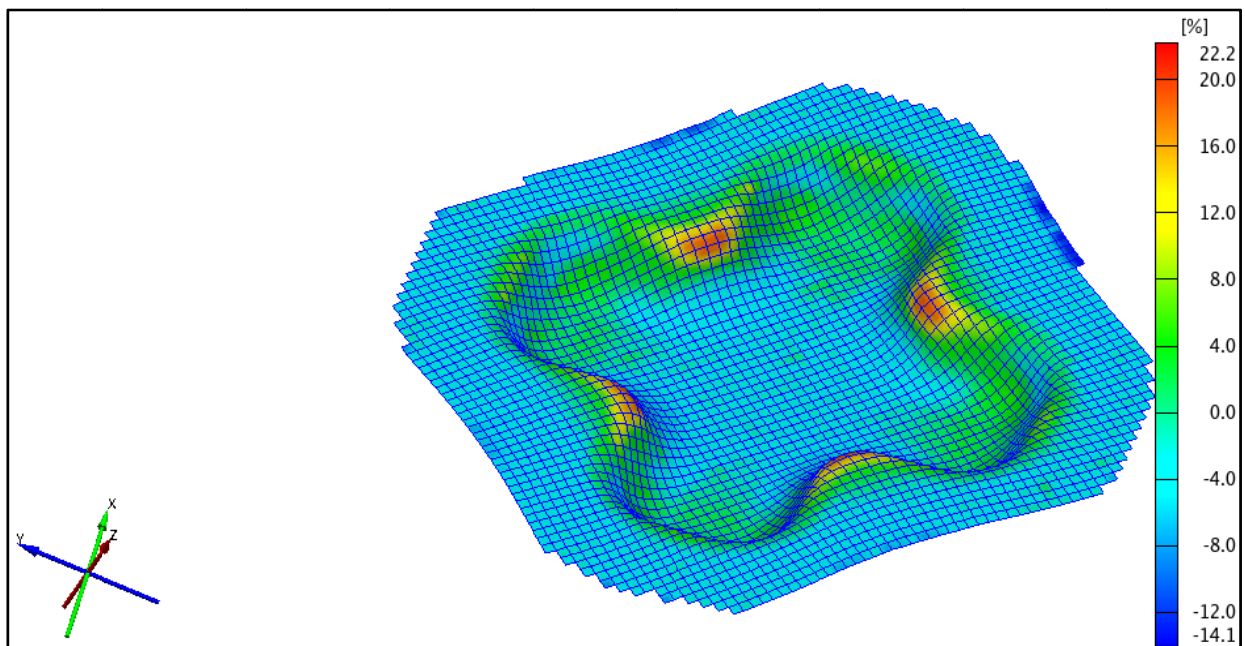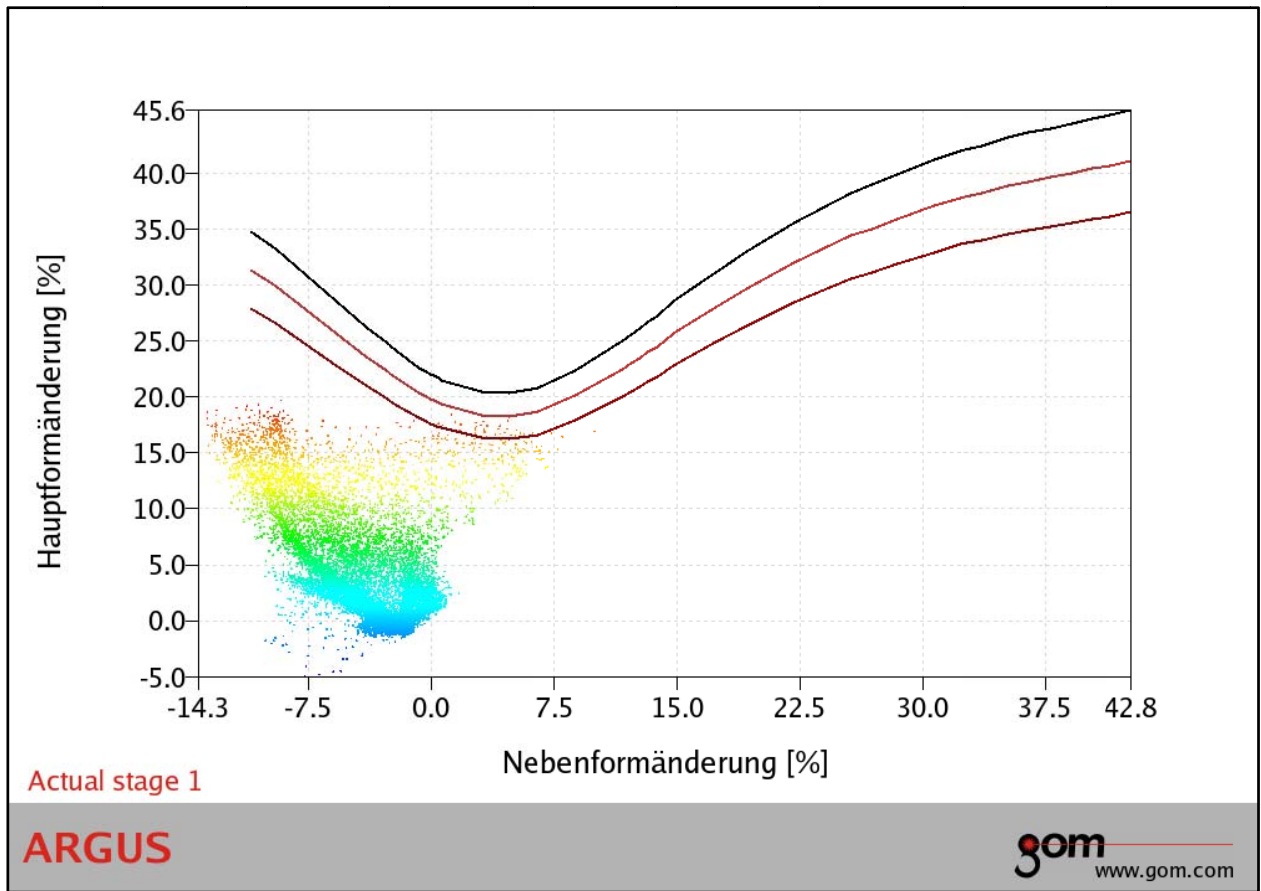
Nr.304   Major Strain   h=32mm

Nr.304   Minor Strain   h=32mm

Nr.304   Forming Limit Diagram   h=32mm
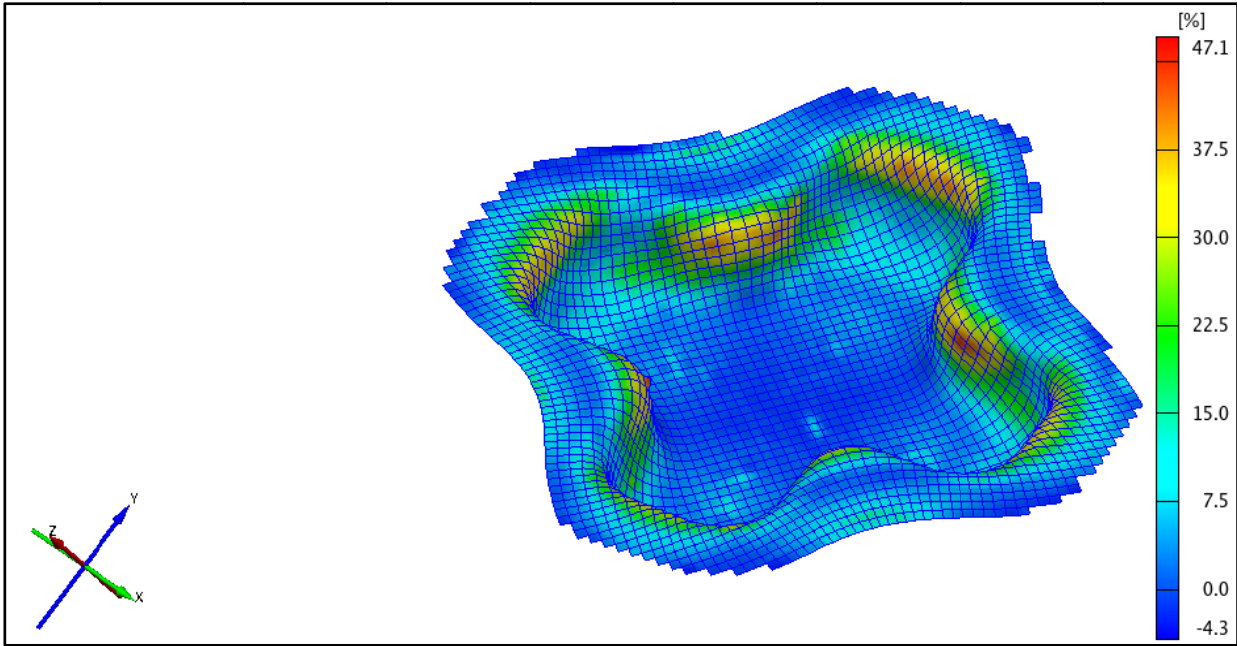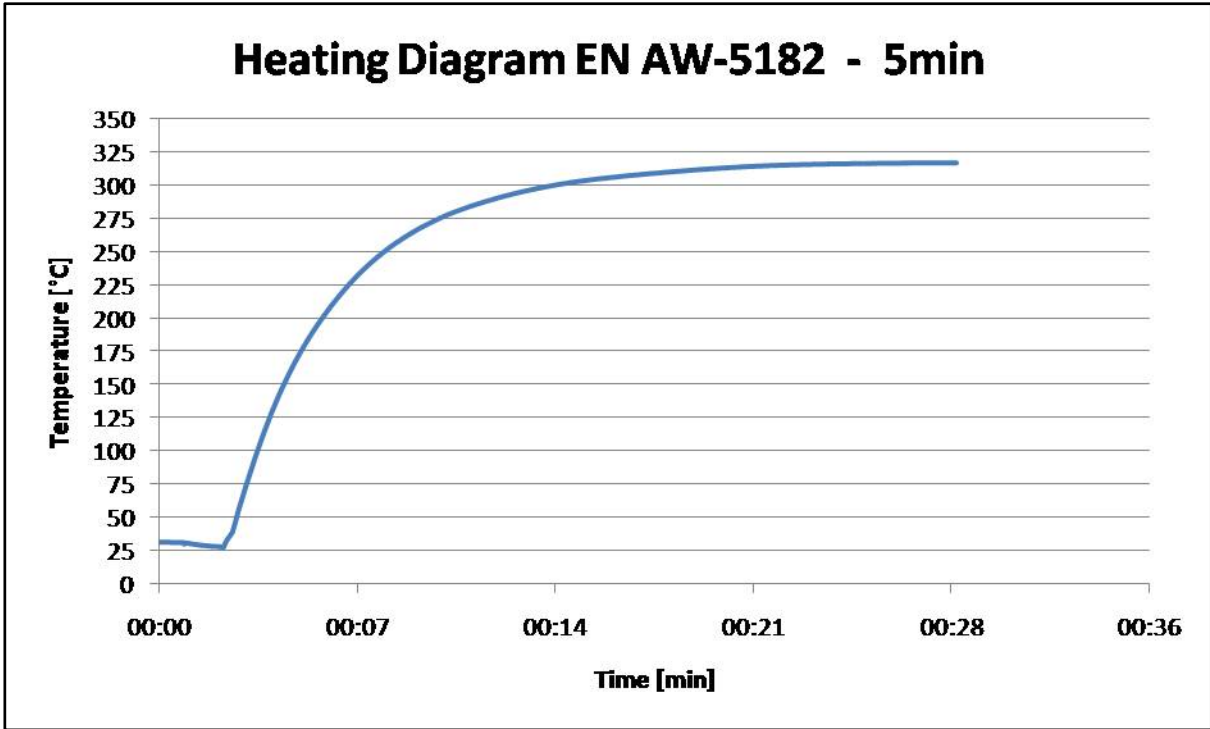

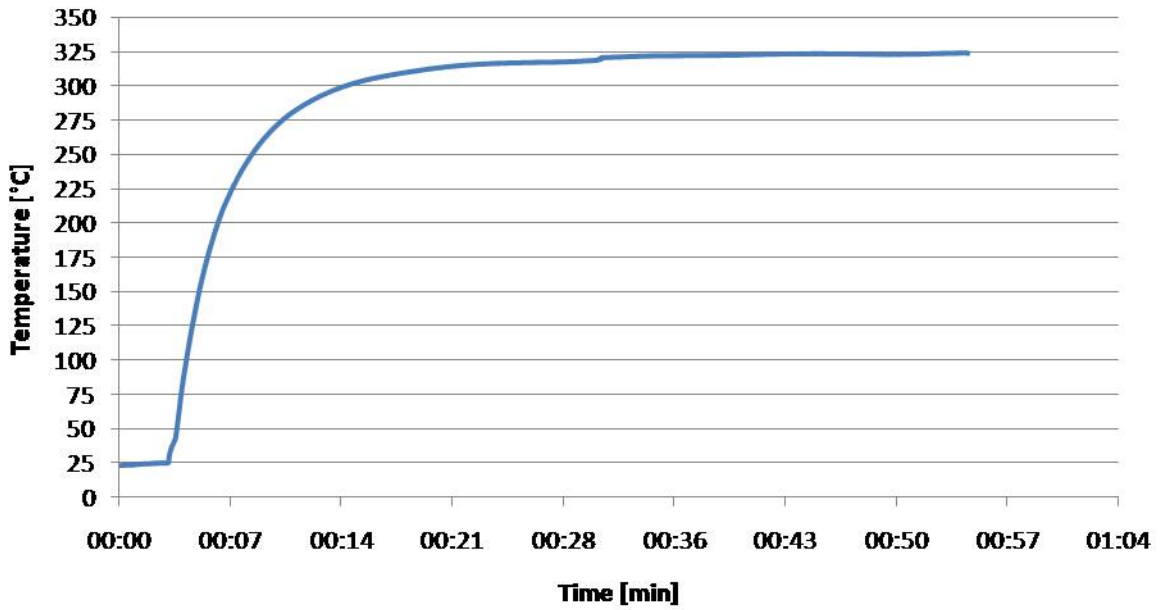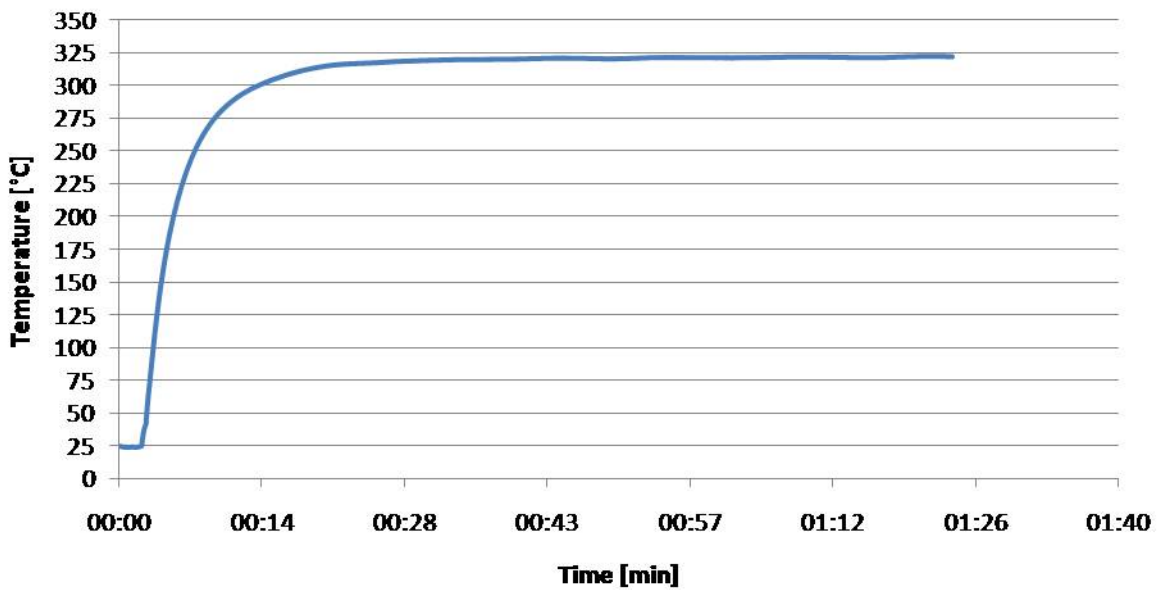**Nr.304   Thinning   h=32mm**
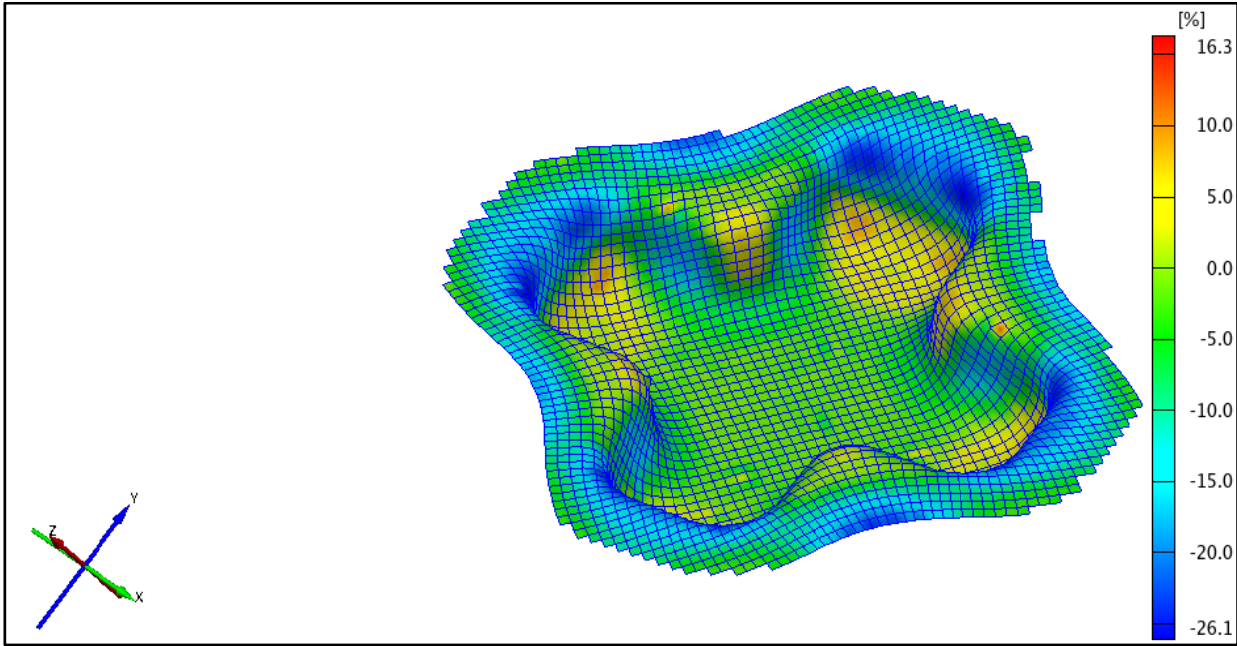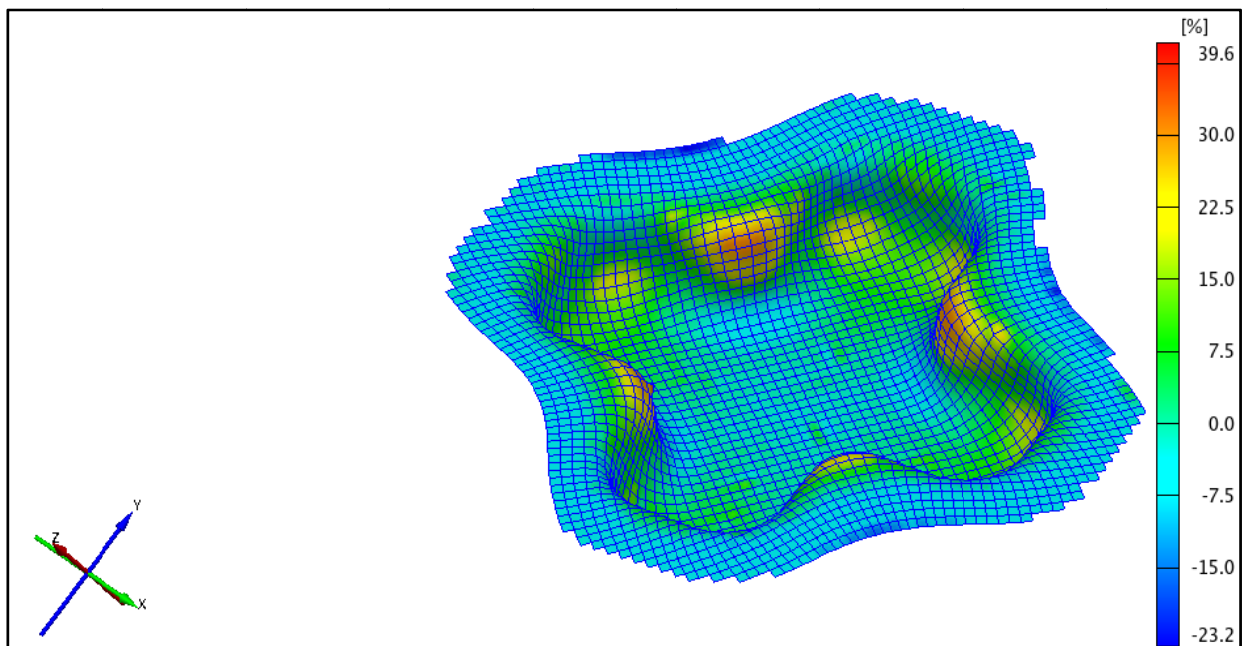
Heating Diagrams

Heating Diagram EN AW-5182 - 5min

Heatin Diagram EN AW-5182 - 15min
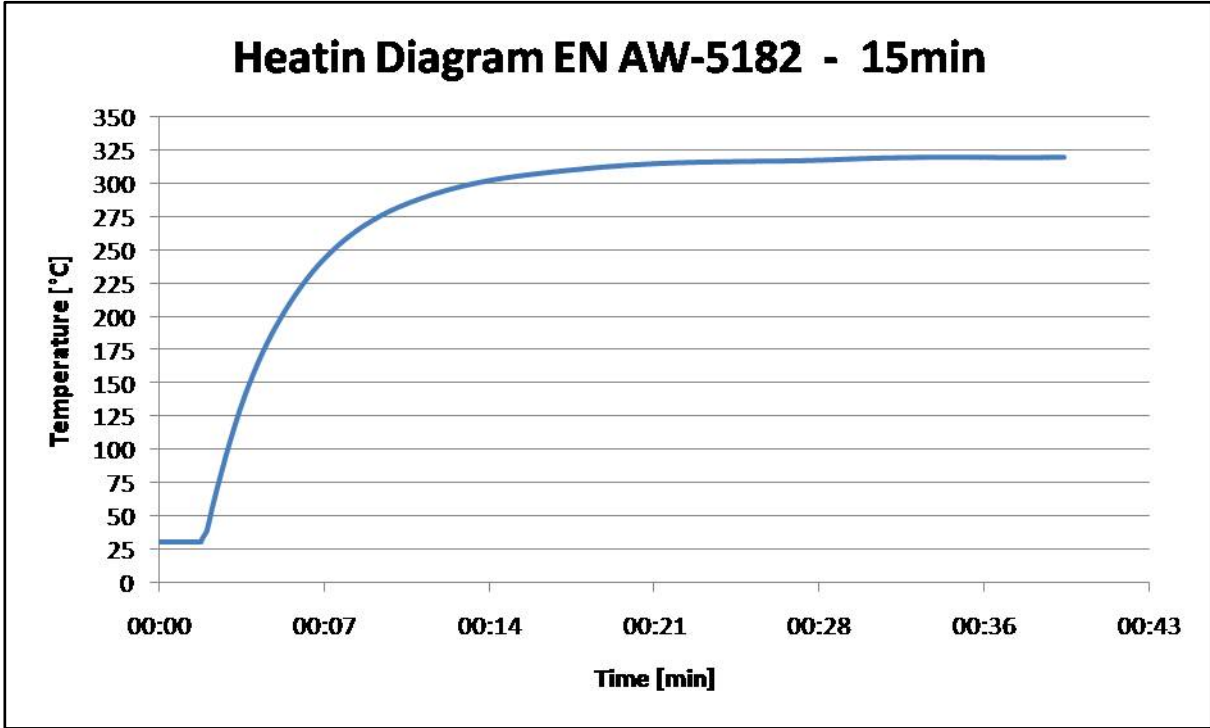
Heating Diagram EN AW-5182 - 30min

Heating Diagram EN AW-5182 - 60min

Heating Diagram EN AW-5182 - 120min